1845

Figure B32: DMA results summary (Top) for Scenario PV-12 (fully laden Qmax passing at 7 knots inbound along channel centreline, 20 knots winds at 300 deg TN), for FSRU Hoegh Esperanza with smaller LNGC Grace Dahlia. FSRU time histories of surge and sway motions (Bottom)

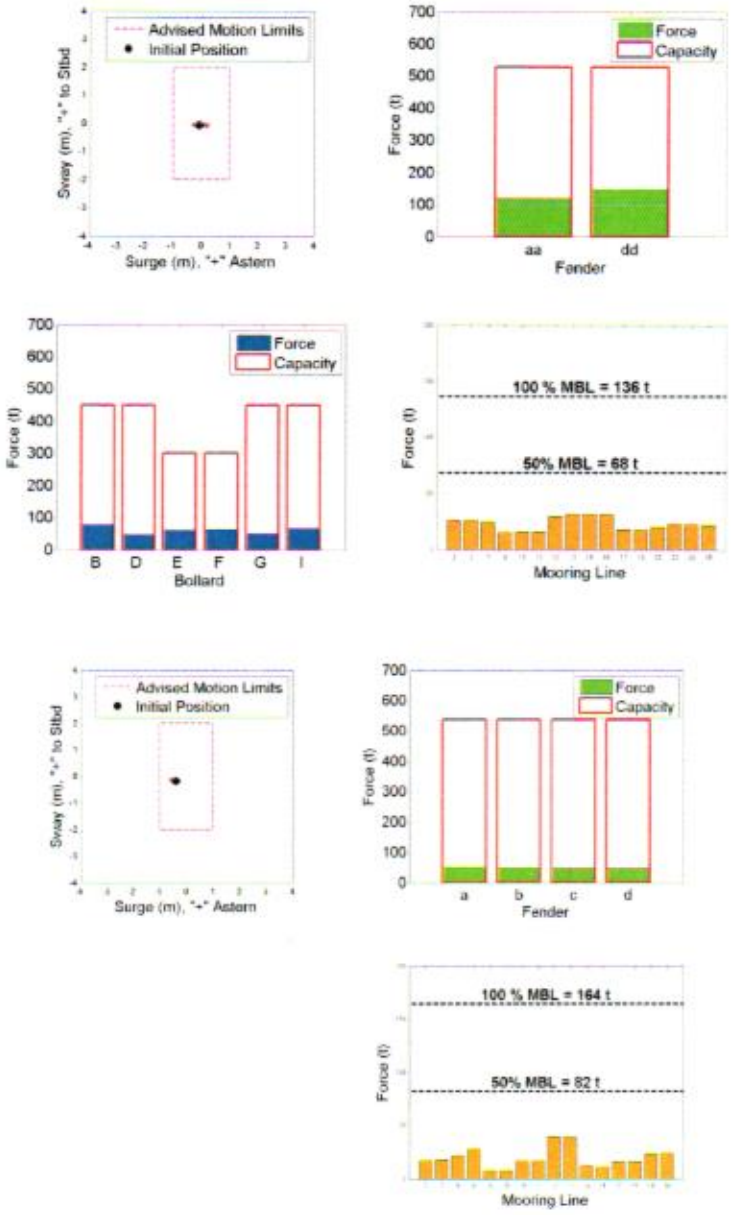

Figure B33: Time histories of surge and sway motions for Scenario PV-12. FSRU motions (Top) and LNGC Grace Dahlia motions (bottom).

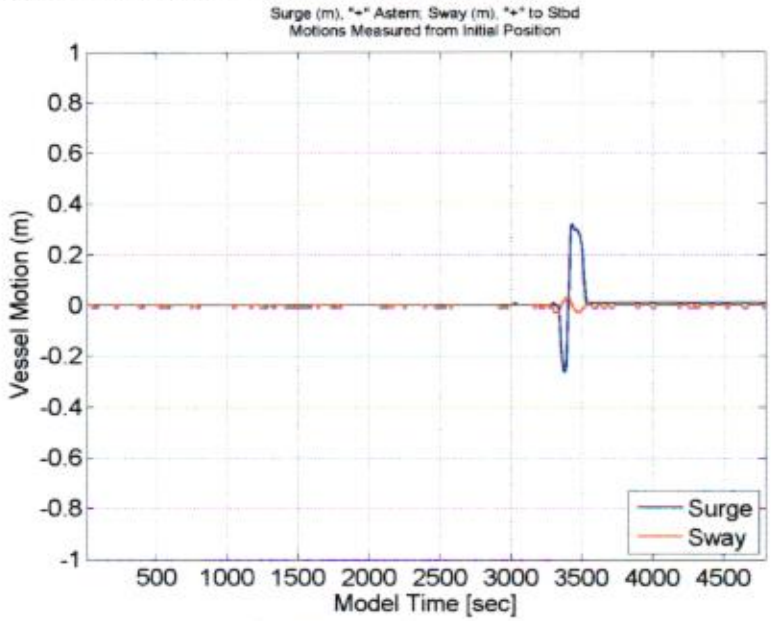

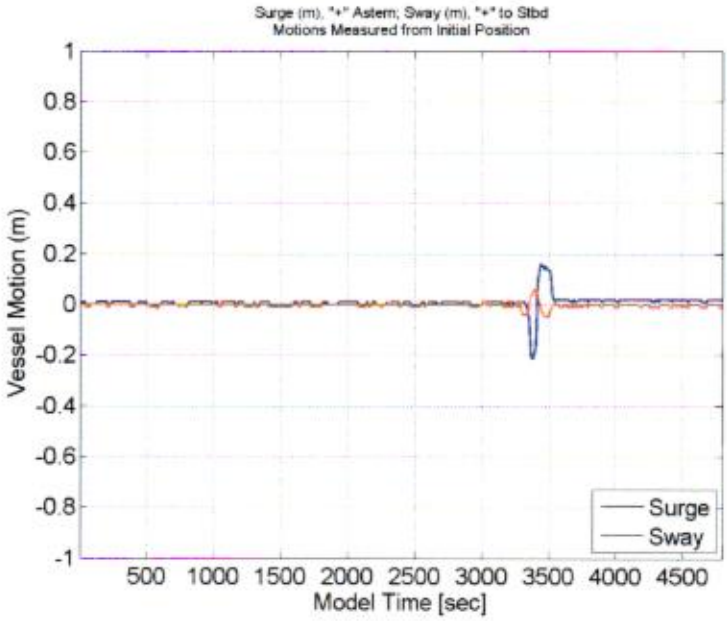

Figure B34: DMA results summary for Scenario PV-13 (fully laden Qmax passing at 7 knots inbound along channel centreline, 20 knots winds at 105 deg TN), for FSRU Hoegh Esperanza with smaller LNGC Grace Dahlia

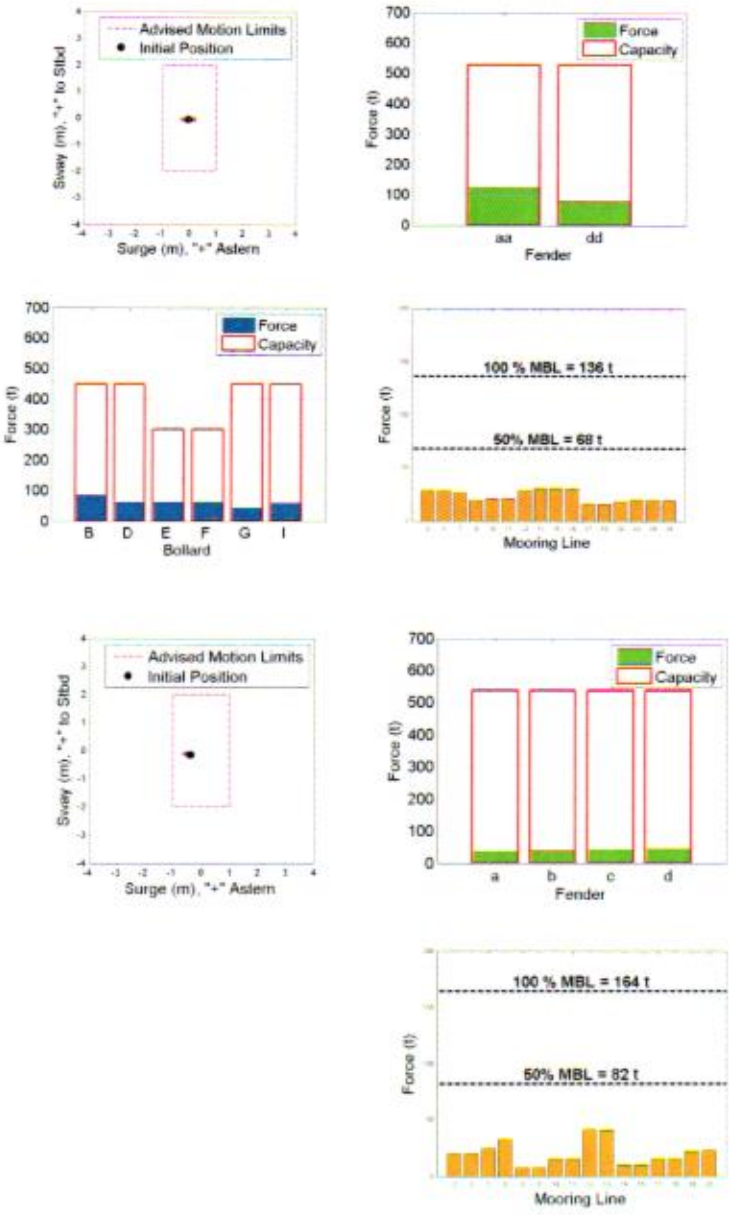

Figure B35: DMA results summary for Scenario PV-14 (fully laden Qmax passing at 7 knots inbound along channel centreline, 20 knots winds at 315 deg TN), for FSRU Hoegh Esperanza with smaller LNGC Grace Dahlia

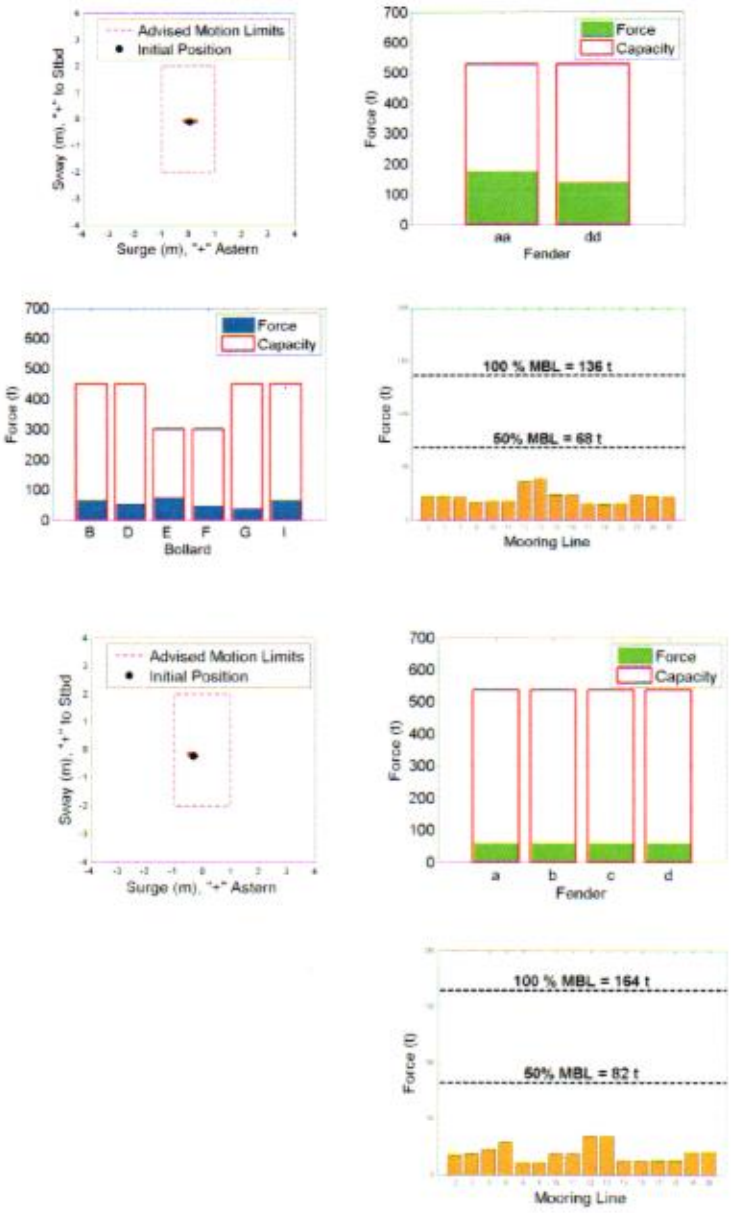

1849

Figure B36: DMA results summary (Top) for Scenario PV-15 (fully laden Qmax passing at 7 knots inbound along channel centreline, 20 knots winds at 45 deg TN), for FSRU Hoegh Esperanza with smaller LNGC Grace Dahlia present.

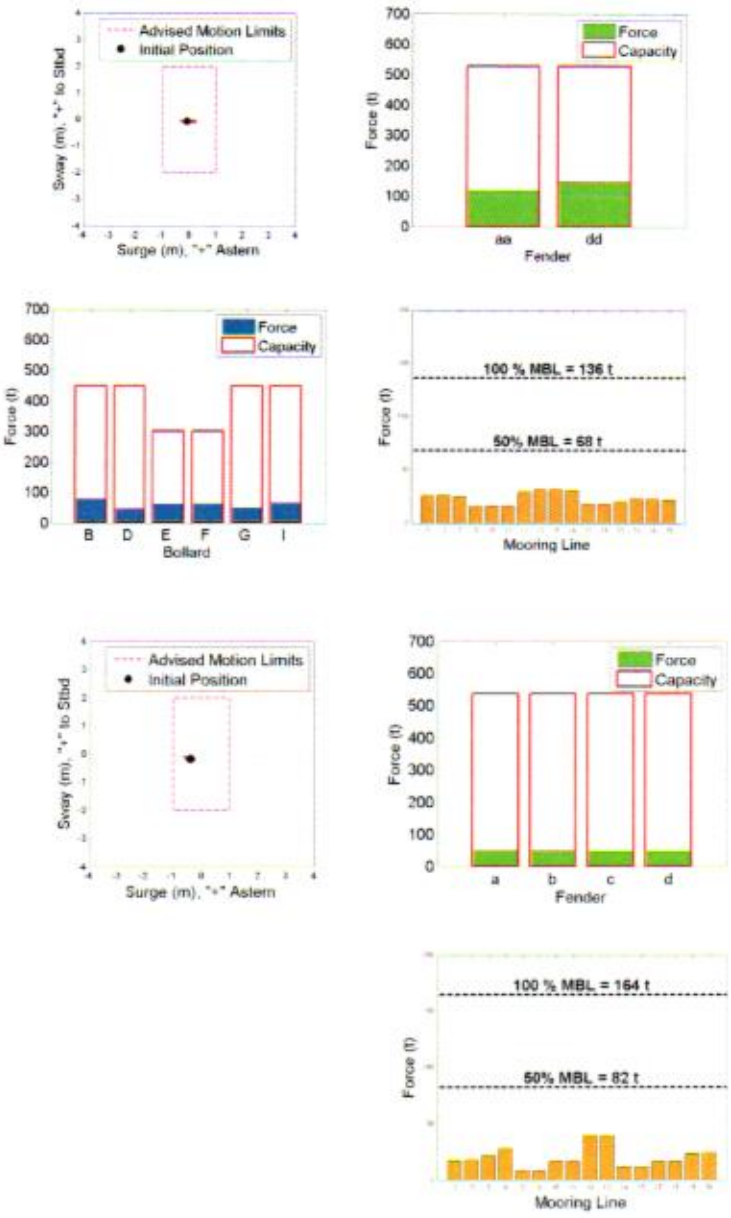

Figure B37: Time histories of surge and sway motions for Scenario PV-15. FSRU motions (Top) and LNGC Grace Dahlia motions (bottom)

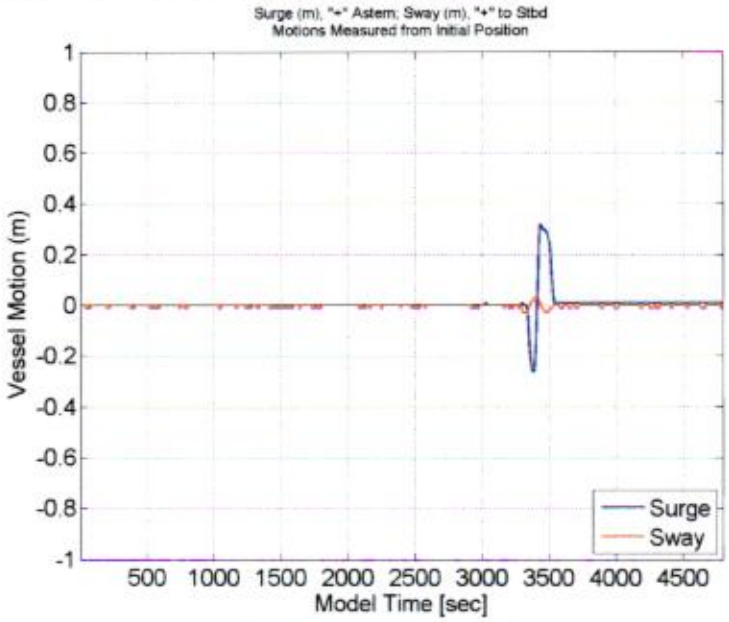

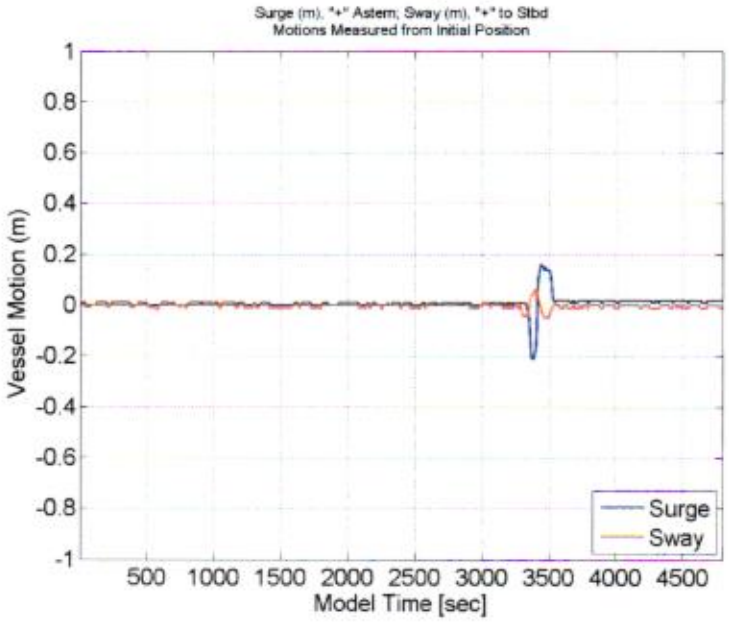

Figure B38: Time histories of surge and sway motions for Scenario PV-16 to PV-21. FSRU motions (Top) and LNGC Grace Dahlia motions (bottom)

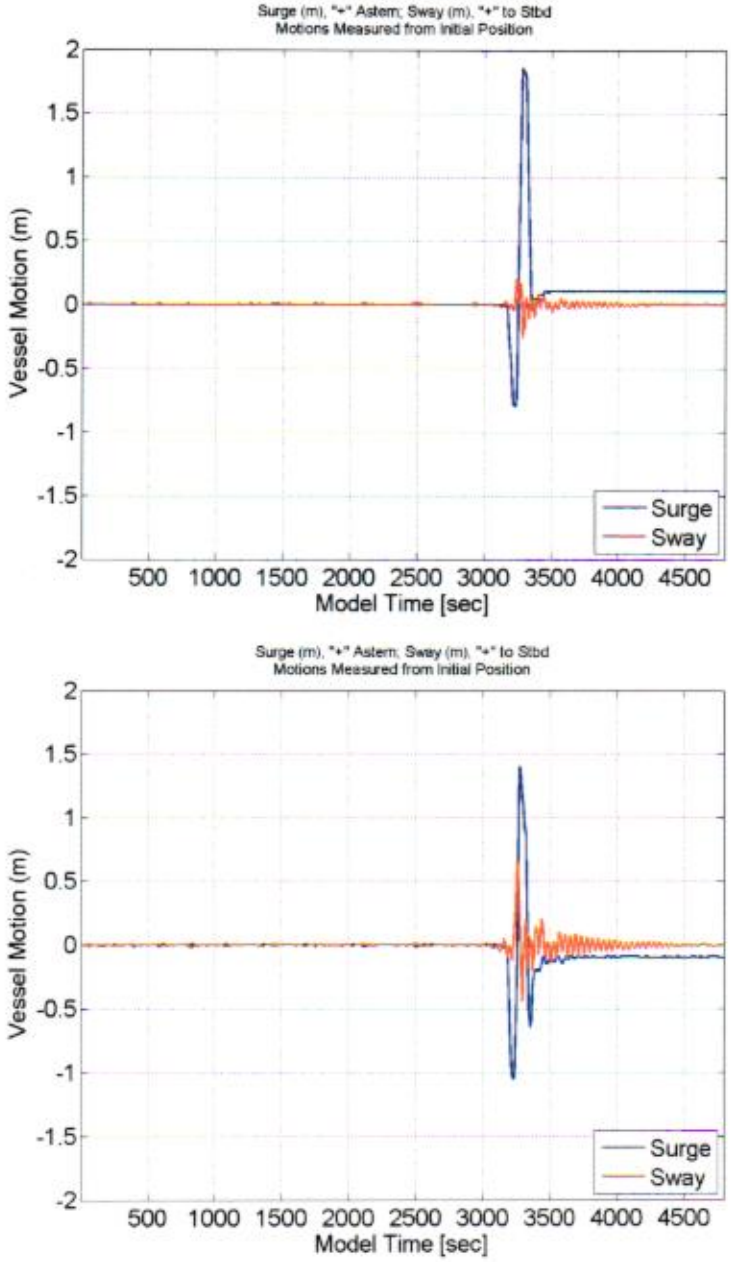

Figure B39: DMA results summary for Scenario PV-17 (fully laden Qmax passing at 10 knots inbound along channel centreline, 20 knots winds at 240 deg TN, 1.5 knots steady currents at 240 deg TN), for FSRU Hoegh Esperanza with Qmax Al Ghuwairiya

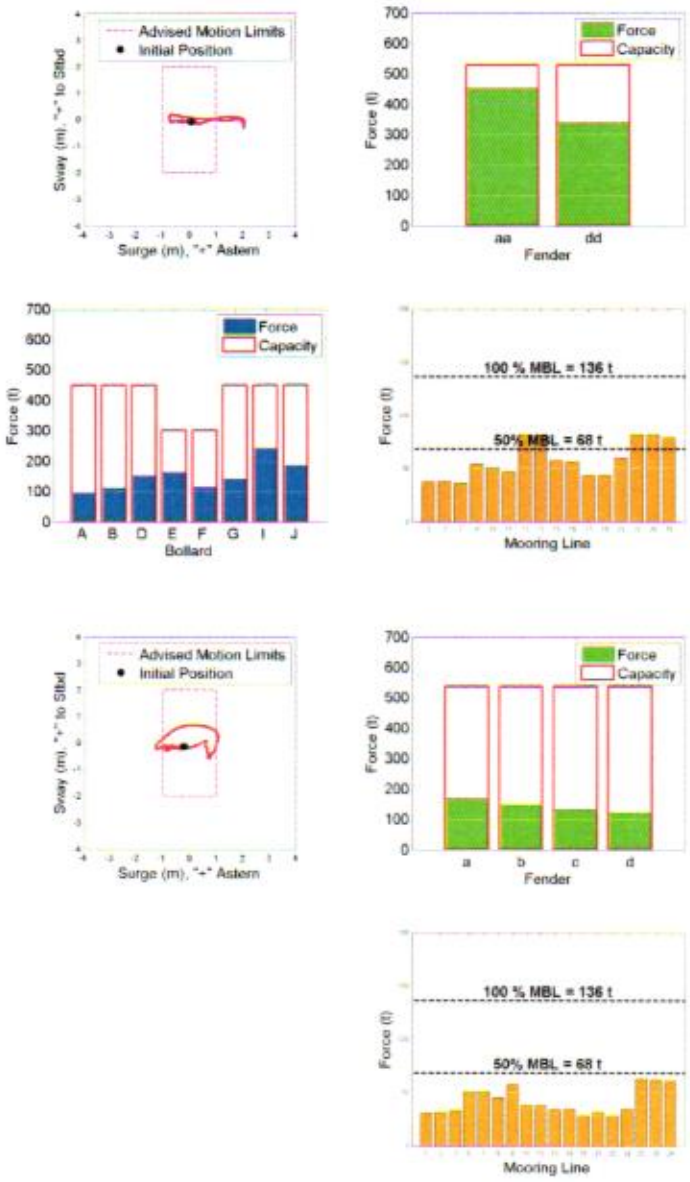

Table B1. Summary of Peak Mooring Forces for Host FSRU Hoegh Esperanza, Scenarios with Environmental Forces only (Fender Configuration FC 1-1)

	Advised Limits	EC-1	EC-2	EC-3	EC-4	EC-5	EC-6	EC-7	EC-8	EC-9	EC-10	EC-11	EC-12	EC-13	EC-14	EC-15
Max Total Force on Bollard A [mt]	450	NA	NA	NA	NA	NA	NA	NA	NA	NA	NA	NA	NA	NA	NA	NA
Max Total Force on Bollard B [mt]	450	113.7	45.6	94.8	89.7	57.4	73.8	112.5	43.5	62.6	83.9	63.9	73.0	114.5	38.7	103.3
Max Total Force on Bollard D [mt]	450	192.7	20.6	161.5	188.7	3.4	124.7	188.3	9.9	84.0	187.5	5.2	53.0	193.0	53.2	140.0
Max Total Force on Bollard E [mt]	300	51.2	7.6	48.3	116.0	81.5	56.1	69.3	1.7	42.1	95.0	81.8	18.6	57.9	46.3	29.9
Max Total Force on Bollard F [mt]	300	34.3	45.4	38.7	21.1	81.7	43.7	28.7	54.0	41.7	13.5	73.3	53.2	26.2	14.2	41.3
Max Total Force on Bollard G [mt]	450	126.8	50.4	169.1	87.3	42.9	157.9	43.2	64.8	122.4	57.4	36.6	54.2	26.4	12.9	29.9
Max Total Force on Bollard I [mt]	450	90.1	37.4	116.7	89.5	98.7	116.6	44.1	42.7	88.3	69.1	58.0	37.0	29.5	31.5	24.3
Max Total Force on Bollard J [mt]	450	NA	NA	NA	NA	NA	NA	NA	NA	NA	NA	NA	NA	NA	NA	NA
Fender aa [mt]	528	138.9	152.2	100.8	134.0	512.9	111.7	77.4	81.5	19.9	120.8	494.2	141.6	60.0	326.3	75.0
Fender dd [mt]	528	50.4	339.4	123.8	0.0	18.3	181.4	0.0	357.1	68.5	0.0	20.5	197.4	0.0	128.8	0.0
Line 2 [mt]	136	40.9	14.8	33.7	32.6	19.0	25.7	40.6	13.8	21.4	30.9	21.3	24.8	41.5	12.5	36.7
Line 3 [mt]	136	39.7	15.1	32.9	31.3	20.2	25.3	39.3	14.3	21.3	29.4	22.1	24.9	40.1	12.3	35.9
Line 7 [mt]	136	33.2	15.7	28.3	25.8	1.4	22.9	32.7	15.5	19.9	23.9	1.8	23.4	33.0	12.0	30.8
Line 8 [mt]	136	55.8	7.1	47.2	56.2	0.7	37.5	55.2	3.8	25.6	56.0	1.5	16.5	56.4	17.9	41.3
Line 10 [mt]	136	68.6	6.7	57.3	69.8	1.3	43.8	68.5	2.9	29.2	66.3	2.1	18.2	68.6	17.8	49.5
Line 11 [mt]	136	68.4	6.9	57.2	69.6	3.5	43.6	68.5	3.3	29.3	65.4	7.3	18.5	68.2	17.5	49.4
Line 12 [mt]	136	24.7	4.2	23.3	55.0	5.1	27.1	33.2	1.4	20.4	45.2	9.3	9.5	27.8	22.6	14.8
Line 13 [mt]	136	26.6	3.3	25.0	61.0	41.0	29.0	36.1	0.3	21.8	49.8	41.2	9.2	30.1	23.7	15.0
Line 15 [mt]	136	17.4	22.8	19.6	10.6	40.5	22.1	14.4	27.1	21.0	6.7	40.7	26.8	13.1	7.0	20.7
Line 16 [mt]	136	16.9	22.6	19.1	10.5	22.0	21.6	14.3	26.8	20.6	6.7	20.0	26.5	13.1	7.2	20.6
Line 17 [mt]	136	43.8	15.3	57.5	32.5	24.0	53.8	15.8	19.2	40.9	22.7	21.6	16.7	10.1	5.5	9.7
Line 18 [mt]	136	44.1	15.9	58.3	31.9	37.1	54.5	15.3	20.1	41.6	21.7	33.6	17.2	9.7	5.0	9.7
Line 22 [mt]	136	40.9	20.1	55.7	25.6	12.1	52.9	13.0	26.7	41.7	14.2	9.9	21.3	6.9	2.4	11.5
Line 23 [mt]	136	28.7	11.5	36.3	31.0	14.9	36.5	16.0	12.8	27.4	24.4	12.8	11.9	11.3	11.7	8.6
Line 24 [mt]	136	30.8	12.7	40.1	30.0	16.0	40.0	14.4	14.6	30.3	22.9	14.0	12.4	9.4	10.2	7.9
Line 25 [mt]	136	30.8	13.2	40.4	28.8	40.2	40.2	13.8	15.4	30.7	21.9	21.1	12.8	8.9	9.7	7.9

Notes:
1. All results indicate peaks occurring within each component, not necessarily coincident in time.
2. Fender, bollard, and mooring line forces are peak loads during the dynamic simulation in metric tonnes (mt).
3. Red cell shows maximum berth fender force in all scenarios.
4. Yellow cells have mooring line loads ~50% of the Minimum Breaking Load; other lines have lower loads for all scenarios.
5. Total bollard loads are resultant loads, including both horizontal and uplift. Red cell shows maximum bollard force in all scenarios.

Table B2. Summary of Peak Mooring Forces for Guest Vessels Qmax Al Ghuwairiya and Smaller LNGC Grace Dahlia, Scenarios with Environmental Forces only (Fender Configuration FC 1-1)

	Advised Limits	EC-4	EC-5	EC-6	EC-10	EC-11	EC-12		Advised Limits	EC-7	EC-8	EC-9	EC-13	EC-14	EC-15
	Guest Qmax Al Ghuwairiya								Smaller LNGC Grace Dahlia						
Max Total Force on Bollard A [mt]	450	174.9	23.0	73.3	184.3	28.6	90.1	Max Total Force on Bollard A [mt]	NA	NA	NA	NA	NA	NA	NA
Max Total Force on Bollard B [mt]	450	89.7	57.4	73.6	83.9	63.9	73.0	Max Total Force on Bollard B [mt]	450	112.5	43.5	62.6	114.5	36.7	103.3
Max Total Force on Bollard D [mt]	450	188.7	3.4	124.7	187.5	5.2	53.0	Max Total Force on Bollard D [mt]	450	188.3	9.9	84.0	193.0	53.2	140.0
Max Total Force on Bollard E [mt]	300	116.0	81.5	56.1	95.0	81.8	18.6	Max Total Force on Bollard E [mt]	300	69.3	1.7	42.1	57.9	46.3	29.9
Max Total Force on Bollard F [mt]	300	21.1	81.7	43.7	13.5	73.3	53.2	Max Total Force on Bollard F [mt]	300	28.7	54.0	41.7	26.2	14.2	41.3
Max Total Force on Bollard G [mt]	450	67.3	42.9	157.9	57.4	36.6	54.2	Max Total Force on Bollard G [mt]	450	43.2	64.8	122.4	26.4	12.9	29.9
Max Total Force on Bollard I [mt]	450	89.5	98.7	116.6	69.1	58.0	37.0	Max Total Force on Bollard I [mt]	450	44.1	42.7	88.3	29.5	31.5	24.3
Max Total Force on Bollard J [mt]	450	40.3	190.8	92.1	17.4	173.9	25.7	Max Total Force on Bollard J [mt]	NA	NA	NA	NA	NA	NA	NA
STS Fender a [mt]	536	0.0	138.6	61.9	0.0	131.9	58.8	STS Fender a [mt]	536	15.9	89.3	39.5	11.9	61.7	15.4
STS Fender b [mt]	536	0.0	97.4	55.0	0.0	99.9	57.5	STS Fender b [mt]	536	25.5	77.0	37.0	21.3	68.5	21.4
STS Fender c [mt]	536	44.9	65.4	48.9	41.4	73.3	61.1	STS Fender c [mt]	536	35.1	67.9	34.5	31.2	75.3	27.5
STS Fender d [mt]	536	96.2	6.9	43.8	90.6	8.8	73.9	STS Fender d [mt]	536	44.7	59.0	32.3	41.2	82.2	33.8
Line 1 [mt]	137	59.6	7.2	24.7	66.4	9.1	29.9	Line 2 [mt]	164	27.9	8.1	16.1	27.4	13.5	22.4
Line 2 [mt]	137	59.1	8.9	24.6	65.8	10.8	30.0	Line 3 [mt]	164	28.6	7.7	16.5	28.4	13.7	23.3
Line 3 [mt]	137	56.2	15.6	24.2	62.1	7.5	30.2	Line 5 [mt]	164	35.7	6.8	20.8	38.0	16.3	31.9
Line 6 [mt]	137	34.7	15.8	20.8	33.6	7.5	13.4	Line 6 [mt]	164	48.2	4.8	25.3	52.5	18.1	43.5
Line 7 [mt]	137	34.5	6.7	20.7	33.5	3.3	13.3	Line 8 [mt]	164	7.5	10.7	3.9	2.9	3.7	-0.8
Line 8 [mt]	137	27.2	15.7	13.4	26.4	6.8	6.7	Line 9 [mt]	164	7.0	11.8	4.0	2.4	4.0	-1.2
Line 9 [mt]	137	37.7	24.4	21.6	36.7	11.4	13.2	Line 10 [mt]	164	13.1	22.5	13.4	9.8	14.7	8.1
Line 11 [mt]	137	17.2	24.4	14.9	14.4	11.4	9.3	Line 11 [mt]	164	12.9	22.5	13.2	9.6	14.6	8.0
Line 12 [mt]	137	17.2	22.4	14.9	14.4	23.0	9.3	Line 12 [mt]	164	31.0	27.6	29.6	34.4	25.1	37.0
Line 13 [mt]	137	18.2	22.4	18.2	18.4	23.0	21.9	Line 13 [mt]	164	30.6	27.3	29.4	34.0	24.7	36.5
Line 14 [mt]	137	19.1	25.2	18.2	18.3	25.7	21.8	Line 14 [mt]	164	4.9	19.9	9.8	1.2	3.3	0.7
Line 18 [mt]	137	14.9	26.5	31.1	8.8	26.7	17.4	Line 15 [mt]	164	4.5	19.7	9.9	0.8	2.6	0.4
Line 21 [mt]	137	14.9	25.7	30.4	9.3	26.3	18.6	Line 17 [mt]	164	8.5	18.9	22.1	6.6	2.5	8.3
Line 22 [mt]	137	14.3	28.1	31.1	7.9	28.4	17.2	Line 18 [mt]	164	8.6	19.0	22.0	6.7	2.7	8.4
Line 24 [mt]	137	14.5	32.5	30.1	8.0	18.9	19.3	Line 19 [mt]	164	14.7	19.6	29.5	12.9	7.0	16.6
Line 27 [mt]	137	13.6	32.9	30.4	6.0	19.4	8.5	Line 20 [mt]	164	15.4	19.9	29.5	13.6	7.6	17.4
Line 28 [mt]	137	13.4	33.2	30.7	5.8	19.7	8.5								
Line 29 [mt]	137	13.3	31.0	31.0	5.7	15.9	8.6								

Notes:
1. All results indicate peaks occurring within each component, not necessarily coincident in time.
2. Fender, bollard, and mooring line forces are peak loads during the dynamic simulation in metric tonnes (mt).
3. Red cell shows maximum STS fender force in all scenarios.
4. Yellow cells have mooring line loads equal to ~50% of the Minimum Breaking Load; other lines have lower loads for all scenarios.
5. Total bollard loads are resultant loads, including both horizontal and uplift. Red cell shows maximum bollard force in all scenarios.

Table B3. Summary of Peak Mooring Forces for Host FSRU Hoegh Esperanza, Scenarios with both Passing Vessel and Environmental Forces (Fender Configuration FC 1-1)

	Advised Limits	PV-1	PV-2	PV-3	PV-4	PV-5	PV-6	PV-7	PV-8	PV-9	PV-10	PV-11	PV-12	PV-13	PV-14	PV-15	PV-16 to PV-21
Max Total Force on Bollard A [mt]	450	NA	NA	NA	NA	NA	NA	NA	NA	NA	NA	NA	NA	NA	NA	NA	NA
Max Total Force on Bollard B [mt]	450	43.7	44.4	43.7	54.2	55.8	55.8	60.8	57.1	63.0	63.9	65.7	77.0	84.8	65.7	77.0	111.3
Max Total Force on Bollard D [mt]	450	45.8	44.6	45.8	53.1	51.9	51.9	43.8	50.2	42.5	52.2	52.0	47.0	61.4	52.0	47.0	161.1
Max Total Force on Bollard E [mt]	300	42.1	39.1	42.1	88.7	84.9	84.9	65.3	80.4	61.1	81.3	75.1	60.8	60.5	75.1	60.8	164.0
Max Total Force on Bollard F [mt]	300	28.0	28.0	28.0	41.3	43.3	43.3	53.5	45.3	56.5	45.9	47.7	62.9	61.8	47.7	62.9	105.2
Max Total Force on Bollard G [mt]	450	40.6	39.6	40.6	53.3	50.2	50.2	56.1	49.6	56.0	41.1	39.3	48.3	43.8	39.3	48.3	117.5
Max Total Force on Bollard I [mt]	450	48.6	46.1	48.6	73.9	69.3	69.3	63.7	66.3	63.3	71.3	66.6	66.5	59.4	66.6	66.5	233.7
Max Total Force on Bollard J [mt]	450	NA	NA	NA	NA	NA	NA	NA	NA	NA	NA	NA	NA	NA	NA	NA	NA
Fender aa [mt]	528	115.5	126.7	115.5	202.5	224.1	224.1	179.1	222.0	164.6	174.5	176.0	119.0	124.9	176.0	119.0	456.9
Fender dd [mt]	528	83.6	86.7	83.6	159.7	166.6	166.6	206.8	175.9	206.5	128.3	139.1	147.4	78.0	139.1	147.4	300.8
Line 2 [mt]	136	14.6	14.9	14.6	18.1	18.7	18.7	20.2	19.1	21.0	21.6	22.2	25.9	28.9	22.2	25.9	37.5
Line 3 [mt]	136	14.6	14.9	14.6	18.2	18.8	18.8	20.5	19.2	21.3	21.7	22.3	26.2	29.0	22.3	26.2	38.1
Line 7 [mt]	136	14.5	14.7	14.5	17.9	18.4	18.4	20.2	18.9	20.9	20.7	21.3	24.9	27.0	21.3	24.9	35.9
Line 8 [mt]	136	15.5	15.1	15.5	18.7	18.2	18.2	15.1	17.5	14.6	17.3	17.0	15.2	19.6	17.0	15.2	55.9
Line 10 [mt]	136	15.3	14.9	15.3	17.6	17.2	17.2	14.5	16.7	14.1	17.7	17.6	15.9	21.0	17.6	15.9	54.6
Line 11 [mt]	136	15.2	14.9	15.2	17.0	16.8	16.8	14.4	16.3	14.0	17.7	17.6	16.1	21.0	17.6	16.1	51.0
Line 12 [mt]	136	20.5	19.2	20.5	41.6	40.7	40.7	31.6	38.6	29.6	39.1	36.2	29.4	29.3	36.2	29.4	82.0
Line 13 [mt]	136	21.6	19.9	21.6	45.1	44.1	44.1	33.8	41.8	31.5	42.2	38.9	31.3	31.2	38.9	31.3	82.0
Line 15 [mt]	136	14.0	14.5	14.0	20.8	21.7	21.7	26.9	22.8	28.4	23.0	24.0	31.6	31.1	24.0	31.6	53.1
Line 16 [mt]	136	14.0	14.5	14.0	20.6	21.5	21.5	26.6	22.6	28.1	22.9	23.8	31.2	30.8	23.8	31.2	52.1
Line 17 [mt]	136	14.1	13.6	14.1	18.0	16.7	16.7	16.9	16.2	17.3	16.4	15.5	18.0	16.4	15.5	18.0	40.1
Line 18 [mt]	136	13.9	13.4	13.9	17.6	16.5	16.5	17.5	16.1	17.9	15.6	14.7	17.5	15.9	14.7	17.5	36.3
Line 22 [mt]	136	13.7	13.5	13.7	20.0	19.2	19.2	22.8	19.4	24.0	16.5	15.6	20.2	18.2	15.6	20.2	49.6
Line 23 [mt]	136	16.6	15.7	16.6	25.8	24.4	24.4	22.0	23.4	21.7	24.8	23.2	22.5	20.4	23.2	22.5	82.0
Line 24 [mt]	136	16.2	15.3	16.2	24.6	23.0	23.0	21.2	22.0	21.2	23.7	22.2	22.3	19.8	22.2	22.3	78.5
Line 25 [mt]	136	15.9	15.1	15.9	23.6	22.0	22.0	20.6	21.1	20.6	22.8	21.3	21.8	19.3	21.3	21.8	73.6

Notes:
1. All results indicate peaks occurring within each component, not necessarily coincident in time.
2. Fender, bollard, and mooring line forces are peak loads during the dynamic simulation in metric tonnes (mt).
3. Red cell shows maximum berth fender force in all scenarios.
4. Yellow cells have mooring line loads exceed 50% of the Minimum Breaking Load; other lines have lower loads for all scenarios.
5. Total bollard loads are resultant loads, including both horizontal and uplift. Red cell shows maximum bollard force in all scenarios.

Table B4. Summary of Peak Mooring Forces for Guest Vessels Qmax Al Ghuwairiya and Smaller LNGC Grace Dahlia, Scenarios with both Passing Vessel and Environmental Forces (Fender Configuration FC 1-1)

	Advised Limits	PV-4	PV-5	PV-6	PV-7	PV-8	PV-9	PV-16 to PV-21		Advised Limits	PV-10	PV-11	PV-12	PV-13	PV-14	PV-15
	Guest Qmax Al Ghuwairiya									Smaller LNGC Grace Dahlia						
Max Total Force on Bollard A [mt]	450	61.3	63.1	63.1	60.7	63.5	61.2	61.2	Max Total Force on Bollard A [mt]	NA	NA	NA	NA	NA	NA	NA
Max Total Force on Bollard B [mt]	450	54.2	55.8	55.8	60.8	57.1	63.0	63.0	Max Total Force on Bollard B [mt]	450	63.9	65.7	77.0	84.8	65.7	77.0
Max Total Force on Bollard D [mt]	450	53.1	51.9	51.9	43.8	50.2	42.5	42.5	Max Total Force on Bollard D [mt]	450	52.2	52.0	47.0	61.4	52.0	47.0
Max Total Force on Bollard E [mt]	300	86.7	84.9	84.9	65.3	80.4	61.1	61.1	Max Total Force on Bollard E [mt]	300	81.3	75.1	60.8	60.5	75.1	60.8
Max Total Force on Bollard F [mt]	300	41.3	43.3	43.3	53.5	45.3	56.5	56.5	Max Total Force on Bollard F [mt]	300	45.9	47.7	62.9	61.8	47.7	62.9
Max Total Force on Bollard G [mt]	450	53.3	50.2	50.2	56.1	49.8	58.0	58.0	Max Total Force on Bollard G [mt]	450	41.1	39.3	48.3	43.8	39.3	48.3
Max Total Force on Bollard I [mt]	450	73.9	69.3	69.3	63.7	66.3	63.3	63.3	Max Total Force on Bollard I [mt]	450	71.3	66.6	66.5	59.4	66.6	66.5
Max Total Force on Bollard J [mt]	450	54.6	50.2	50.2	53.0	48.3	51.9	51.9	Max Total Force on Bollard J [mt]	NA	NA	NA	NA	NA	NA	NA
STS Fender a [mt]	536	52.9	61.2	61.2	74.1	64.0	71.0	71.0	STS Fender a [mt]	536	54.8	56.7	50.7	37.3	56.7	50.7
STS Fender b [mt]	536	58.2	66.4	66.4	70.8	68.4	67.4	67.4	STS Fender b [mt]	536	55.0	56.7	49.1	39.0	56.7	49.1
STS Fender c [mt]	536	63.4	71.6	71.6	67.8	73.0	63.9	63.9	STS Fender c [mt]	536	55.2	56.7	47.6	41.5	56.7	47.6
STS Fender d [mt]	536	68.7	76.9	76.9	68.2	77.8	65.8	65.8	STS Fender d [mt]	536	55.5	56.9	46.4	44.2	56.9	46.4
Line 1 [mt]	137	20.3	20.9	20.9	19.9	21.0	20.0	20.0	Line 2 [mt]	164	18.6	18.0	17.1	19.7	18.0	17.1
Line 2 [mt]	137	20.3	20.9	20.9	20.1	21.1	20.2	20.2	Line 3 [mt]	164	18.8	18.2	17.4	19.9	18.2	17.4
Line 3 [mt]	137	20.8	21.4	21.4	20.6	21.6	21.1	21.1	Line 5 [mt]	164	22.9	22.6	21.5	24.6	22.6	21.5
Line 6 [mt]	137	22.9	22.1	22.1	18.6	21.3	18.0	18.0	Line 6 [mt]	164	29.0	28.6	27.5	32.9	28.6	27.5
Line 7 [mt]	137	22.9	22.1	22.1	18.6	21.3	18.0	18.0	Line 8 [mt]	164	11.3	10.9	7.5	7.8	10.9	7.5
Line 8 [mt]	137	15.3	14.5	14.5	11.4	13.7	10.8	10.8	Line 9 [mt]	164	11.5	11.0	7.7	7.7	11.0	7.7
Line 9 [mt]	137	23.8	22.8	22.8	18.9	22.0	18.2	18.2	Line 10 [mt]	164	18.6	18.5	16.6	15.4	18.5	16.6
Line 11 [mt]	137	19.8	19.6	19.6	17.9	19.3	17.4	17.4	Line 11 [mt]	164	18.6	18.4	16.6	15.3	18.4	16.6
Line 12 [mt]	137	19.8	19.6	19.6	17.9	19.3	17.4	17.4	Line 12 [mt]	164	33.3	34.5	39.5	41.4	34.5	39.5
Line 13 [mt]	137	20.4	21.1	21.1	22.5	21.4	23.2	23.2	Line 13 [mt]	164	32.9	34.0	39.0	40.9	34.0	39.0
Line 14 [mt]	137	20.3	21.0	21.0	22.5	21.3	23.1	23.1	Line 14 [mt]	164	13.0	12.3	11.4	10.1	12.3	11.4
Line 18 [mt]	137	17.8	17.2	17.2	19.5	17.2	20.2	20.2	Line 15 [mt]	164	12.7	11.8	11.2	9.8	11.8	11.2
Line 21 [mt]	137	18.8	18.4	18.4	20.8	18.4	21.6	21.6	Line 17 [mt]	164	14.3	12.9	15.9	15.3	12.9	15.9
Line 22 [mt]	137	17.8	17.0	17.0	19.4	17.0	20.0	20.0	Line 18 [mt]	164	14.3	12.9	15.9	15.3	12.9	15.9
Line 24 [mt]	137	19.4	19.1	19.1	21.8	19.1	22.7	22.7	Line 19 [mt]	164	20.3	19.9	23.0	22.2	19.9	23.0
Line 27 [mt]	137	18.4	17.0	17.0	17.8	16.3	17.4	17.4	Line 20 [mt]	164	20.8	20.4	23.6	22.9	20.4	23.6
Line 28 [mt]	137	18.2	16.7	16.7	17.7	16.1	17.3	17.3								
Line 29 [mt]	137	18.0	16.5	16.5	17.6	15.9	17.3	17.3								

Notes:
1. All results indicate peaks occurring within each component, not necessarily coincident in time.
2. Fender, bollard, and mooring line forces are peak loads during the dynamic simulation in metric tonnes (mt).
3. Red cell shows maximum STS fender force achieved in all scenarios.
4. Yellow cells have mooring line loads equal to ~50% of the Minimum Breaking Load: other lines have lower loads for all scenarios.
5. Total bollard loads are resultant loads, including both horizontal and uplift. Red cell shows maximum bollard force achieved in all scenarios.

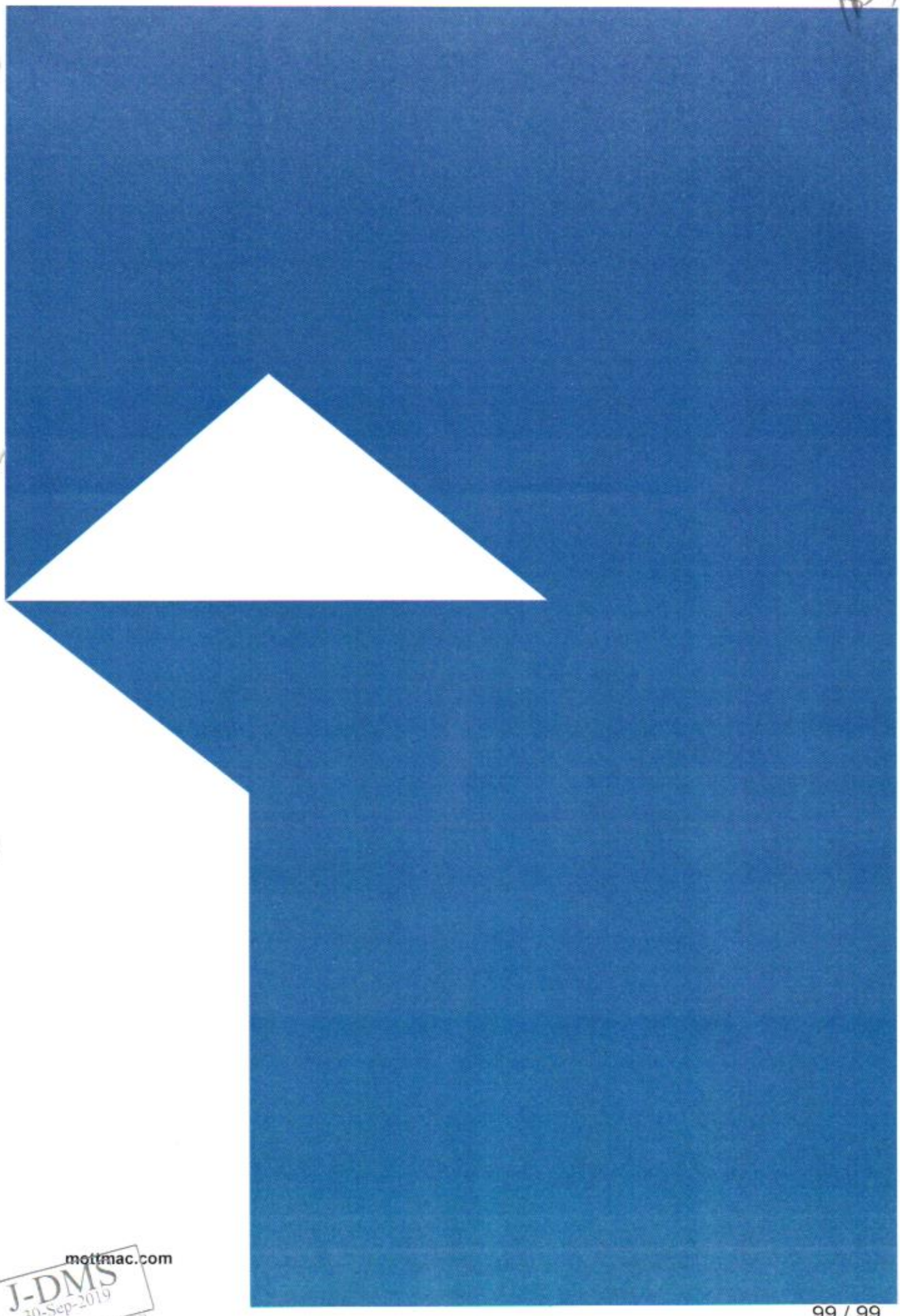

1858

1959

JOB No.	DOC. No.	Rev.
0-8069-20	**S-000-13M0-221**	**2**

DATE 12 - Sep - 2019 SHEET 1 OF 92

PREP'D	F. Cogordan	
CHK'D	K. Uchino	
APP'D	K.Kou	

SEDIMENTATION STUDY

Tabeer LNG Project / FEED

FOR FINAL FEED

REV.	Date	Page	DESCRIPTION	PRE'D	CHK'D	APP'D
0	29-Mar-19	ALL	Issue for Review	N. Inoue	K.Uchino	K.Kou
1	05-Aug-19	ALL	Issue for Final FEED	F. Cogordan	K.Uchino	K.Uchino
2	12-Sep-19	3,4,39,44,48, 75,79	Issue for Final FEED	F. Cogordan	K.Uchino	K.Kou

JGC JGC CORPORATION

Contents

1. INTRODUCTION

1.1. Scope

The specification covers to determine sand/mud transport regime and accretion rates in the dredged approach channel to the project following development of the berth facilities.

2. SUMMARY

2.1. Results of Sedimentation Analysis

The aim of FEED was to quantify sedimentation in the approach and nearshore channels, berth and turning basin area. The offshore region and islands around the nearshore channel are understood to be characterized by fine sand. In contrast, sediments in the approach channel comprise silt and clay. These different sediment types are thought to merge gradually in the area adjacent to Muchak Island. To correctly represent the different dynamical properties of these sediment types, two modelling approaches have been undertaken in this phase of the works:

Sand Transport model (ST) - for the non-cohesive sandy sediment in the nearshore and approach channel; and
Mud Transport model (MT) – for the muddy cohesive sediments in the approach channel, berthing and turning basin.

The results obtained from both models show that, in general, the approach channel is mainly dominated by sand processes, with some additional mud deposition during the monsoon season. Whereas, the area of the turning circle and the berths is dominated by deposition of cohesive sediments.

The volume of sand and mud deposited in the approach channel and project site have been added together. A table with the estimated deposition over the years is included in Appendix A in report. As a result of analysis, in the area of the turning basin and the berth pocket, no significant sand accretion is observed.

As regards to the uncertainty pertaining to the sediment transport modeling, especially on restrictions and calculation limitations, the following points are noted.

- Restrictions from availability of calibration data:
Limited information was available to calibrate the mud transport model. However, extensive literature review established that the suspended sediment concentration in the estuary is small, in the range of 25 to 180mg/l. Survey data used to calibrate the model from SSC values at site between 20mg/l and 40mg/l, with peak concentrations during the ebb tide of up to 150mg/l. Hence, literature data and measured data agreed reasonably well, and it was eventually possible to use this data for model calibration purpose.

- Calculation limitation on computed concentration:
During neap tides, the model slightly underestimates the suspended sediment load by approximately 10mg/l. However, since the suspended sediment concentrations are low, this underestimation is considered not to affect the model results greatly, especially when the monsoon seasonal effects are factored in.

- Restrictions from duration of calibration data:
The model was calibrated with data collected outside the monsoon season, in March 2019. It is recommended to collect data during the monsoon season in order to check that the

values assumed in this modelling study are appropriate.

- General comment on model performance and limitations:
It is considered that the model results are broadly conservative and reflect the expected cohesive sediment behavior and associated accretion around the Project site and more widely in the approach channel. Nevertheless, the mud transport result presented in this study must only be used as a guide to likely sedimentation rates and if used to assess dredging requirements must also include some element of uncertainty to mitigate risks.

3. APPENDIX

Appendix-1_FEED_Phase-Sediment_transport_P6

1863

MOTT MACDONALD

JGC

Pakistan FSRU FEED Phase

Sediment Transport

11 September 2019
Confidential

Mott MacDonald
Mott MacDonald House
8-10 Sydenham Road
Croydon CR0 2EE
United Kingdom

T +44 (0)20 8774 2000
F +44 (0)20 8681 5706
mottmac.com

JGC Corporation

Pakistan FSRU FEED Phase

Sediment Transport

11 September 2019
Confidential

Issue and Revision Record

Revision	Date	Originator	Checker	Approver	Description
P1	27/03/19	S Costa	DM Price	JJ Williams	Draft for comments
P2	13/05/19	S Costa	DM Price	JJ Williams	Comments addressed
P3	04/07/19	S Costa	DM Price	S Barker	MT chapter completed – Draft for comments
P4	25/07/19	S Costa	DM Price	JJ Williams	Final – Comments addressed
P5	01/08/19	S Costa	DM Price	JJ Williams	Final – Additional Comments addressed
P6	10/09/19	S Costa	DM Price	JJ Williams	Final – Additional Comments addressed

Document reference: 396490 | 004 | P6

Information class: Standard

Contents

Tables

Figures

1871

Executive summary

JGC corporation (JGC) is undertaking Basic Design services for the marine facilities associated with the FEED Design services in Chann Waddo Creek, near Port Qasim, Karachi, Pakistan, hereafter termed "the Project".

Mott MacDonald was commissioned to undertake the sediment transport studies for FEED of the Project. The primary aim of FEED was to quantify sedimentation in the approach and nearshore channels. The offshore region and islands around the nearshore channel are understood to be characterised by fine sand. In contrast, sediments in the approach channel comprise silt and clay. To correctly represent the different dynamical properties of these sediment types, two modelling approaches have been required in FEED:

- Sand transport model (ST) - for the non-cohesive sandy sediment in the nearshore channel; and
- Mud transport model (MT) - for the muddy cohesive sediments in the approach channel.

The models were setup using MIKE modules and calibrated/validated with the existing information. For the MT a data campaign was undertaken in order to obtain suspended sediment concentration at the site, over a tide, during spring and neap tide conditions. the samples were used to support the mud transport calibration. No calibration data existed at this stage for the sand transport model. This was verified by comparing the model results to available anecdotal dredging records.

This report is based on best presently available data and predictions. Climate change within the design life of the project is expected; the consequences of which are unknown. It can, however, be expected that such consequences will have an impact on the conclusions reached herein.

In summary, the sediment transport models indicated that:

- There are important potential net sand transport pathways, both in the nearshore and in the approach channels which can lead to sand deposition. The nearshore sand is generally driven towards the channels and then offshore creating deposition in the nearshore channel and an intertidal sandbank offshore;
- The sand transport modelling results indicate accretion of up to 2m in the entrance to the approach channel, mainly in the areas close to the islands;
- In the area of the turning circle and the berth, no significant accretion of sand is predicted;
- Mud deposition is related to the offshore concentrations and is predicted to increase in the monsoon season. The present simulations assume 4 months of interrupted monsoon conditions. In the worst-case scenario considered, this gives rise to a deposition of around 0.45m/year at the edges of the turning circle; and
- The calculation of mud deposition by the model is highly dependent on the assumed properties of the bed layers, and therefore, results should be treated as being indicative only.

When interpreting the model results it is important to understand the model limitations. Both the sand transport and mud transport models have been built with the limited available information. This has required assumptions to be made. While both models have been calibrated/verified within the constraints imposed by available data, the results presented in this report should be treated as indicating the expected sediment accretion rates and locations rather than absolute figures. It is noted also that sediment transport formulae and models have a significant empirical

foundation and often relate best to the data set upon which they were derived. At best sediment transport can only be predicted to within a factor of two or three (e.g. Schoonees & Theron, 1995; Camenen & Larroudé, 2003; Winter, 2007; Papanicolaou et al., 2008; Amoudry & Souza, 2011) and thus model precision must always be treated with caution and allowances made for inaccuracies.

1875

1 Introduction

1.1 Project Background

JGC corporation (JGC) is undertaking Basic Design services for the marine facilities associated with FEED Design services in Chann Waddo Creek, near Port Qasim, Karachi, Pakistan, hereafter termed the Project.

During Pre-FEED of this work, Mott MacDonald Ltd. (MML) undertook a numerical modelling study of hydrodynamics to support the Project. The study used a range of survey and existing data to build and calibrate a two-dimensional, depth-averaged, MIKE21 flexible mesh (FM) hydrodynamic (HD) model using bathymetry that encompasses the Project site, the complex network of surrounding tidal channels and intertidal mudflats and mangroves and the coastal and offshore areas. The model was driven by a global tidal model at the offshore boundary and was calibrated and validated using measured tidal flows obtained at four locations around the Project site using ADCP instruments.

In addition, an assessment of post-dredging channel hydrodynamics around the Project site was undertaken. The results showed a small reduction of the current speed around the dredging pockets. For additional information please refer to MML (2018) hydrodynamic modelling report (Ref. 396490-002-A).

Pre-FEED also included a spectral wave model to simulate wave conditions outside and within the approach channel and Project site. The model was built using Mike 21 Flexible Mesh (FM) Spectral Wave (SW) and was driven by offshore waves and wind. The model was calibrated, validated and used to obtain extreme waves conditions in the project site. For additional information please refer to MML (2018) wave modelling report (Ref. 39639-003-A).

In this report a distinction is made between: (a) the existing dredged channel extending offshore from Bundal Islands that forms part of the access to Qasim Port, hereafter termed "the nearshore channel"; and (b) the channel that connects the nearshore channel and the Project site, hereafter termed "the approach channel". These channels are shown in Figure 1.

With reference to the models and data from Pre-FEED, the primary aim of FEED is to quantify sedimentation in the approach and nearshore channels. The offshore region and islands around the nearshore channel are understood to be characterised by fine sand. In contrast, sediments in the approach comprise silt and clay. These different sediment types are thought to merge gradually in the area adjacent to Muchak Island (Figure 1). To correctly represent the different dynamical properties of these sediment types, two modelling approaches have been required in FEED:

- Sand transport model (ST) – for the non-cohesive sandy sediment in the nearshore channel; and
- Mud transport model (MT) – for the muddy cohesive sediments in the approach channel.

1.2 Report Structure

The report comprises:

- Chapter 2 – Sand transport modelling;
- Chapter 3 – Mud transport modelling; and
- Chapter 4 – Conclusion and recommendations.

2 Sand Transport Modelling

2.1 Introduction

A MIKE 21 Flexible Mesh sand transport model (MIKE21 FMST) for the Pakistan FSRU Pre-FEED was setup to determine the sand transport regime and accretion rates in the dredged approach channel to the Project following development of the berth facilities. The MIKE21 FMST model is driven by two dynamically linked modules: (a) the Hydrodynamic (HD) Module and; (b) the Spectral Wave (SW) Module previously presented in the Mott MacDonald (2018) hydrodynamic and wave modelling reports (396490-002-A and 39639-003-A, respectively).

2.1.1 Study area

The main features of the study area comprising the nearshore and approach channels, principal islands and the Project site are shown in Figure 1.

Figure 1: Study area

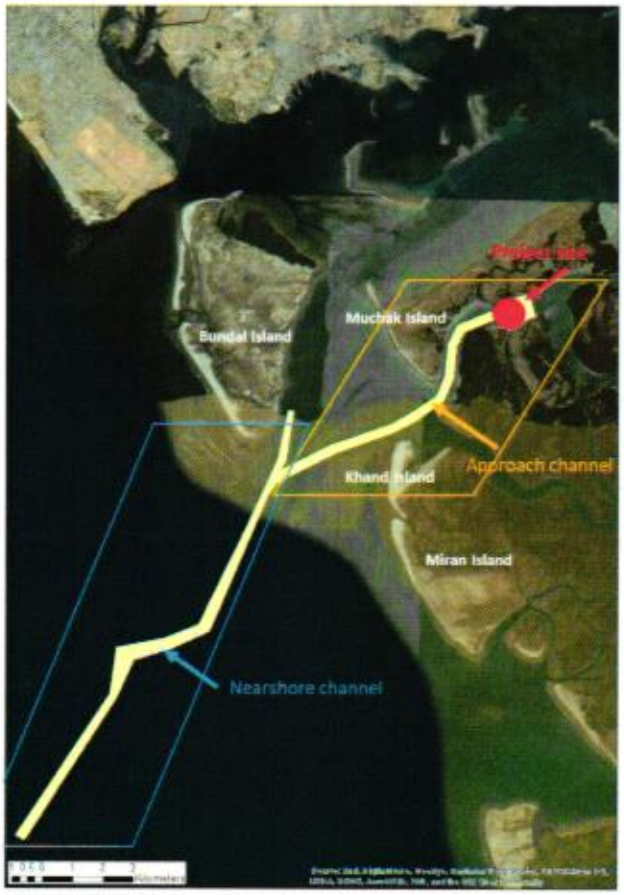

Source: Mott MacDonald, 2019

2.2 Background

2.2.1 Littoral drift

On the coast of Pakistan, littoral drift is driven predominately by wave action during the southwest monsoon. In waters west of Karachi Port, littoral drift is predominantly in an easterly direction. However, littoral drift between Karachi to Phitti Creeks is complicated by the local topography. The Hydraulic Research Station Report EX557 (1971) indicates a littoral drift division on Bundal Island with roughly equal proportions of sediment being transported north and south from a location around the middle of the island. This is supported by evidence of coastal retreat of this and other islands in the delta region. At most locations south of Bundal Island, littoral drift is variable in direction and determined by seasonal and other meteorologically-driven changes in wave direction. The net effect of littoral transport is the deposition of littoral sediments into the Project approach channel (see Section 2.2.2).

2.2.2 Dredging records

Anecdotal historical evidence gathered by JGC and made available to Mott McDonald on 18 February 2019, details dredging requirements for the nearshore channel to the Project site (Figure 2). These data show that:

- Between navigation buoy 1 and buoy 9, dredging in the range 2.5 to 3.0 million m^3 is required every year after the monsoon;
- Between navigation buoy 12 and buoy 14, dredging in the range 1.5 to 2.0 million m^3 is required annually; and
- At other location within the confines of the nearshore channel, dredging in the range 0.5 to 1.0 million m^3 is required at other (variable) locations every two years. There is no information available for the project site.

Estimates of dredge volume requirements in Phitti Creek of around 1.7 Million m^3 per annum for the period 1973 to 1974 were reported by Hydraulics Research (Hydraulics Research Report Ex698). These figures were derived from trial dredging and scaled-up to reflect the dredging requirements for the 8km length of Phitti Creek. These earlier estimations of dredging requirements therefore agree broadly with the values reported above.

In addition, according to the feasibility study undertaken in 2002 from the deepening and widening of Port Qasim navigation channel (Hennessy *el al*, 2002), the nearshore channel is infilling approximately 1.5m during the annual SW monsoon season. An average of 2.5 million cubic metres of material are removed from the whole channel, up to Port Qasim, each year, with almost 90% of this dredged from the nearshore channel. Most of the removed material is fine sand, according to the report.

While these dredging records are broadly informative, their accuracy cannot be established. Further, the bulk density of the dredged material and the proposition of cohesive and non-cohesive sediments is unknown making interpretation of these data problematic. For these reasons we do not consider that the dredging records provide sufficiently robust evidence for model calibration and/or validation purposes. Nevertheless, these data provide evidence of sedimentation in the shipping channels around the Karachi area and indicate that the monsoon period probably gives rise to more sedimentation that at other times of the year. It is not unreasonable to anticipate that sedimentation will occur in the approach channel to the project site, and at the project site itself. The sand and mud transport modelling studies presented here aim to provide the best possible estimates of sedimentation using the available information.

Figure 2: Anecdotal dredging information for the Project nearshore channel

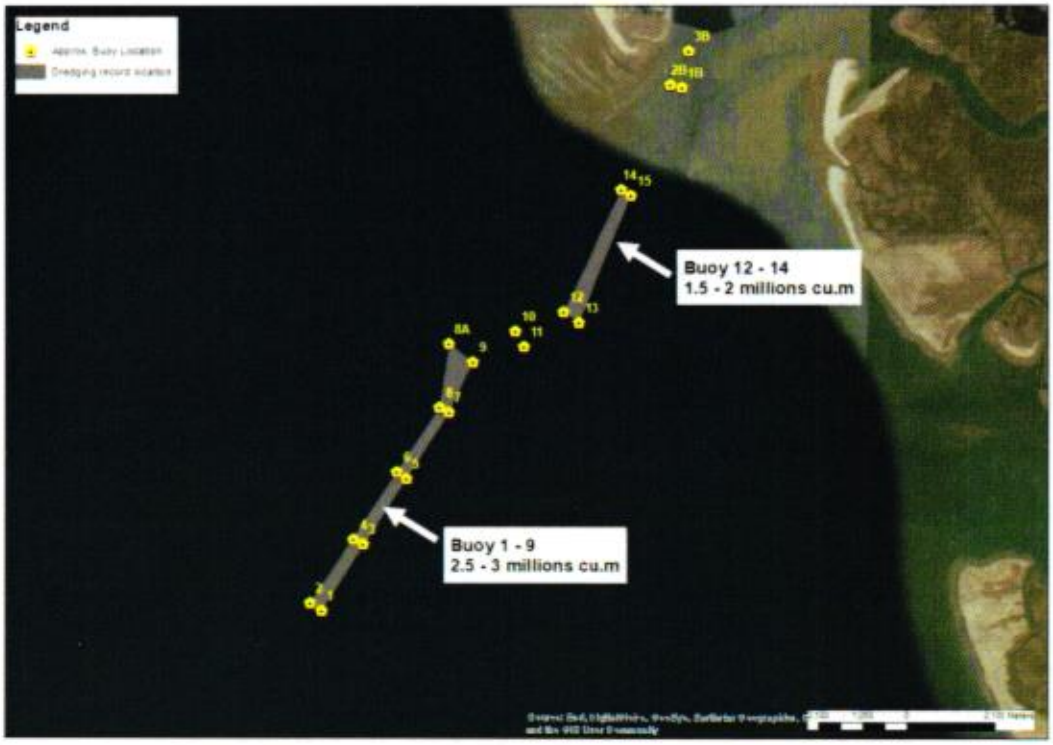

Source: Anecdotal Dredging information provided by JGC, 18 February 2019

2.3 Approach

A schematic diagram of the ST modelling approach is shown in Figure 3. Dynamic links with the hydrodynamic and spectral wave modules provides MIKE21 FMST with the required input data on tidal and wind-driven current speeds, water depths and wave stirring effects. The method is founded on the morphological waves and tide approach described in Section 2.6. The Pre-FEED HD and SW calibrated models were used to setup the coupled model, including sand transport (ST). The coupled model was run with waves and water levels only, to allow the model to warm-up prior to the sediment transport module being started.

Figure 3: Modelling approach

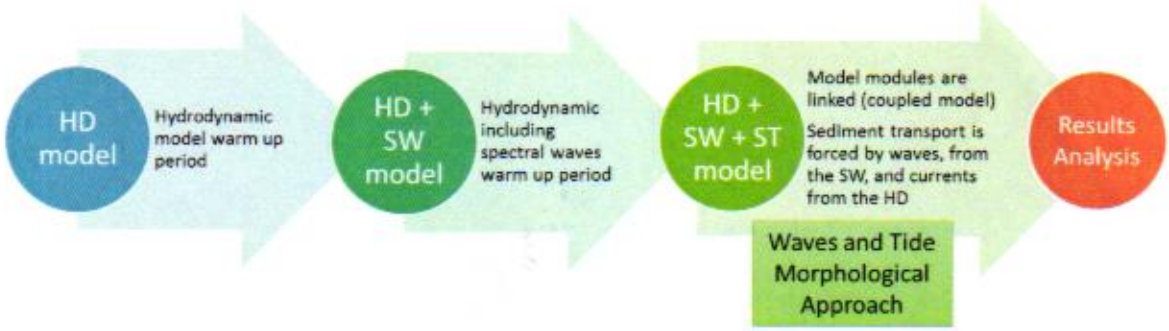

Source: Mott MacDonald, 2019

2.4 Model domain and mesh

The model domain and mesh reported in Mott MacDonald, 2018. Pakistan FSRU - Hydrodynamic Modelling Study (396490-002-A) were largely unaltered for the MIKE 21 FMST model. The domain extended approximately 150km offshore with an approximate width of 100km (Figure 4) and, following normal modelling practice, the resolution of the model mesh was defined as being coarser in the offshore region where mesh element edge lengths were approximately 2000m. The mesh resolution progressively increased shoreward to reach around 15m to 20m, measured between element centres, in the nearshore areas and at the Project site.

Figure 4: Model domain and flexible mesh for the Mike 21 FMST model

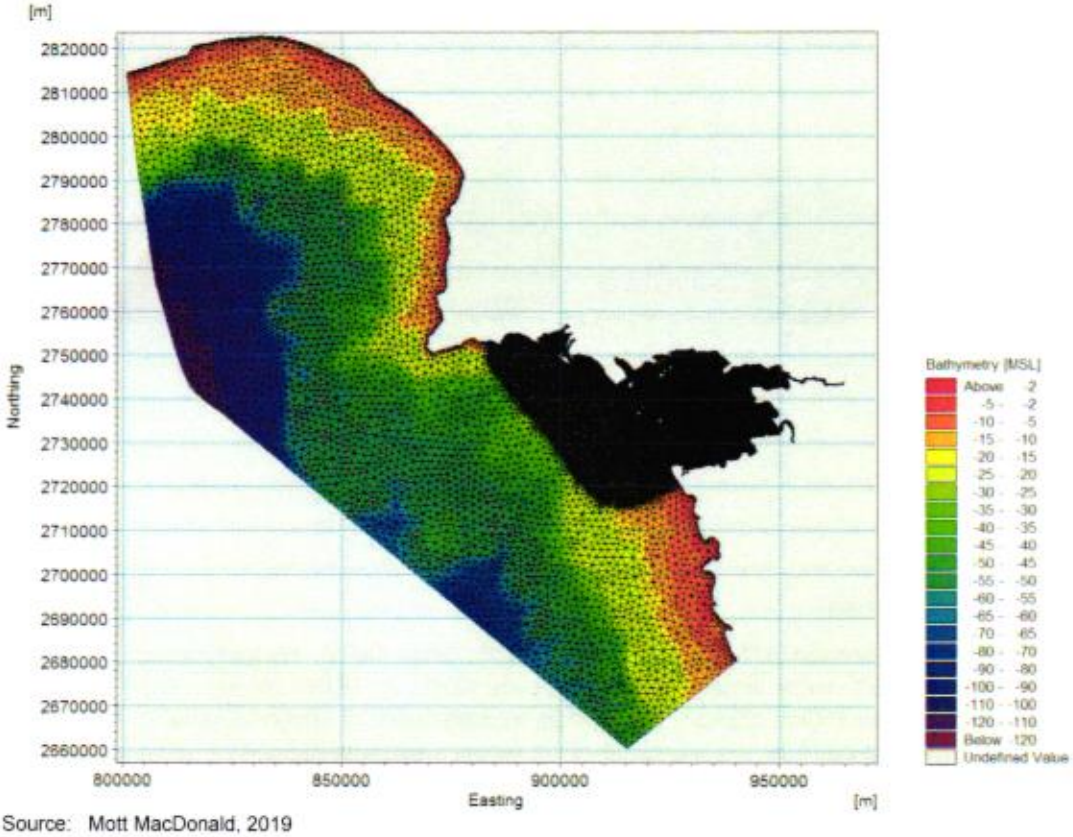

Source: Mott MacDonald, 2019

Some small modifications to the Pre-FEED MIKE21 model bathymetry mesh were made:

- To accommodate some minor updates in bathymetric survey data, the MIKE21 FMST mesh and bathymetry were slightly modified from those described and used during the HD model setup and calibration presented in Mott MacDonald, 2018. Pakistan FSRU - Hydrodynamic Modelling Study (396490-002-A); and
- To resolve in greater detail the wave-driven currents likely to play a role in the transport of sediments into the dredged approach channel, the MIKE 21 FMST mesh resolution in the nearshore and around the islands was increased up to 15m to 20m, measured between element centres (Figure 5). This resolution is normally considered to be sufficient to resolve surf zone processes.

It is also noted that the study area is characterised by broad and shallow intertidal areas (Figure 5). The initial model results showed that waves break at the seaward edge of the intertidal flats and in doing so, they lose a significant portion of their energy. Waves propagating shoreward from this break point are much smaller and continue to dissipate energy due to bed friction as they propagate further inshore. These model results are in agreement with the Hennessy *el al* (2002) report. Therefore, the nearshore model mesh, comprising at least 8 elements, provides sufficient resolution to capture wave processes in the nearshore breaking zone (including wave-driven currents) with sufficient resolution to meet the requirements of the present study. This view is supported by evidence showing that nearshore wave-driven currents make only a small contribution to the total sediment transport in the main channel.

Figure 5: Increased mesh resolution around the nearshore islands

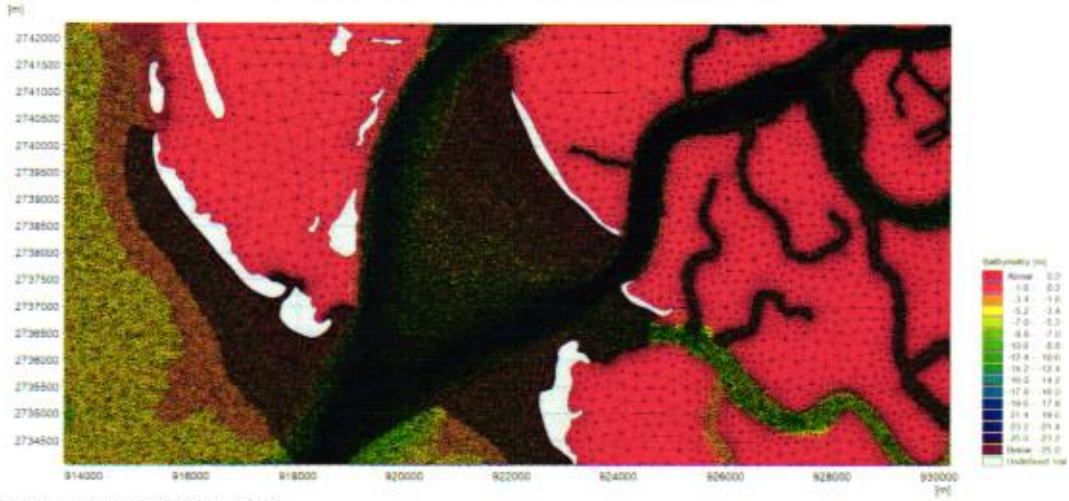

Source: Mott MacDonald, 2019

Following previous work, the model was set up in geographical latitude and longitude coordinates based on the WGS84 horizontal datum. The vertical datum for the model bathymetry and boundary conditions is referenced to Mean Sea Level (MSL).

The model bathymetry in the MIKE 21 FMST model included the dredging of the approach channel, turning circle and the berth basin defined in the Pre-FEED study. Figure 6 shows the dredging requirements in order to obtain the necessary minimum depth of -15.94mMSL (which is -14m CD) with a side slope of 1:5. This demonstrates that the changes to bathymetry required for the Project are relatively minor when considered in the wider context of the entire approach channel.

Figure 6: Bathymetry difference showing the zones of dredging

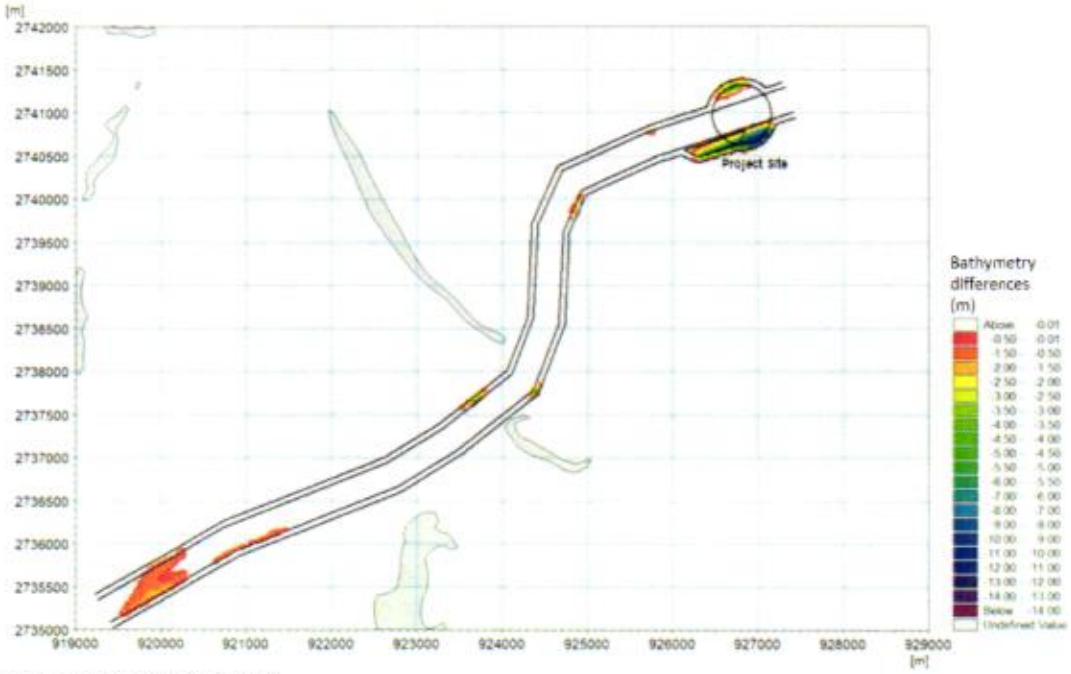

Source: Mott MacDonald, 2019

The nearshore approach channel (see Figure 7) is also included in the model bathymetry with a depth of -17.24mMSL. Some adjustments to model bathymetry were required in order to merge smoothly the approach channel with the nearshore channel and the bathymetry was modified to comply with the minimum depth requirements, (Figure 7).

Figure 7: Changes to the MIKE 21 FMST bathymetry to merge the nearshore channel and the approach channel: (a) Nearshore channel location and minimum depth of -15.3mCD (-17.24m MSL); (b) original bathymetry of Pre-FEED model; and (c) modified bathymetry to merge both channels.

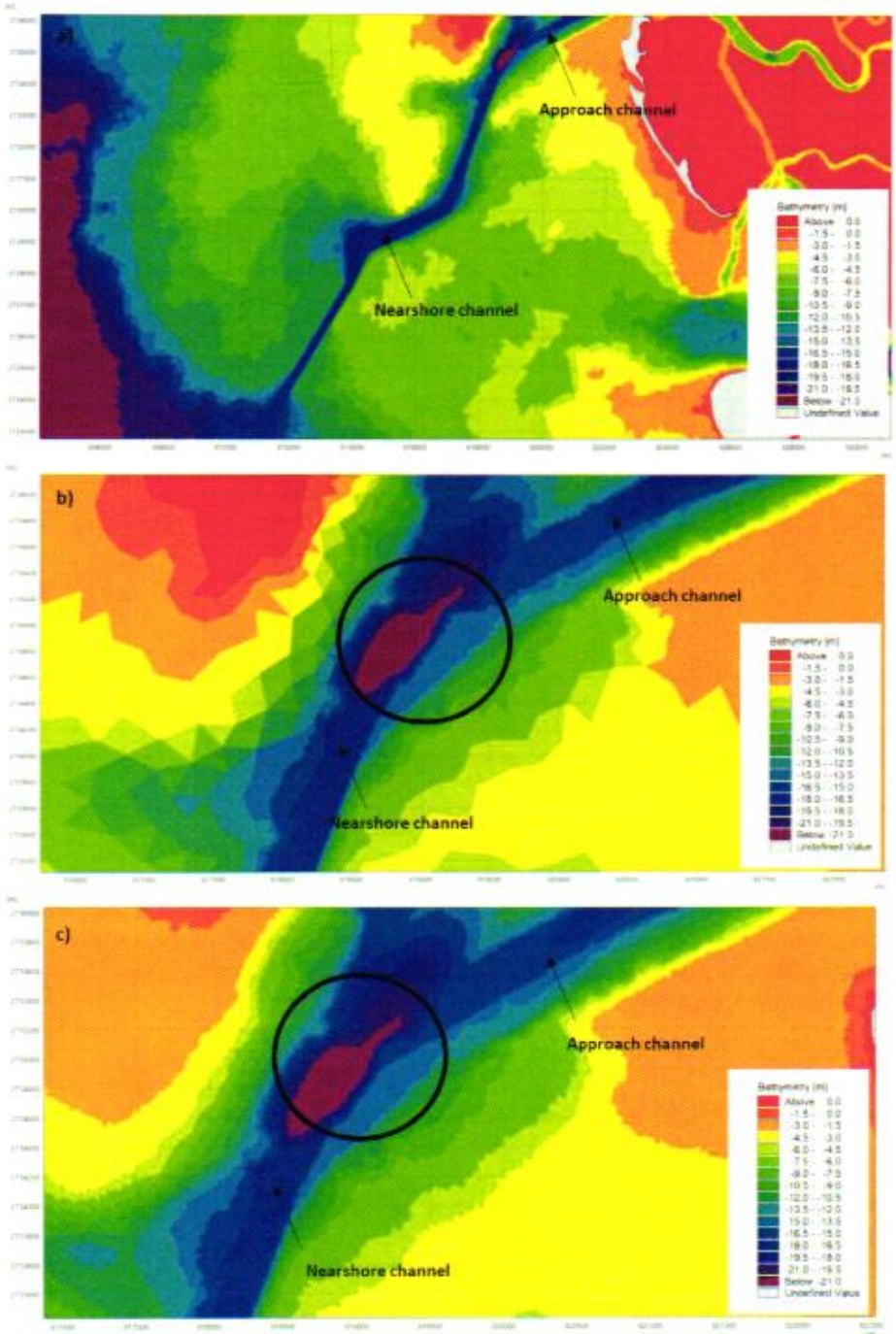

Source: Mott MacDonald, 2019

The bathymetry of the nearshore islands was also modified. In the absence of measured bathymetric or topographic data for these areas, the equilibrium beach profile to the depth of closure (Bruun rule) was used to modify the model bathymetry. The Bruun rule defines an equilibrium beach profile using

$$h(y) = Ax^{2/3}$$

where h is the water depth at a seaward distance, y, and A is a scale parameter which depends primarily on sediment characteristics (Dean, 1991). A sediment with a d_{50} of 0.17mm was used as described in more detail in the sand transport assumptions of Section 2.9. The Bruun rule was used to define the beach profile in front of the island and was adjusted in order to merge it with the available data further offshore. Figure 8 shows the interpreted bathymetry around the nearshore islands. Qualitatively, this agrees broadly with available aerial images of the site. In the absence of any suitable data this approach was considered to be appropriate.

Figure 8: Nearshore island bathymetry (m MSL). The equilibrium profile rule was used as a guidance to create the bed levels in these areas.

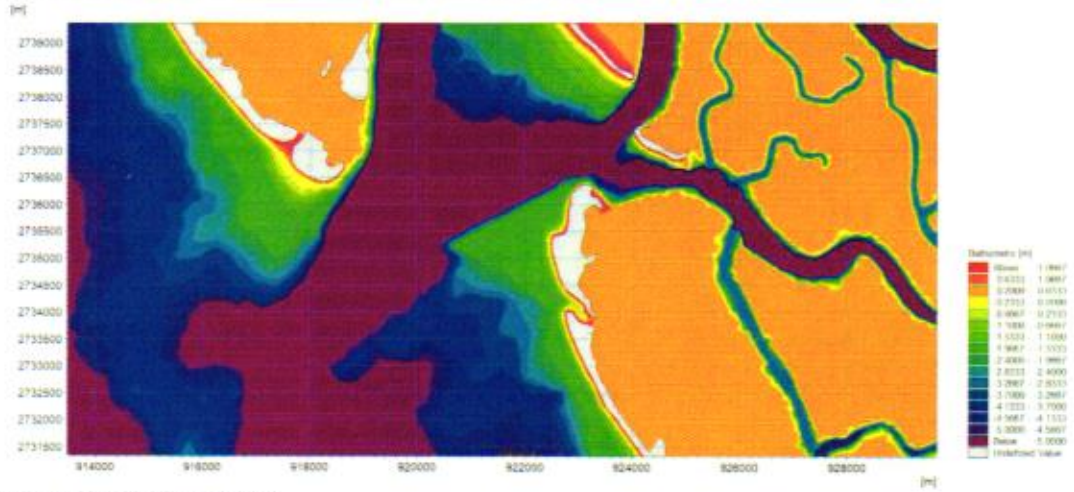

Source: Mott MacDonald, 2019

No other changes to the model bathymetry were made. For information regarding the rest of the dataset used to build the model bathymetry please refer to Mott MacDonald, 2018. Pakistan FSRU - Hydrodynamic Modelling Study (396490-002-A).

2.5 Boundary conditions

MIKE21 provides tidal data from a fully-validated Global Tidal Model with a grid resolution of 0.125 degrees. These data were used to define the water level boundary conditions for the hydrodynamic model, as described in Mott MacDonald, 2018. Pakistan FSRU - Hydrodynamic Modelling Study (396490-002-A). The MIKE 21 HD model has one continuous open offshore boundary located at water depth greater than 120m (MSL), Figure 9. Time-varying water levels along this model boundary are predicted using tidal constituents and include spatial variation along the boundary to capture the variable tidal range and associated phase differences.

The SW model is driven by waves and wind conditions along the same boundary, as described in Section 2.8 of this report. It is assumed that waves conditions are spatially invariant at this deep-water offshore location.

Figure 9: Location of model boundaries in the MIKE21 HD model

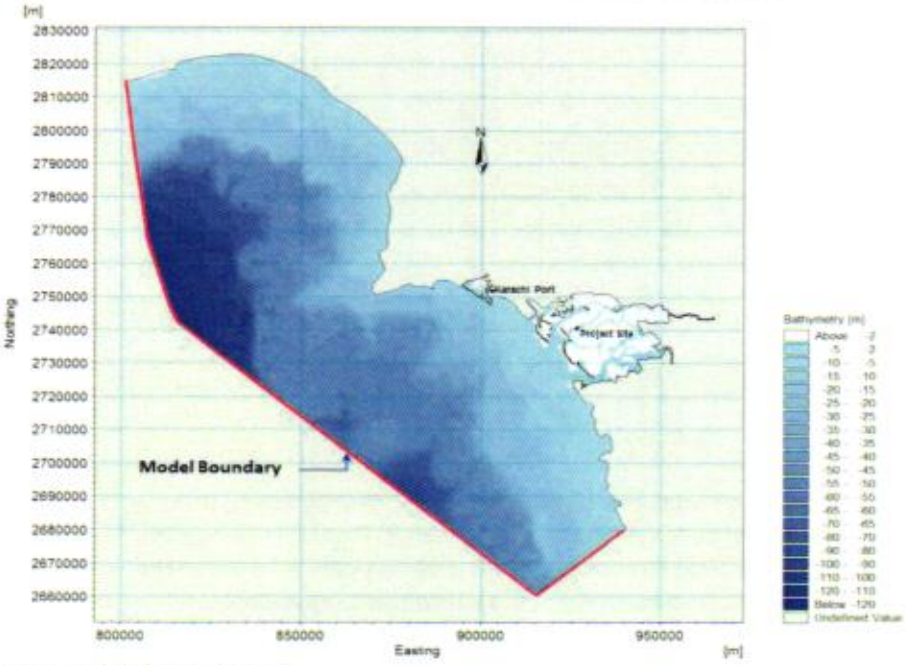

Source: Mott MacDonald, 2019

2.6 Morphological conditions

Coastal models are generally complex and computationally intensive. In order to maintain a balance between data availability, model complexity and computational effort, a schematisation of model inputs is often used. Since the primary aims of the Pakistan FSRU FEED Phase model is to better understand sediment mobility and how this may impact on channel sedimentation, the schematisation of hydrodynamic and waves conditions was used to represent an annual wave-current climate driving sand transport. This approach has used the *morphological tide* and *morphological wave* concepts.

2.6.1 Morphological tides

A morphological tide is defined here as the tide that when repeated will produce the same sediment transport as a Spring-Neap tidal cycle. To determine the morphological tide, a sediment transport model for a point (MIKE Litdrift module) was run for a full spring-neap tidal cycle and the total sediment transport rates determined at several locations. The sediment transport rates for each tide (high water to high water) during the full spring-neap tidal cycle was then calculated and factored up to simulate the whole period of the spring-neap cycle.

The results indicate that the tide on 10/06/2016 21:45 to 11/06/2016 22:25 (Figure 10) produced the closest total sediment transport when factored to account for the whole period of the spring-neap cycle.

Figure 10: First morphological tide approximation

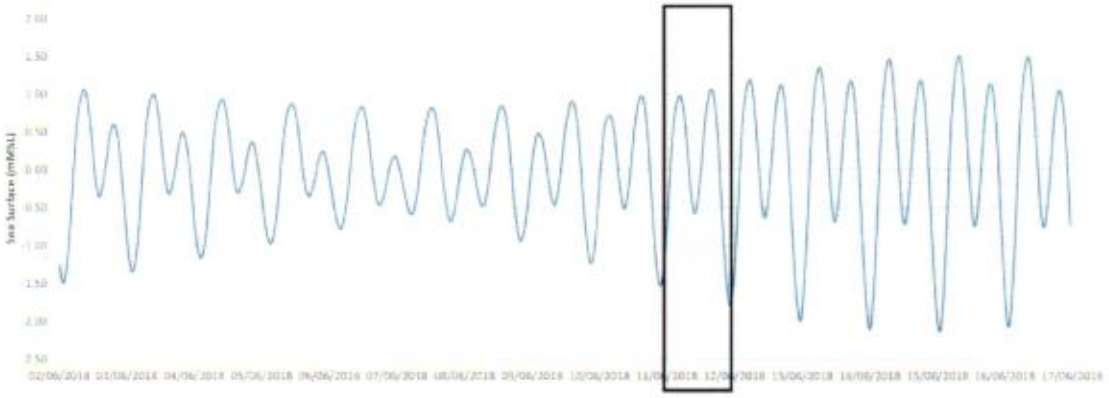

Source: Mott MacDonald, 2019

However, in order to ensure that the transport was not underestimated, and that all intertidal areas were flooded by the tide, a tide with a slightly larger range was selected. Figure 11 shows the selected final morphological diurnal tide of 25hrs, from 13/06/2016 6:00 to 14/06/2016 7:00. The figure also shows the total model simulation time assumed in the subsequent simulations.

Figure 12 shows an example of the cumulative transport calculated at a point in the study area. The figure shows the initial selected tide and the final morphological tide. The results indicate that there is very limited transport during Neap tides, while there is significant transport during Spring tides. Looking at these results, it was decided that selecting a larger tidal range to represent the morphological tide would be more conservative and would ensure that the results do not under estimate the potential transport.

Figure 11: Final morphological tide and model simulation time

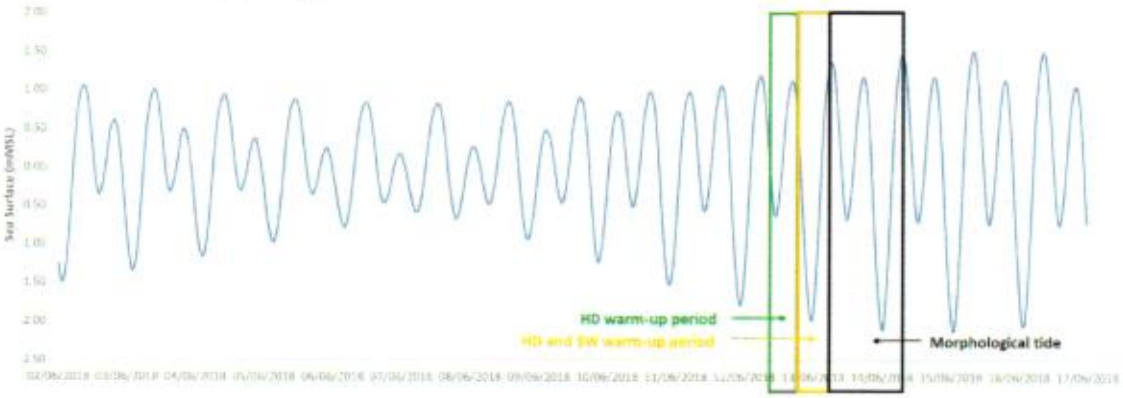

Source: Mott MacDonald, 2019

Figure 12: Cumulative transport for a point for a neap-spring cycle, including water level. Both the initial and the final morphological tides are shown.

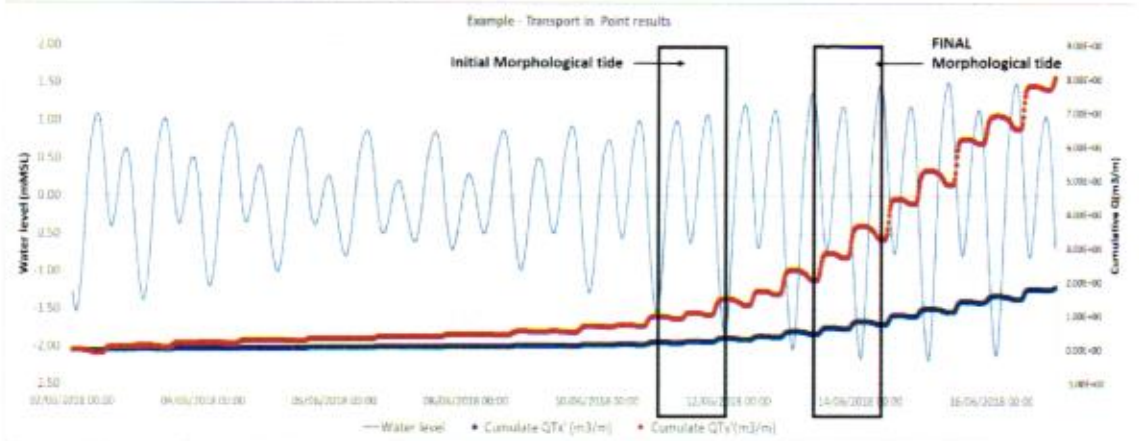

Source: Mott MacDonald, 2019

2.6.2 Morphological waves

To define morphological (or representative) waves, the full wave climate is reduced to a set of representative (morphological) wave-wind conditions. Running model simulations with a number of these representative wave conditions for a morphological tidal period and multiplying wave-current impacts on morphology by a factor related to the frequency of occurrence of a given wave condition, enables estimation of the annual sand transport rates.

Morphological waves were derived by the Energy Flux Method (EFM) described by Benedet *et al.* (2016) where the wave energy flux, *Ef*, of each wave record from a wave time series is calculated using

$$Ef = \left(\rho g \frac{Hs^2}{8}\right) Cg \qquad (1)$$

where ρ is the water density (1025 kg/m^3), g is the acceleration due to gravity (9.81 m/s^2), Hs is the significant wave height, and Cg is the deep-water wave group celerity.

In the approach, the wave climate was first split into 5 directional sectors with each sector containing 1/5th of the total wave energy as defined by Eq. 1 (Figure 13). Each sector was then further sub-divided by wave height before determining the frequency of occurrence of wave conditions within each direction and wave height class. The morphological wave energy, direction, period and height were then obtained for each wave class calculated according to the mean wave energy flux of each wave class.

Wave height is calculated from the mean wave energy of each class, deriving it from the above formula (1). Wave direction and peak period corresponds to the mean value of each class.

Figure 13: Definition of directional bins by the Energy Flux Method (EFM) with each wave direction class containing 1/5 of the total wave energy (upper two panels). Sub-division of each direction class into 20-height classes, each containing 1/20th of the total wave energy, is shown in the bottom panel. Note that this is an example only and does not represent the conditions at the project site.

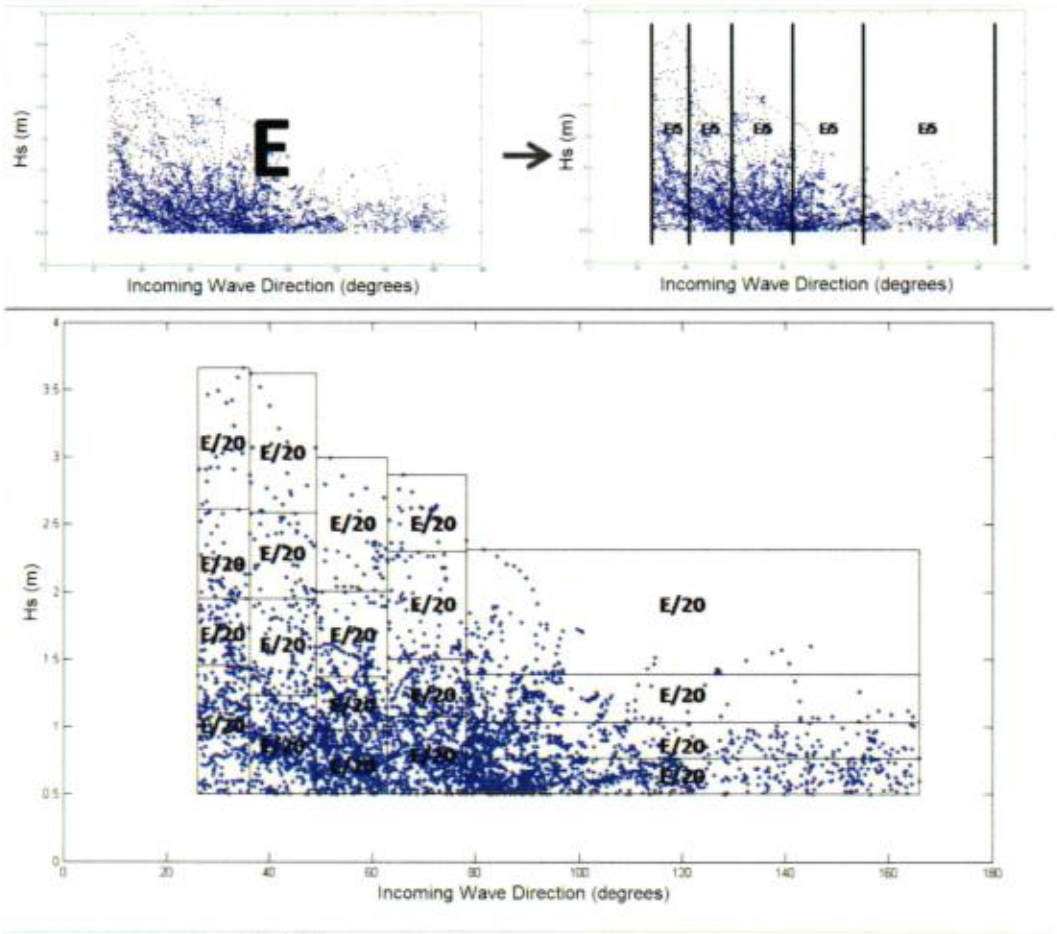

Source: After Benedet *et al.*, 2016

For the Pakistan FSRU FEED MIKE21 FMST model, the EFM was applied to the *Oceanweather* data point (Figure 14). This included simulated wave data from 1979 to 2016 at intervals of 1 hour. Figure 15 shows a wave rose derived from this offshore wave data.

Figure 14: *Oceanweather* data point selected for the morphological wave analysis

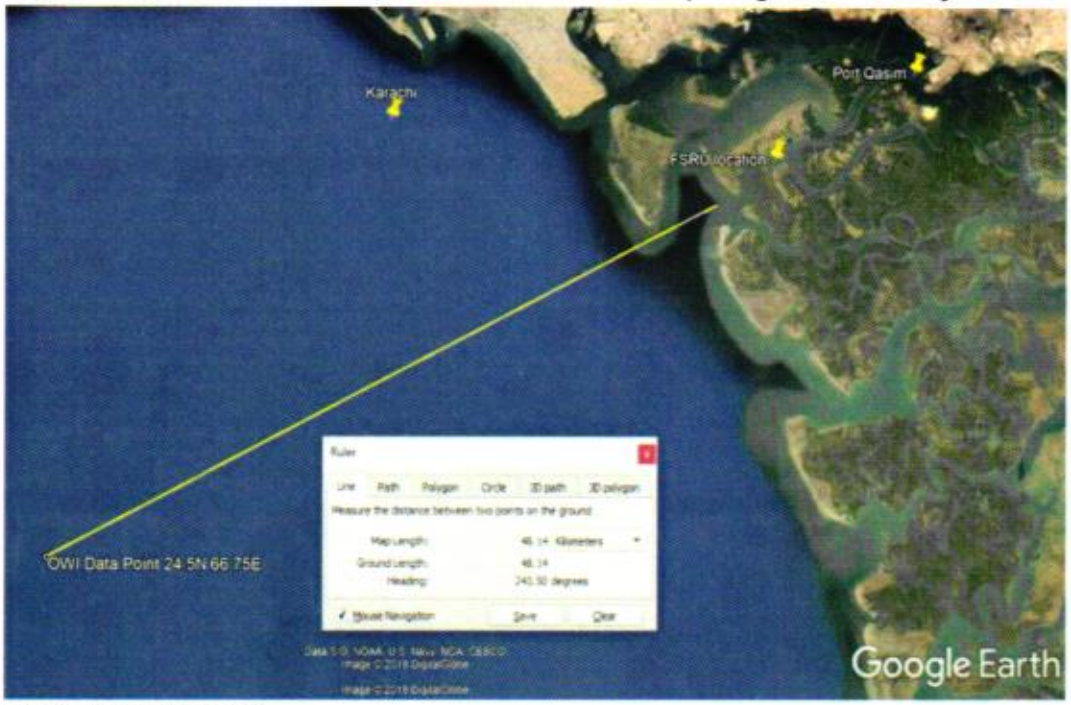

Source: Google Earth, 2019

Figure 15: *Oceanweather* data wave rose

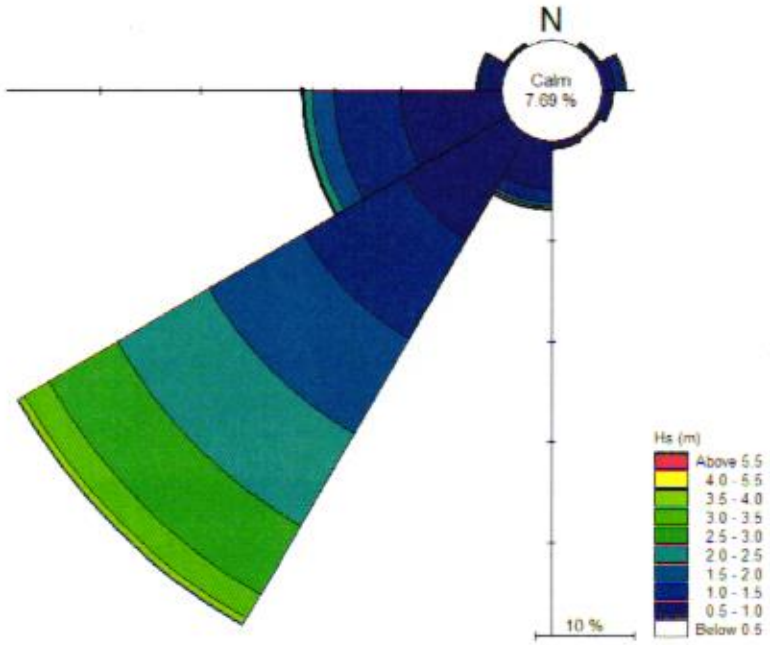

Source: Mott MacDonald, 2019. Contains *Oceanweather* data, 2018

The *Oceanweather* data is plotted in Figure 16 showing: (a) wave height vs. wave direction; and (b) wave energy vs. wave direction. Please note that the direction of the waves is defined as the direction that waves are travelling from. Both figures show that there is a clear dominant wave direction, with larger waves coming from the 210 deg N to 240 deg N sector. Figure 15 shows that waves from the southwest (225 deg. N) dominate the records in terms of height and energy.

Figure 16: *Oceanweather* data distribution against wave direction: (a) wave height (Hs) against wave direction, (b) energy flux against direction.

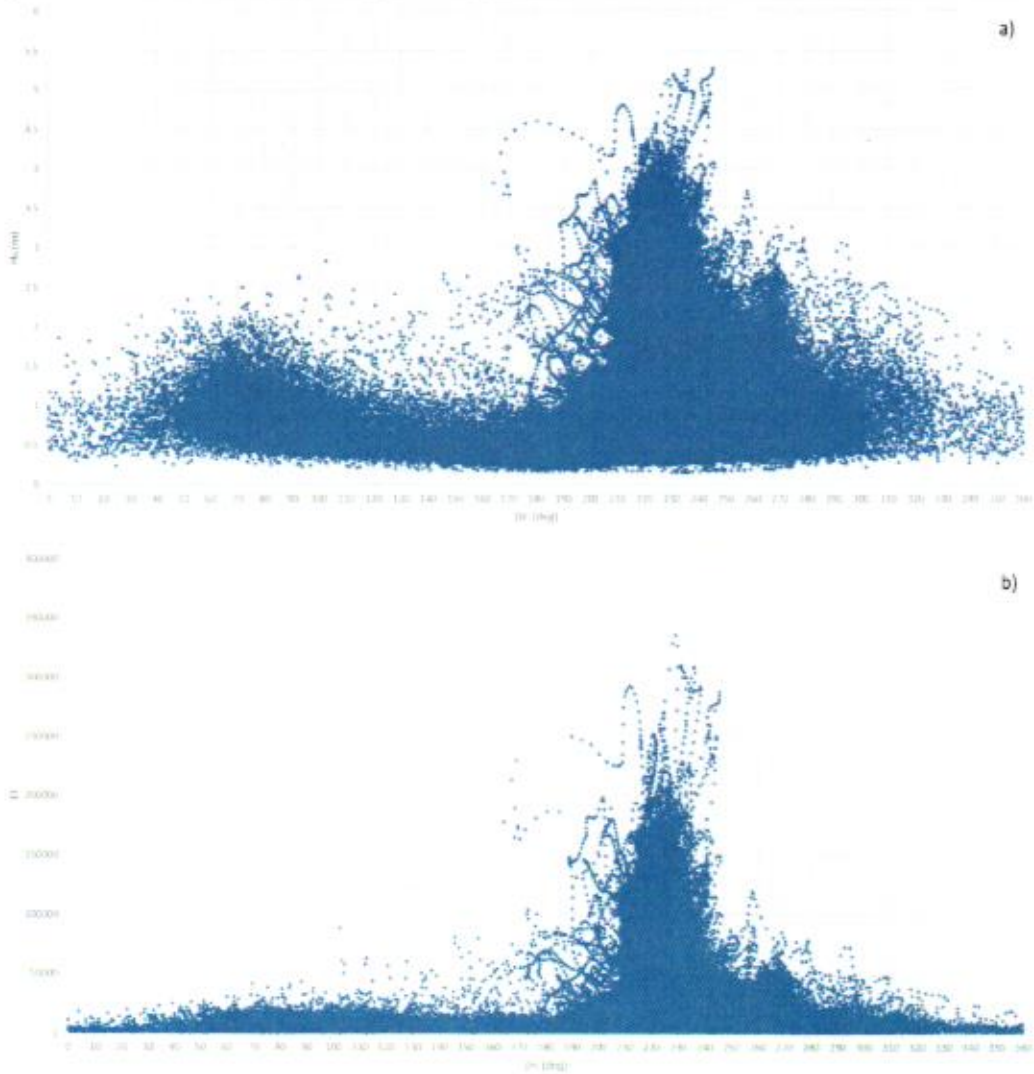

Source: Mott MacDonald, 2019. Contains *Oceanweather* data, 2018

The results of the waves schematisation are shown in Table 1 and Figure 17. Here the wave climate has been discretised into 11 wave conditions and 1 calm condition. The waves have been further discretised into six main directions based on the energy distribution shown in Figure 16b and include:

- 150 to 180 deg. N;

- 180 to 210 deg. N;
- 210 to 240 deg. N;
- 240 to 270 deg. N;
- 270 to 300 deg. N; and
- 300 to 330 deg. N.

All waves coming from 330 to 150 deg. N direction were considered calm conditions. Please note, that the direction of this wave sector indicates that they are travelling away from the site, and therefore, they do not contribute to wave conditions in the study area. In terms of wave height, each of the direction classes have been sub-divided into different sub-classes.

As previously noted in Figure 16, Figure 17 shows that almost 80% of the energy comes from the 210 to 240 deg. N sector (E3). Some significantly smaller energy contribution can be observed in the adjacent sectors, 180 deg. N to 220 deg. N (E2) and 240 deg. N to 270 deg. N (E4). The remaining waves have an almost insignificant contribution to the total energy observed in this offshore point. It is noted also that these smaller waves will also have negligible impacts with regards to sediment mobility and need not be considered further.

Figure 17: Schematisation of *Oceanweather* data point to derive morphological waves using the EFM.

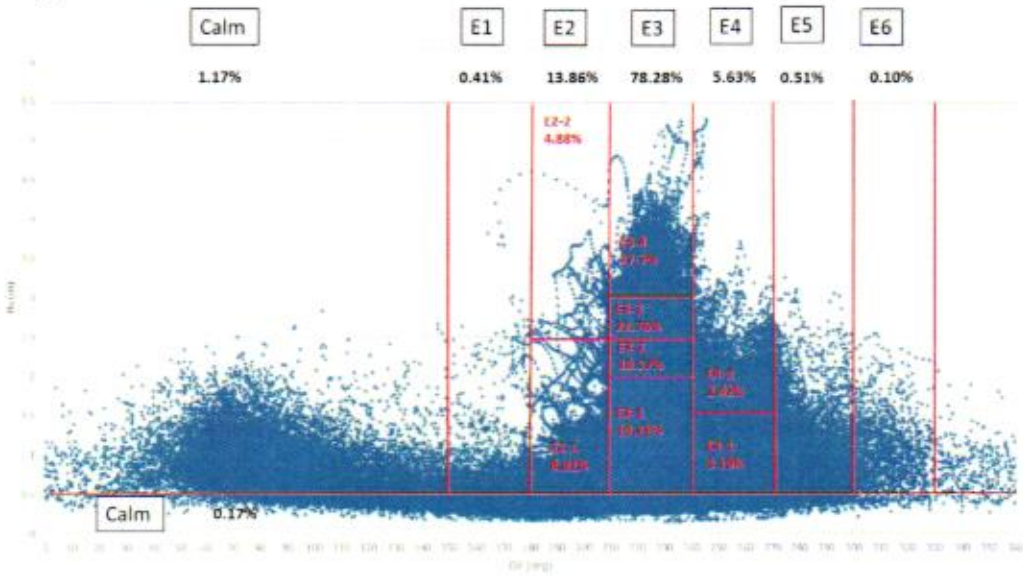

Source: Mott MacDonald, 2019

Table 1 summarises the selected morphological waves, with their corresponding wave direction and peak period. Please note, that in the case of the calm condition, wave height, direction and peak period were selected considering the most relevant processes to the project site. While a large amount of the waves corresponding to the calm conditions are from the northeast direction (Figure 17), as noted above, these waves would not have any effect on the site and therefore, the calm condition direction was selected to be irrelevant to the study.

Table 1: Morphological waves calculated with the EFM at the *Oceanweather* data point

Morphological wave scenario	Hs (m)	Direction (deg. N)	Tp (s)	% of the total energy
E1-1	0.96	173	11.1	0.4
E2-1	1.31	206	11.2	8.9
E2-2	2.89	209	12.2	4.9
E3-1	1.27	229	8.9	19.2
E3-2	2.25	224	10.0	18.6
E3-3	2.75	223	11.0	22.8
E3-4	3.41	224	11.4	17.7
E4-1	0.97	257	6.4	3.2
E4-2	1.99	258	6.8	2.4
E5-1	1.14	286	6.0	0.5
E6-1	1.11	316	5.8	0.1
Calm	0.25	225	5.0	1.3

Source: Mott MacDonald, 2019

2.6.3 Morphological waves boundaries conditions

Based on the relationship between wave height and hourly wind speed at the *Oceanweather* point, estimates of the corresponding wind speed and wind direction were derived for each of the morphological wave conditions. It is noted that only the wind-wave component of the wave data was used to define the wind direction.

The relationship between the wind speed and the wave direction was found by fitting a regression curve through the data, although there was a significant amount of scatter. The final regression used correspond to $wind\ speed = 6\sqrt{Hs}$

A similar approach was used to determine a relationship between the wind direction and the wave direction (sea waves only): $wind\ direction = 0.9842 * wave\ direction$

The derived wind speed and direction for each morphological wave condition at the *Oceanweather* data point are summarised in Table 2.

Table 2: Estimated wind speed and direction related to morphological waves conditions

Morphological wave scenario	Wind speed (m/s)	Wind direction (deg. N)
E1-1	5.9	171
E2-1	6.9	203
E2-2	10.2	206
E3-1	6.8	225
E3-2	9.0	220
E3-3	9.9	219
E3-4	11.1	221
E4-1	5.9	253
E4-2	8.5	254
E5-1	6.4	282
E6-1	6.3	311
Calm	No wind	No wind

Source: Mott MacDonald, 2019

It is noted that the morphological conditions (wind and waves) were derived at the *Oceanweather* data point located in the middle of the model domain, approximately 20km from the offshore boundary (Figure 18).

Figure 18: Location of the *Oceanweather* data point with respect of the model boundary

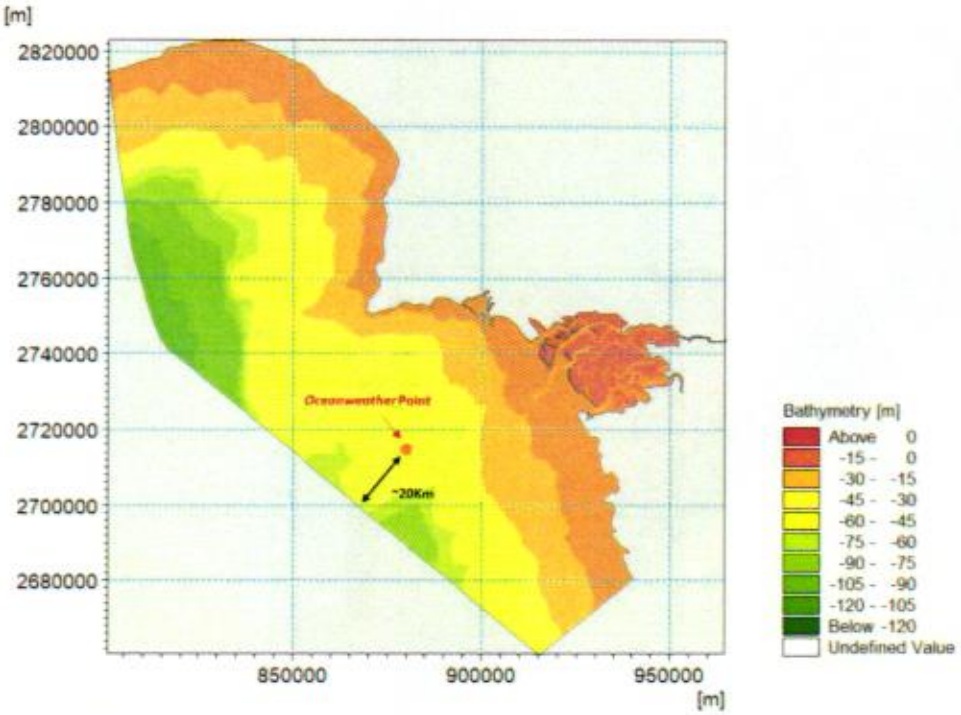

Source: Mott MacDonald, 2019

The morphological waves, applied to the existing model boundaries (Figure 9), would be modified by wind over the longer fetch and therefore, would tend to overestimate wave conditions at the *Oceanweather* data point. To overcome this issue, the wind field was applied in the SW model module only east of the *Oceanweather* data point using wind maps appropriate for each of the simulated morphological conditions. An example wind map is shown in Figure 19. The final morphological wave and wind conditions are shown in Table 3.

Figure 19: Wind map example used in the morphological simulation to ensure that the morphological waves, applied to the model boundary were not being modified by the wind before the *Oceanweather* data point.

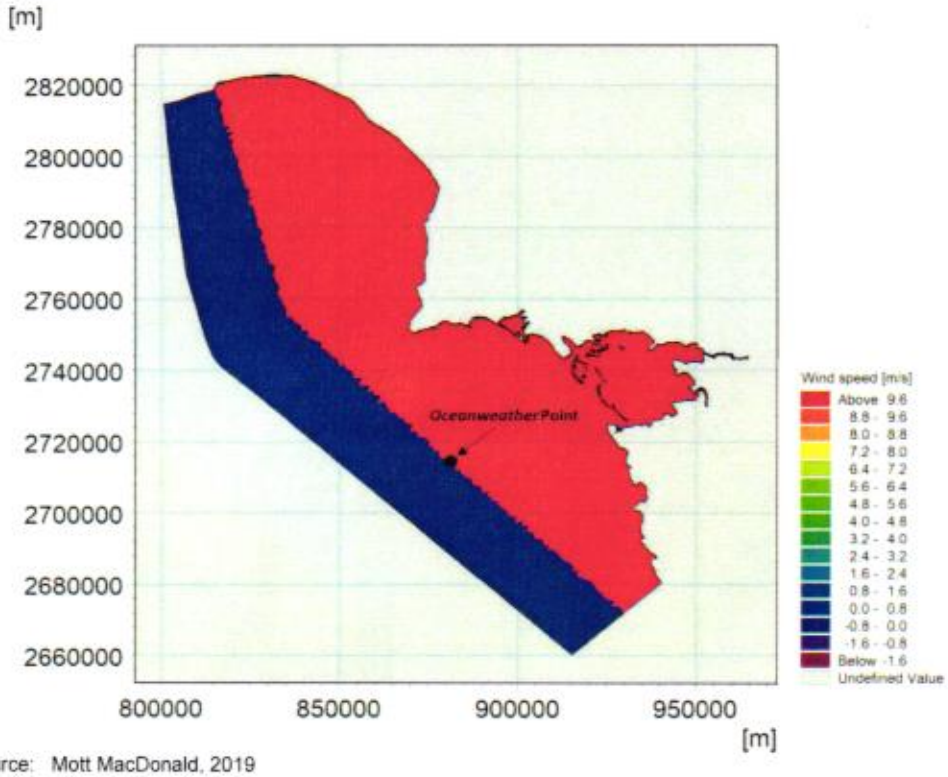

Source: Mott MacDonald, 2019

Table 3: Morphological waves and wind conditions at the *Oceanweather* data point (derived from hourly data)

Morphological wave scenario	Hs (m)	Direction (deg. N)	Tp (s)	Wind speed (m/s)	Wind direction (deg. N)
E1-1	0.96	174	11.1	5.9	171
E2-1	1.31	206	11.2	6.9	203
E2-2	2.89	209	12.2	10.2	206
E3-1	1.27	229	8.9	6.8	225
E3-2	2.25	224	10.0	9.0	220
E3-3	2.75	223	11.0	10.0	219
E3-4	3.41	224	11.4	11.1	221
E4-1	0.97	257	6.4	5.9	253
E4-2	1.99	258	6.8	8.5	254
E5-1	1.14	286	6.0	6.4	282
E6-1	1.11	316	5.8	6.3	311
Calm	0.25	225	5	No wind	No wind

Source: Mott MacDonald, 2019

2.7 Hydrodynamic (HD) module setup

The HD module was setup as described in Mott MacDonald, 2018, (396490-002-A) and the wave radiation stresses (from the Mike 21 SW model) were added. This allowed wave-driven currents to be simulated and enabled a more realistic simulation of processes resulting in an enhancement to mobilisation and transport of sediment.

2.8 Spectral Wave (SW) module setup

The SW model was setup following the SW calibration, undertaken in Mott MacDonald (2018) wave modelling report (39639-003-A). To allow the simulation of morphological conditions the following changes were made:

- The model used the water level from the HD module, but was run without taking into account the tidal current influences;
- Wind was included as a constant value applied only from the locations east of the *Oceanweather* point (Section2.6.3); and
- Morphological waves defined the wave boundary conditions and were applied at the model boundaries.

2.9 Sand transport (ST) module setup

Limited information regarding the sediment properties was available at this stage. The *Factual Geotechnical Investigation Report for Geotechnical Investigation for Pakistan FSRU Project* (STS, 2018) contained information regarding a borehole campaign in the area of interest. The report is reviewed in more details in Chapter 3, but in general indicated that surficial sediment at the Project site and other locations in the area, is dominated by fine sediment, mainly clay and silt. Limited information regarding the sand fraction is available in the *Factual Geotechnical Investigation Report*.

The MIKE21 FMST model was setup with the following conservative assumptions:

- A median grain size (d_{50}) of 0.17mm was selected, with a grading of 1.1 corresponding to fine sand;
- The sand is composed of silica with a density of 2650 Kg/m^3;
- There is no morphological development of the seabed (e.g. erosion/accretion or bedforms) and therefore, no subsequent feedback upon waves, hydrodynamic and sand transport calculations (i.e. a fixed bed model);
- Sand depth (sand bed thickness) is unlimited and is available throughout the whole model domain; and
- The model has zero sediment flux gradient at the boundaries.

The MIKE21 FMST model was forced both by waves, obtained from the SW module, and tides/currents, from the HD module. Sand transport rates were derived using an efficient look-up table pre-generated to define transport rates for any combination of water depth, bed slope, current, wave condition and sediment property properties which are representative of the expected range, and within the model domain.

2.10 Sand transport results

The large-scale and detailed annual net potential sand transport patterns for the study area, obtained with the MIKE21 FMST model, are shown in Figure 20 to Figure 22. Since it is assumed that sand availability is unlimited across the whole model domain, the term "potential" has been

used to indicate this. The annual net potential sand transport has been derived for all the morphological scenarios, then factored together according to their percentage of occurrence (Table 1).

The annual net potential sand transport vectors shown in Figure 20 indicate that as expected the currents in the channels create a net ebb dominant sand transport direction. The nearshore sand transport is generally driven towards the channels and then offshore. The intertidal areas in front of the nearshore islands show that littoral and tidal transport moves sand towards and into the main channels. Additionally, pathways can be seen that help form the sand banks which are evident on the southern ends of Bundal and Muchak Islands, and the northern end of Khand Island (see Figure 1).

The vectors show that sand transport into the dredged nearshore channel is predicted, and therefore deposition would be expected. The patterns would agree with the existing dredging records, were large amount of sediment is extracted from the southern areas of the nearshore channel (Figure 2 and Section 2.2.2).

The high current velocities areas observed in deeper water (refer to the bottom of Figure 20) are simply a reflection of the higher current velocities predicated by the model. The direction of net sand transport is offshore and while the amounts of material being transported is subject to some unavoidable uncertainty associated with the empirical nature of the transport formula, the net direction is well defined in the model and thus provides confidence in the conclusion reaches regarding sand accumulation in the approach channel.

Figure 20: Annual net potential sand transport patterns for the study area

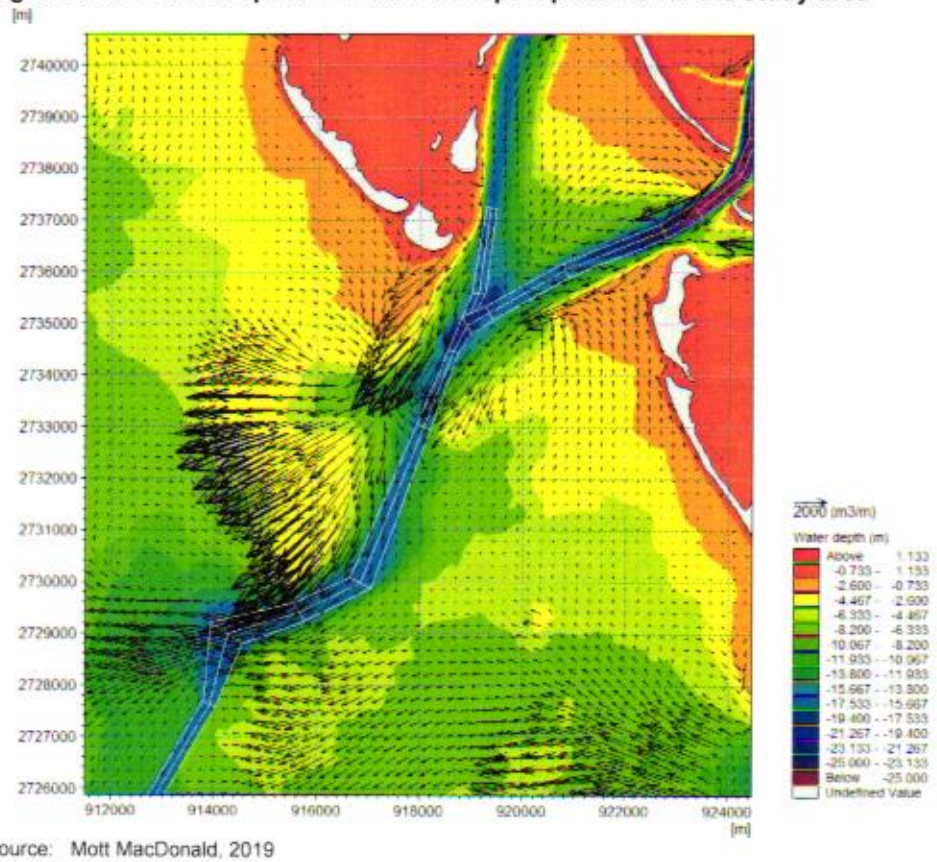

Source: Mott MacDonald, 2019

Figure 21 shows, in more detail, the annual net potential sand transport patterns in the approach channel. While sand transport from the nearshore areas towards the main channel due to tidal and waves forcing is predicted, sand availability will greatly limit local accretion.

Figure 22 shows the predicted annual sand transport patterns in the berths and turning circle. The image indicates that in general the transport is southwards, due to the ebb dominance of the tidal currents and thus if fine sand is available it is unlikely to accrete in these areas.

Figure 21: Annual net potential sand transport patterns for the approach channel

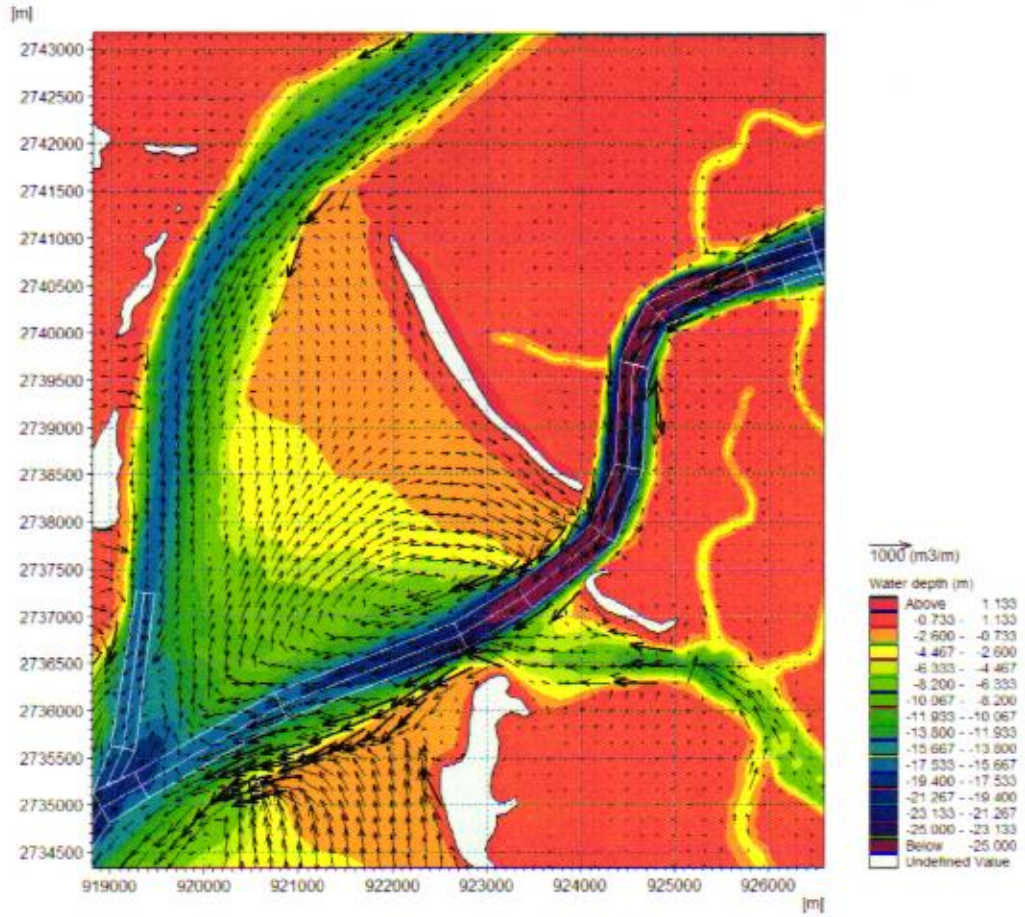

Source: Mott MacDonald, 2019

Figure 22: Annual net potential sand transport patterns for the berths and turning circle area

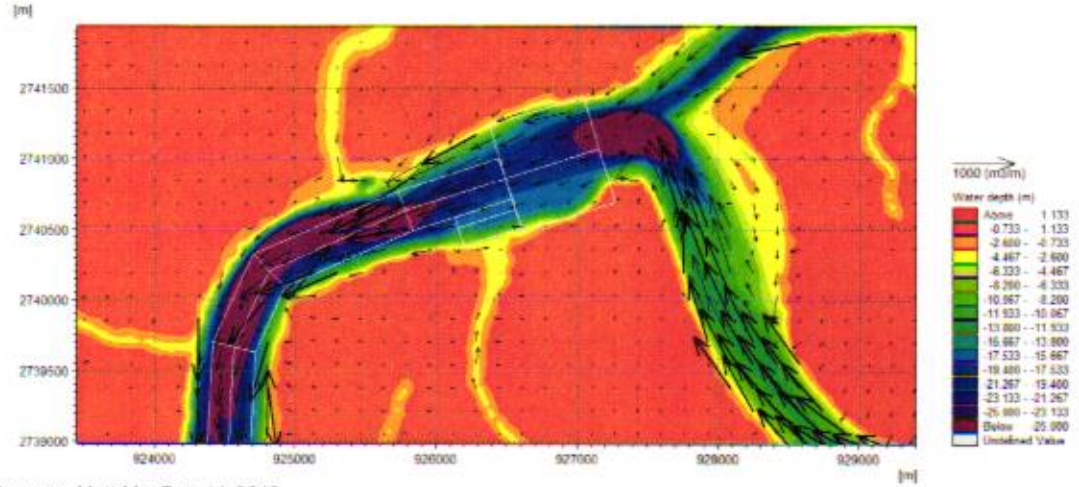

Source: Mott MacDonald, 2019

To understand further the sand transport regime in the study area, the proposed nearshore and approach channels and the berths have been sub-divided into a series of *Analysis Boxes* (Figure 23) both along their length and across their axes. Sand entering and leaving each *Analysis Box* has then been used to calculate the annual sediment budget and the corresponding changes in bed elevation.

Figure 23: Pakistan FSRU sand transport *Analysis Boxes*. (a) analysis boxes in the nearshore and approach channels; (b) detail of boxes in the approach channel.

Source: Mott MacDonald, 2019

The method used to estimate the sediment volume change for each of the *Analysis Boxes* (Figure 24) involves calculation of the sediment flux crossing the sides of each *Analysis Box* to obtain a sand transport budget. Put simply, if more sand enters than leaves each box, accretion will occur and *vice versa*. Assuming a sediment porosity of 0.4, the annual changes in bed level were calculated using the resulting sediment volume change data in each *Analysis Box*.

Figure 24: Schematic representation of how the sediment deposition or erosion is calculated for each *Analysis Box* using the sediment flux across each section and the area of each *Analysis Box*. The sedimentation is estimated for one year with a sediment porosity value of 0.4

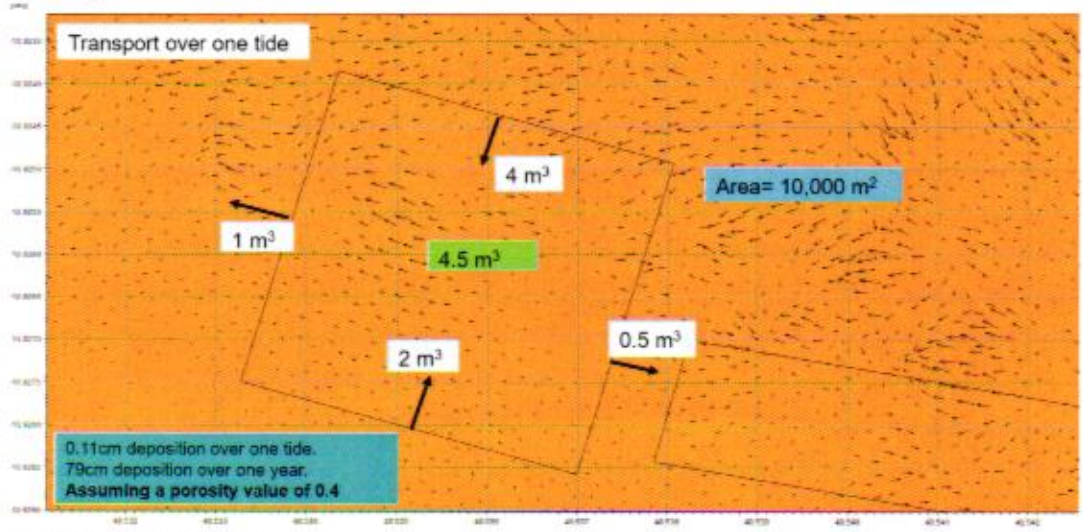

Source: Mott MacDonald, 2019

Sand budgets were obtained for all the *Analysis Boxes* and for all morphological scenarios by considering the net sand fluxes into/out of each box. Average erosion/accretion rates were then derived over the area of a given box. As previously described, the results were then factored together to give an annual erosion/accretion depth using the corresponding occurrence of each scenarios (Table 1).

The results of this box analysis are shown in Figure 25. The figure indicates significant deposition in several areas of the nearshore channel and the proposed approach channel. This deposition ranges from less than 1m to up to 3.5m in one year.

Figure 25: Total annual average bed level change for the entire study area.

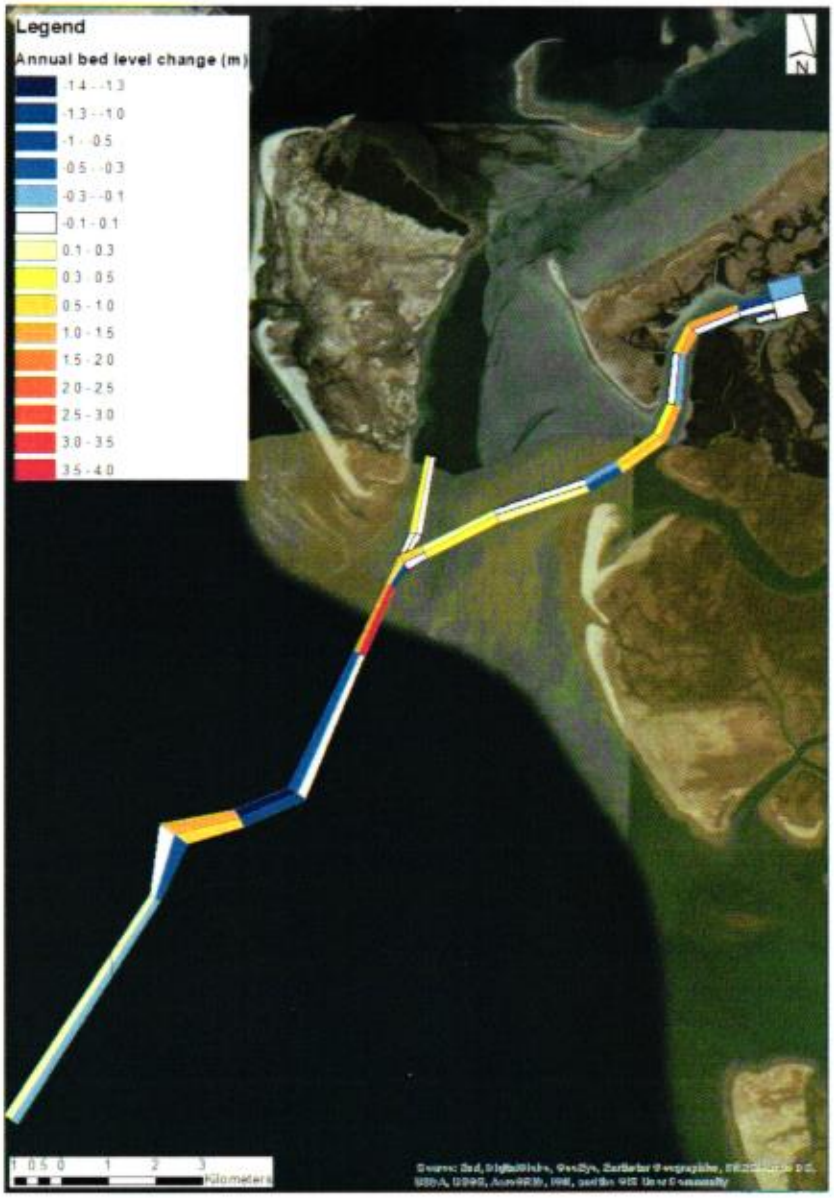

Mott MacDonald, 2019
Note: Positive numbers are showing accretion, while negative numbers are indicating erosion.

2.10.1 Sedimentation in the nearshore channel

When interpreting the sand transport predictions, it should be kept in mind that:

- The model assumes an unlimited sand supply available;
- The morphological (representative) conditions do not account for infrequent extreme events explicitly;
- Fluvial sediment inputs are unknown and assumed to be zero;

- Owing to extensive water extraction for irrigation and dams at many locations along the river course, the delta area around the project site now receives very little sediment from fluvial sources. Consequently, the seaward limit of the delta is now subject to moderate erosion. During the flood tide, modelling shows there is sediment ingress into the tidal channels around the project site. In the case of sand size sediments, the ebb-dominated flows act to flush material imported primarily as bedload during the flood tide seaward again so that there is little or no net deposition. In the case of cohesive material, this remains in suspension and is easily transported into and up the tidal channels where is can deposit in favourable conditions. Depending on the location, the subsequent ebb tide may not have stuffiest velocity to resuspend this material; and
- Account is taken of sand-sized sediments only. In the upper reaches of the approach channel, cohesive sediments dominate.

Noting carefully that the sediment budget calculations take a conservative view and assume an unlimited source of sandy sediments, Figure 26 shows the calculated potential annual bed level change for the nearshore channel. In general, it shows a combination of accretion and erosion areas in the dredged channel, with deposition in the range 3.5m to 4m in some areas (e.g. Box 16-1). The areas with deposition are correlated with the transport patterns previously shown in Figure 25, and are related to sand transport into the channel from shallower areas.

Figure 26: Total annual average bed level change for the nearshore channel.

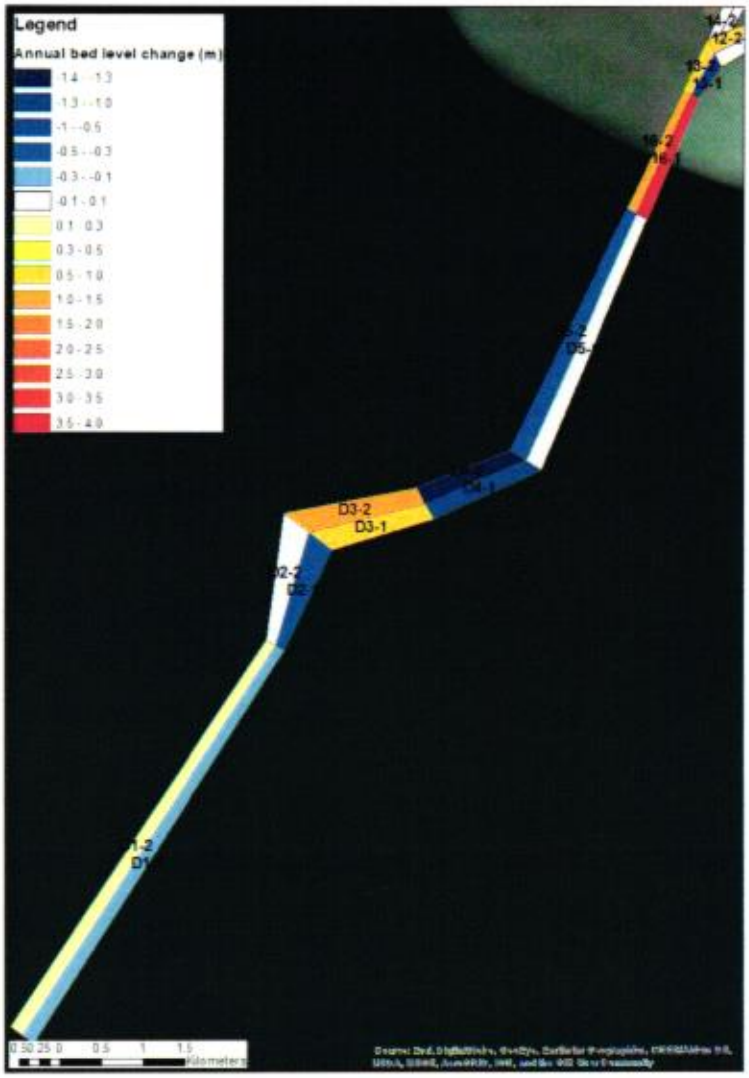

Donald, 2019
Note: Positive numbers are showing accretion, while negative numbers are indicating erosion.

The deposition rates obtained have been compared to the anecdotal evidence of dredging records provided by JGC (2019) and previously described in Section 2.2.2. According to the information presented in Figure 2, the annual nearshore channel dredged volume is between 4 million m^3 and 5 million m^3 per year, after the monsoon season.

The results obtained in this study indicate a sand deposited volume in the nearshore channel of the order of 1.8 million m^3 over the simulated year. This number is about 2.5 times lower than the dredging records. However, it is important to understand that dredge volumes and MIKE 21 FMST model predictions cannot be directly compared since:

- The MIKE 21 FMST model predictions only consider sand and the anecdotal dredging records do not provide any information regarding the characteristics of the dredged material, grain size or water content to discriminate the percentage of sand; and

- It is assumed that the dredge data are yearly records. However, the timeline is not confirmed.

The results obtained in this study are also in agreement with the volumes reported by Hennessy *el al.* (2002) study, which reference dredging volumes of 2.5 million m^3 per year.

While the existing uncertainties prevent direct comparisons between model predictions and dredging data, the agreement is sufficiently close to conclude that model predictions are reasonably reliable if one assumes sediment deposition in the nearshore channel is a combination of sand and mud.

2.10.2 Sedimentation in the approach channel and berths

Smaller sand deposition rates are predicted in the approach channel, (Figure 27). The results indicate a maximum deposition up to 2m, mainly in the areas close to the islands. As shown previously in the sediment patterns, Figure 21, there is a sediment transport pathway driven by tide and wave action, from the nearshore islands into the channels, leading to the deposition in the approach channel.

In the area of the turning circle and the berth, no significant sand accretion is observed. Indeed, there is actually some evidence of erosion associated with the local increasing in flow speeds due to the enlargement of the tidal prism. It should be noted however that the evidence suggests that cohesive sediment exists in and around the berths/turning circle and therefore these results require further examination using the mud transport model presented in Chapter 3.

In terms of potential sand deposition volumes, the results are showing a deposition of the order of 1.2 million m^3 over the simulated year, from Box 1 to Box 11. Figure 27 also provides an indication of the areas where accretion is likely to happen and where the dredging effort should be focussed.

As with all sediment modelling, due to the number of assumptions and the modelling limitations, it is good practice to consider a safety factor when the estimated volumes are used to determine dredging requirements in order to take into account, the model limitations and the selected approach

Figure 27 provides an indication of the areas where accretion is likely to happen and where the dredging effort should be focussed.

Annual sand accretion of the order of 1.2 million m^3 is predicted in the approach channel.

Figure 27: Total annual average bed level change for the approach channel and berths.

Donald, 2019
Note: Positive numbers are showing accretion, while negative numbers are indicating erosion.

2.11 Summary and conclusions

A MIKE21 FMST sand transport model for the Pakistan FRSU – FEED, was setup to determine the sand transport regime in the study area. The model was also used to understand accretion rates in the dredged nearshore and approach channels and berth facilities.

Since the primary aims of the work is to better understand sediment mobility and how this may impact on channel sedimentation, the schematisation of hydrodynamic and wave conditions was undertaken using the morphological tide and wave concept. In the case of the tide, a 25 hours

period was selected for the simulations since the study area is driven by mixed diurnal/semi-diurnal tides.

In addition, the effect of the wave-driven currents has been included in the model, since it was considered potentially important in the nearshore areas around the islands. Wave-driven currents could be an additional source of sediments into the dredging channel and in order to be represented in the model, the mesh resolution in the nearshore areas was increased to 25m, as per the project site mesh resolution.

The results of the modelling indicate that:

- There are important potential net sand transport pathways, both in the nearshore and in the approach channel which can lead to sediment deposition. The nearshore sediment is generally driven towards the channels and then offshore creating deposition in the channel and an intertidal sandbank growing in an offshore direction;
- The predicted sand accretion location in the nearshore channel agrees broadly with the existing anecdotal dredging records;
- The results indicate annual accretion of up to 2m in the entrance to the approach channel, mainly in the areas close to the islands;
- In the area of the turning circle and the berth, no significant sand accretion is observed, and there is evidence of localised erosion. The accretion of cohesive sediments at this location is considered in Chapter 3; and
- Annual sand accretion of the order of 1.2 million m^3 is predicted in the approach channel. In the nearshore channel the annual accretion is estimated of the order of 1.8 million m^3 over the simulated year.

When interpreting the model results it is important to understand the model limitations. At best, sand transport modelling is accurate to a factor of two or three but can be subject to larger errors in some circumstances (*cf.* Schoonees & Theron, 1995; Camenen & Larroudé, 2003; Winter, 2007; Papanicolaou et al., 2008; Amoudry & Souza, 2011). Further, taking a conservative view, it has been assumed that sand is unlimited in availability (from erosion) and for deposition. Any hard, non-erodible substrate will act to reduce the sand transport potential. The presence of cohesive and other material will increase the potential rates of deposition. The sand transport result should be treated therefore as being indicative since the sand transport rates obtained using the model are based on assumptions about the size, density and availability of mobile sediments.

The results presented have been estimated using a morphological modelling approach representing the typical annual wave and tidal conditions at the site. The impact of storms, and their effect on the sedimentation in the area, has not been undertaken. Extreme events by their nature will enhance sediment mobility for relatively short periods and it is highly recommended that they are investigated as part of the detailed design.

3 Mud Transport Modelling

3.1 Introduction

Suspended sediments at the project site comprise: (a) resuspended fine, mainly cohesive sediments which are mobilised from the bed during peak tidal flows; (b) suspended sediment from sources upstream (east) of the Project site; and (c) suspended sediments from sources downstream (west) and offshore from the Project site. Together, these sources combine and give rise to the observed suspended sediment concentrations (SSC) at the Project site. Using the MIKE by DHI mud transport module (MIKE21 FMMT, hereafter termed the MT model) driven by the existing calibrated MIKE21 FMHD model, (hereafter termed the HD model) the modelling work reported here aims to reproduce as closely as possible the temporal and spatial variations in SSC measured in March 2019 (Section 4.3.1). Using this calibrated model, with an update to the bathymetry to represent the proposed layout, it has been possible to identify areas of sediment accretion and thus provide guidance on the likely maintenance dredging requirements for the FSRU facility.

This section of the report:

- Provides available background information to inform the interpretation of sediment dynamics around the Project site;
- Details the establishment, calibration and validation of the MT model for baseline conditions; and
- Presents results from the MT model for the Project, focussing on changes to sedimentation processes and on the likely maintenance dredging requirements.

It is noted from the outset that in common with many studies of this nature, the availability of data relating to bed sediment composition and the concentration and provenance of suspended sediments are extremely limited. While these data limitations have been supplemented by field measurements and laboratory analyses, it has been necessary to make a range of broad assumptions during the model build and calibration phases. These assumptions are based on experienced gained in past studies and the skill and knowledge of the modelling team and have been examined systematically in several sensitivity analyses reported below. This approach provides a well-founded basis for subsequent comparative studies of scheme impacts for this strategy.

The MT module is based on the cohesive sediment formulae from Mehta *et al.* (1989). The model is driven by the HD model-derived currents that define the bottom shear stress and include descriptions of bed sediment strength, sediment entrainment and deposition thresholds and suspended sediment settling velocities (accounting for flocculation and hindered settling, Lumborg *et al.*, 2012). The MT module is appropriate for estuaries where a large proportion of the sediments have cohesive properties. As reported in Section 3.2.4, the area encompassing the Project site is dominated by mudflats composed of clays and silty sands and remnants of consolidated sediment. Use of the MT model is thus appropriate for these conditions.

3.1.1 Study area

As described in the Sand Transport modelling chapter, the study area encompasses a nearshore channel, an approach channel and the project site. These sections are shown in Figure 28.

Figure 28: Study area

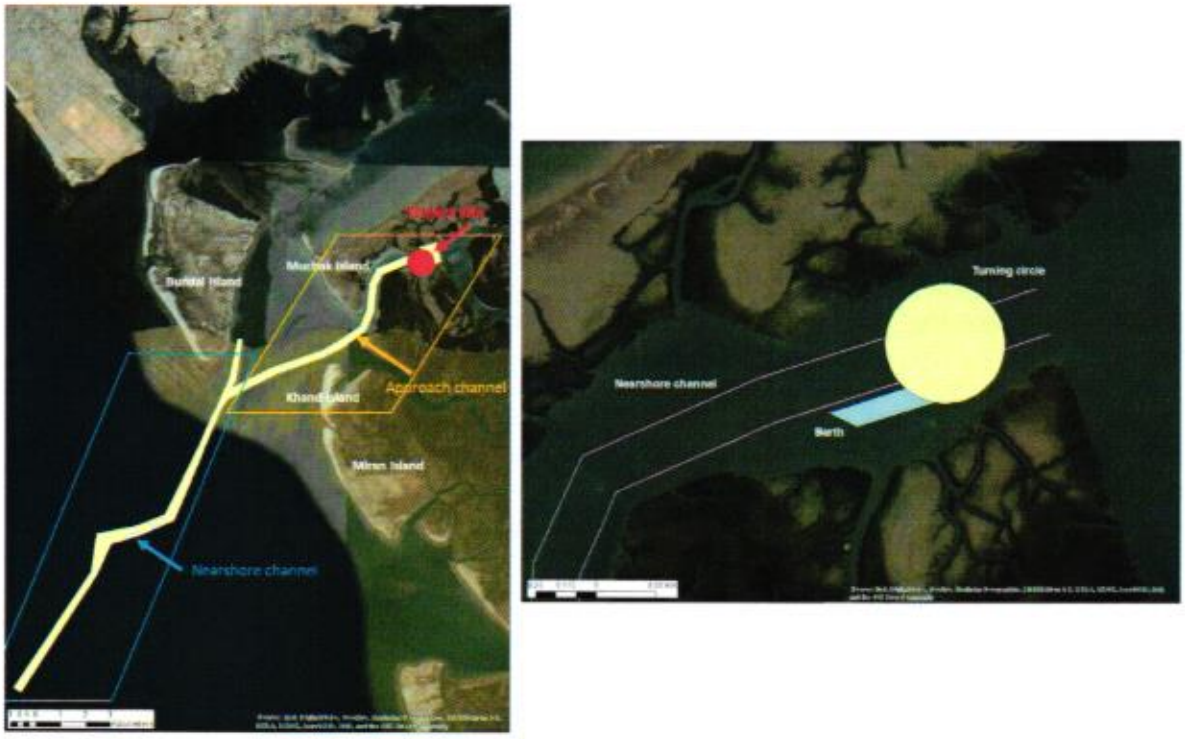

Source: Mott MacDonald, 2019

However, for the Mud Transport modelling, it is important to identify the different creeks and channels that are part of the estuary. The suspended sediment concentrations available in the literature are always related to the creek's names, and therefore, the image below has been added to help to locate and relate the information

1809

Figure 29: Creek, islands and channel in the study area.

Source: Mott MacDonald, 2019

3.2 Background

3.2.1 Geology and geotechnical

The geology of the project site comprises quaternary deltaic deposits of fine sands, silt and mud and forms part of the extensive Indus delta (Figure 30, Global Environmental Management Services - GEMS, 2017).

Figure 30: Geology of the Project area

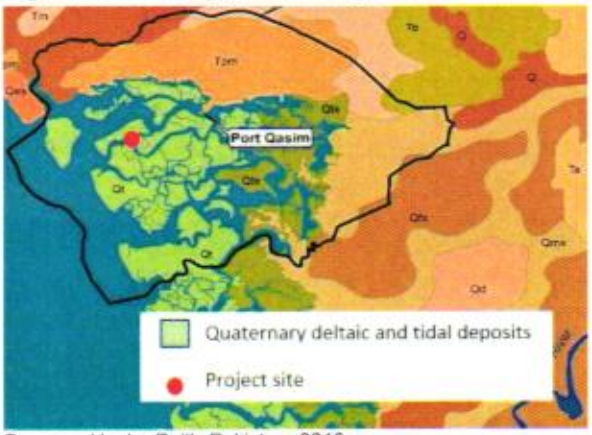

Source: Hagler Bailly Pakistan, 2016

3.2.2 Suspended sediments

Total suspended sediment (TSS) concentration and turbidity were measured on 11 March 2017 at four locations (Figure 31, Table 4) and reported in GEMS, 2017. The measurement locations are north east of the Project site in Phitta Creek and may not therefore be representative of the local conditions for the present study.

The relationship between reported TSS values (in units of mg/l) and turbidity (in nephelometric turbidity units, NPU, Table 4) is weak, indicating that backscatter readings from the turbidity meter are influenced by both organic and non-organic suspended sediments. Unfortunately, no further information is provided in the GEMS (2017) report to reconcile this.

Figure 31: Location of TSS and turbidity measurements, 11 March 2017

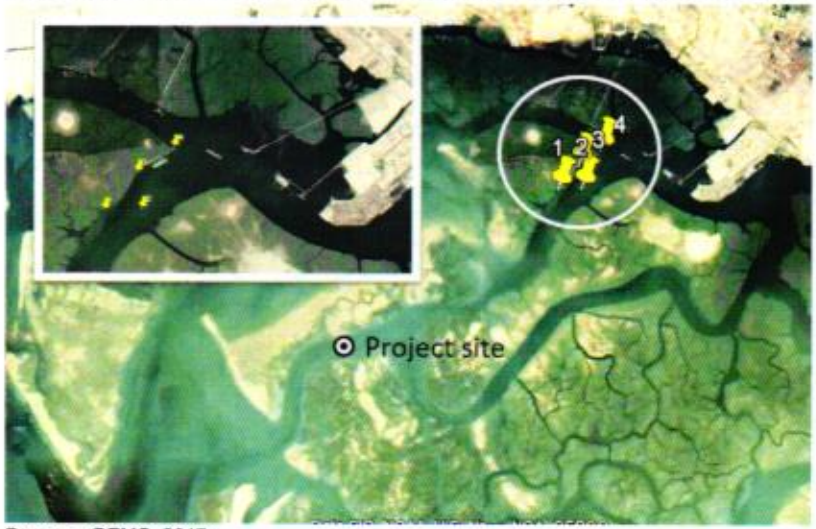

Source: GEMS, 2017

Table 4: GEMS suspended sediment sampling results – 11 March 2017

	Sample 1	Sample 2	Sample 3	Sample 4
North	24° 45' 59.0"	24° 46' 00.0"	24° 46' 24.0"	24° 46' 39.5"
East	67° 16' 36.4"	67° 17' 02.6"	67° 16' 59.4"	67° 17' 25.0"
TSS (mg/l)	12	10	<5	12
Turbidity (NPU)	4	2	5	6

Source: GEMS, 2017

Suspended sediment concentration values measured monthly at two locations in Phitta Creek (Figure 32) are also reported by Naz *et al.* (2014) for the period January 1998 to December 1998. These samples were obtained as part of a study looking at meso-zooplankton and other biological components of the suspended sediments and no information is provided regarding the sampling or analysis methodology. It is possible that this was unsuitable for TSS *per se*. Table 5 shows concentration values less than 1.0mg/l and the minimum and maximum TSS values are around one order of magnitude less than the GEMS data (Table 4). Unfortunately, there is insufficient information to enable reconciliation of these data differences.

The above research also refers to the Rizvi *et al.* (1994) study, which found higher suspended sediment concentrations due to the southwest monsoon (May to August), up to 110-115 mg/l in

Gharo Creek, and lower values during March, September and November. According to the research the higher suspended sediment load is due to the greater tidal flows and wind speeds.

Figure 32: Location of sediment samples in Phitta Creek.

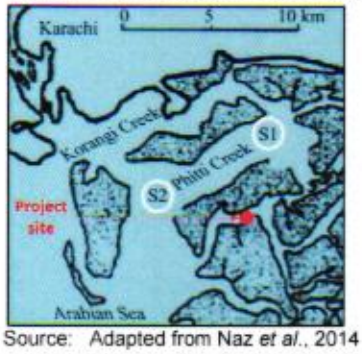

Source: Adapted from Naz *et al.*, 2014

Table 5: Suspended sediment concentration values from Phitta Creek

	S1			S2		
	mean	min	max	mean	min	max
Concentration (mg/l)	0.69±0.05	0.01	0.20	0.065±0.04	0.01	0.02

Source: Naz *et al.* (2014)

According to Environmental Impact Assessment for the Engro Fast Track LNG Regasification Project, prepared by Environmental Management Consultants (EMC) in 2014, the suspended sediment concentration in the creek areas have an annual range of 25-170 mg/l. The higher values are observed, similar to the previous research, during the southwest monsoon period (May to August). The average suspended load during June-July was, according to the report, between 80-115 mg/l. However, EMC (2014) reported higher values (115-170 mg/l) at some places in the Phitti/Koragi /Kadiro creek system. Lower suspended sediments concentrations (25-50 mg/l) were recorded from September to March each year. The research indicated that the suspended load in the creeks also exhibits variations with the degree of turbulence during the tidal cycle. Furthermore, during the flood season (June to September) in the Indus River (located 100km south of the site), the suspended load rises to about 400 mg/l in Khobar Creek. Please note that no information is available regarding how the above data has been collected.

In addition, according to Harrison *et al.* (1997), the suspended load in Isaro Creek ranged from about 100 to 180 mg/l (measured in 1991, but no addition information available). Harrison *et al.* (1997) explains the high suspended load in the creeks are because of the fine sediments (about 5 % sand, 75 % silt and 20% clay). These fine sediments are easily suspended by high tidal currents (0.5 to 1.5 m/s) caused by semi-diurnal tidal ranges of up to 4 m during spring tides.

All the above available information has been plotted in Figure 33. Please note that the locations of the suspended sediments are approximated, and they should be only used as a general guidance for the potential suspended sediment concentrations observed in the creek system.

Figure 33: Approximate location of suspended sediment measures available in the literature.

Source: Mott MacDonald, 2018

The uncertainties associated with data discussed above therefore demonstrates clearly the need to acquire *in situ* suspended sediment information at the Project site to avoid ambiguities during the MT model calibration process. This has been addressed by the surveys undertaken by TCI in March 2019 (Section 3.2.2).

3.2.3 Dredge volumes

As previously mentioned in the Sand Modelling Chapter (Section 2.2.2), information provided to Mott MacDonald by JGC on 18 February 2019 details anecdotal dredging records for the approach channel to the Project site. While providing a broad indication of possible dredging requirements, and while they have some value, they are of anecdotal nature and therefore must be interpreted with caution.

3.2.4 Borehole information

The STS (2018) report provides information on sediment core analysis for 9 locations: BH-01 to BH-04 at the Project site and BH-11 to BH-15 in Phitta Creek (Figure 34). Information from the borehole report has been extracted and used to define several MT model setup parameters.

Figure 34: Location of boreholes BH-11 to BH-15. Boreholes BH-1 to BH-04 were at the Project site.

Source: STS, 2018

Table 6: Summary of near-surface sediment properties at Locations BH-01 to BH-04

Sediment	BH-01	BH-02	BH-03	BH-04
Sand depth	None	None	None	None
Clay/silt depth	0 to 6.8m	0 to 4.5m	0 to 7.5m	0 to 4.0m

Source: STS, 2018

Table 7: Summary of near-surface sediment properties at Locations BH-11 to BH-15

Sediment	BH-11	BH-12	BH-13	BH-14	BH-15
Sand depth	0 to 10.5m	None	0 to 3.5m	1.0 to 20.0m	0 to 1.5m
Clay/silt depth	None	0 to 2.5	None	0 to 1.0	None

Source: STS, 2018

Table 8: Description and properties of surficial sediments from borehole data at sites BH-01 to BH-04

Location	Description	Sand (%)	Silt (%)	Clay (%)
BH - 01	Clay / Silt: brownish grey, silty clay / clayey	6.6	45.4	48
	silt, traces of sand	2.8	51.5	45.7
		2.8	58.7	38.5
		5	42.5	52.5
		7.6	59.9	33.1
BH - 02	Clay /Silt: brownish grey, very soft,	3.2	43.3	53.5
	silty clay / clayey silt, traces of sand	4.2	51.5	44.3
		3.2	41.4	55.4
		3.2	34.3	62.5
BH - 03	Clay / Silt: brownish grey, very soft, silty	8.8	45.5	45.7
	clay / clayey silt, traces of sand	4.6	59.6	35.8
		8.6	44.3	47.5
		4.6	59.5	35.9
		7.4	43.5	49.1
BH - 04	Clay: brownish grey, silty, traces of sand	9.2	41.9	48.9
		6.4	45.5	48.1
		4.2	34	61.8

Source: STS, 2018

Data in Table 7 and Table 8 indicate that surficial sediment at the Project site and at more distant locations are dominated by fine sediment. With clay content by percentage exceeded 50% in most case (Table 8) the physical behaviour of the material will conform to typical cohesive sediments. Using these data, the density of surficial sediments was determined to be in the range 1,300 kg/m^3 to 2,005 kg/m^3. These values provide some guide for subsequent MT model calibration, especially in terms of the deeper and more consolidated sediment layers.

3.3 MT model setup

Following DHI guidance the MT model was set up using all available information and estimates of several required site-specific parameters including the threshold for erosion and accretion and for bulk density. Following standard practice, the model calibration was undertaken iteratively, using successive model results to guide adjustments to key MT parameters (erosion/accretion properties, bed thickness initial conditions, initial SSC, boundary conditions, etc.) and to define the initial conditions for subsequent MT model runs. By this means, it was possible to converge the SSC values predicted by the MT model towards values defined by the calibration data (SSC) described below. The selection of initial values for MT parameters was guided by DHI recommendations and the experience of the modelling team in other projects.

Our approach to calibration of the MT model has been founded on what we believe to be the most reliable data available, albeit limited in spatial and temporal extent to achieve the best modelling

outcome possible. However, it should be specifically noted that it is well recognised that without extensive data defining the nature and behaviour of the estuarine sediments, the establishment of an accurate MT model is extremely difficult to achieve. Nevertheless, although the model is unable to provide accurate specific values for sediment erosion and accretion it will allow assessment of the relative changes that may result from the FSRU Project. It is considered therefore that the model has a capability to address concerns associated with potential changes to sediment budgets and morphology, and the associated maintenance dredging as required in this study.

The MT model calibration aimed fundamentally to optimise agreement between model predictions and measurements of suspended sediments at the three sampling locations. Calibration of the model for suspended sediments was undertaken for Spring and Neap tides.

The calibration period selected was:

- **Spring tide**: 21 to 23 March 2019 – Tide range of approx. 2.8m (at Port Qasim); and

The validation period selected was:

- **Neap tide**: 29 to 31 March 2019 – Tide range of approx. 1.4m (at Port Qasim).

3.3.1 Calibration and validation data

Although an extensive review of the published literature was undertaken to identify suitable datasets, only a limited amount of data was identified as being suitable for the purposes of calibrating the model.

3.3.1.1 Suspended sediment concentrations (SSC)

Suspended sediment data was collected for a spring tide (21-23 March 2019) and neap tide (29-31 March) by TCI. The data were collected at three locations (Figure 35) using Niskin Bottles. At each location, the water samples were obtained at two depths (near-bed and mid-water) over a 13-hour period (Low water to High water to Low water) at 30-minute (MET1), or 1-hour intervals (MET3 AND METnew). For additional information regarding the survey, please refer to the TCI (2019) report.

Figure 35: Suspended sediment samples locations

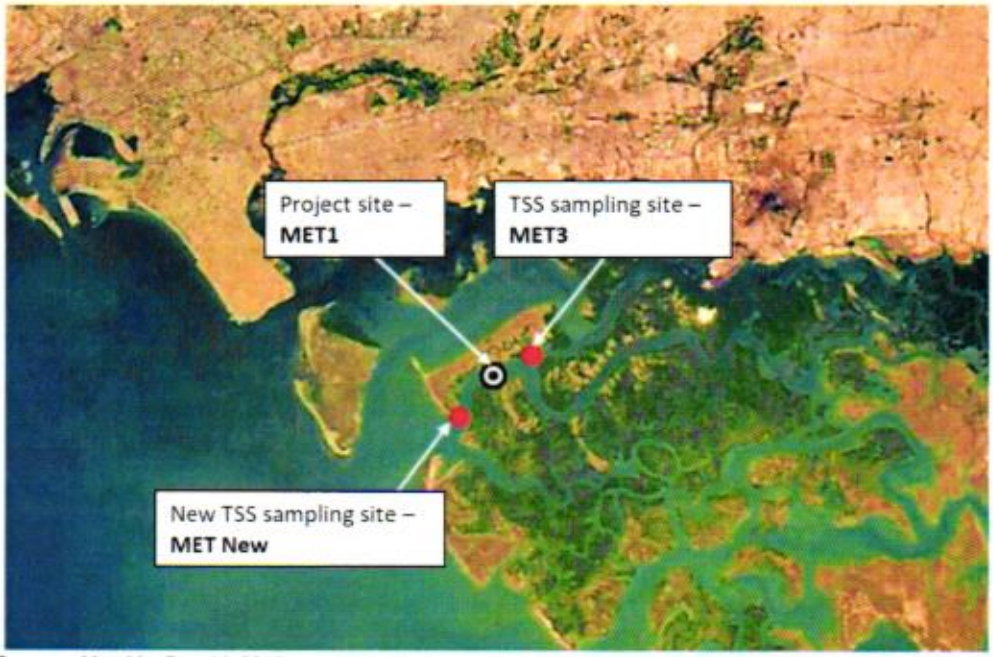

Source: Mott MacDonald, 2019

Table 9 provides a summary of the suspended sediment sampling campaign.

Table 9: Suspended sediment sample campaign summary

	MET1	MET3	MET New
Location – Long/Lat (WGS84)	67.212878, 24.720592	67.22972222, 24.72934444	67.19194444, 24.6980500
Approx. water depth (m MSL)	-14.5	-17.5	-24.7
Spring sample	22nd March	21st March	23rd March
Neap sample	30th March	29th March	31st March
Sampling interval	0.5 hr	1 hr	1 hr

Source: Mott MacDonald, 2019

The SSC results are shown in Figure 36a (spring tide) and Figure 36b (neap tide) for the three locations, including the modelled water level for the project site. Please note that due to the proximity of the sample locations, the water level at the site has been used as a reference for the three locations.

The sample results show that, in general, background SSC values range between 20mg/l to 40mg/l. This is similar to the values reported by EMC (2014), which quotes SSC values of the order of 25-50 mg/l from September to March.

The results indicate that there is no clear pattern between the bottom and the middle water depths SSC values. The samples show similar SSC values for both the bottom (red lines) and the middle water depths (blue lines), Figure 36, but there is no evidence that indicates higher SSC values at the bottom or the middle water, which could potentially indicate that there is good mixing in the water column.

1917

The SSC time-series also show short peak concentrations for the spring tide during the ebb phase (Figure 36a). The peaks concentrations are both in the middle and bottom depths samples, depending on the location. Again there is no clear relationship between bottom and middle water SSC values.

The spring tide SSC values are plotted against the current speed and the water level at each sampling location in Figure 37. Please note that the currents were extracted at each sample location to ensure the correct comparison between sediment concentrations and phase of the tide. The figure shows that the peak concentration tends to occur during the ebb tide, generally close to the peak in the current speeds. This suggests that the recorded peak concentrations could be related to local erosion of the bed close to the sample location. This increase in the SSC values is not observed during the flood tide, potentially due to the smaller current speed.

The sample results are, in general terms, in agreement with the ebb dominance of the estuary in that the peak of SSC is observed to occur during the ebb tide. In addition, the peak in SSC can be observed in all three samples, which provide some confidence in the measured data.

It is important to note that the results do not show a clear influx of SSC into the estuary. The influx of offshore sediment would be expected at the METnew location during the flood tide phase if sufficient suspended sediment was available. However, there is no evidence for this which suggests that, at least during the sampling period, the suspended sediment in the estuary is re-worked local sediment, with little or no input of sediment from the coastal area.

During monsoon seasons, the suspended sediments concentrations in the estuary are expected to increase and be more influenced by the offshore availability of material. A sensitivity test regarding the effect of the monsoon season has been undertaken as part of the model calibration and is reported in Section 3.7.

Figure 36: Suspended sediment concentrations at the three samples locations for (a) spring tide and (b) neap tide. Please note that 100mg/l are equivalent to 0.1kg/m³.

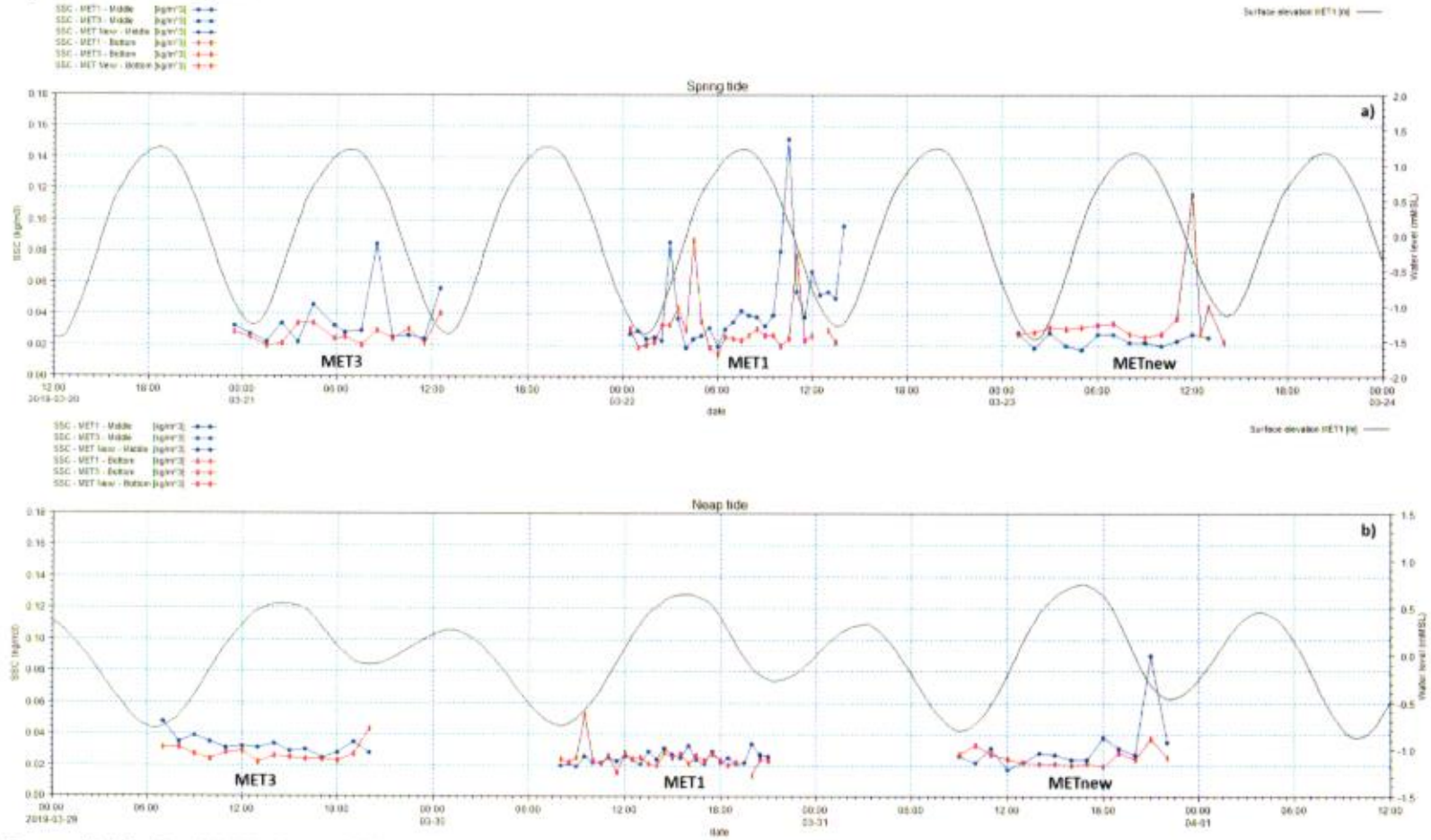

Source: Mott MacDonald, 2019. Contains TCI data, 2019.

Figure 37: Suspended sediment concentrations at the three samples locations for the spring tide, plotted with water level and current speed for each site. Please note that 100mg/l are equivalent to 0.1kg/m3.

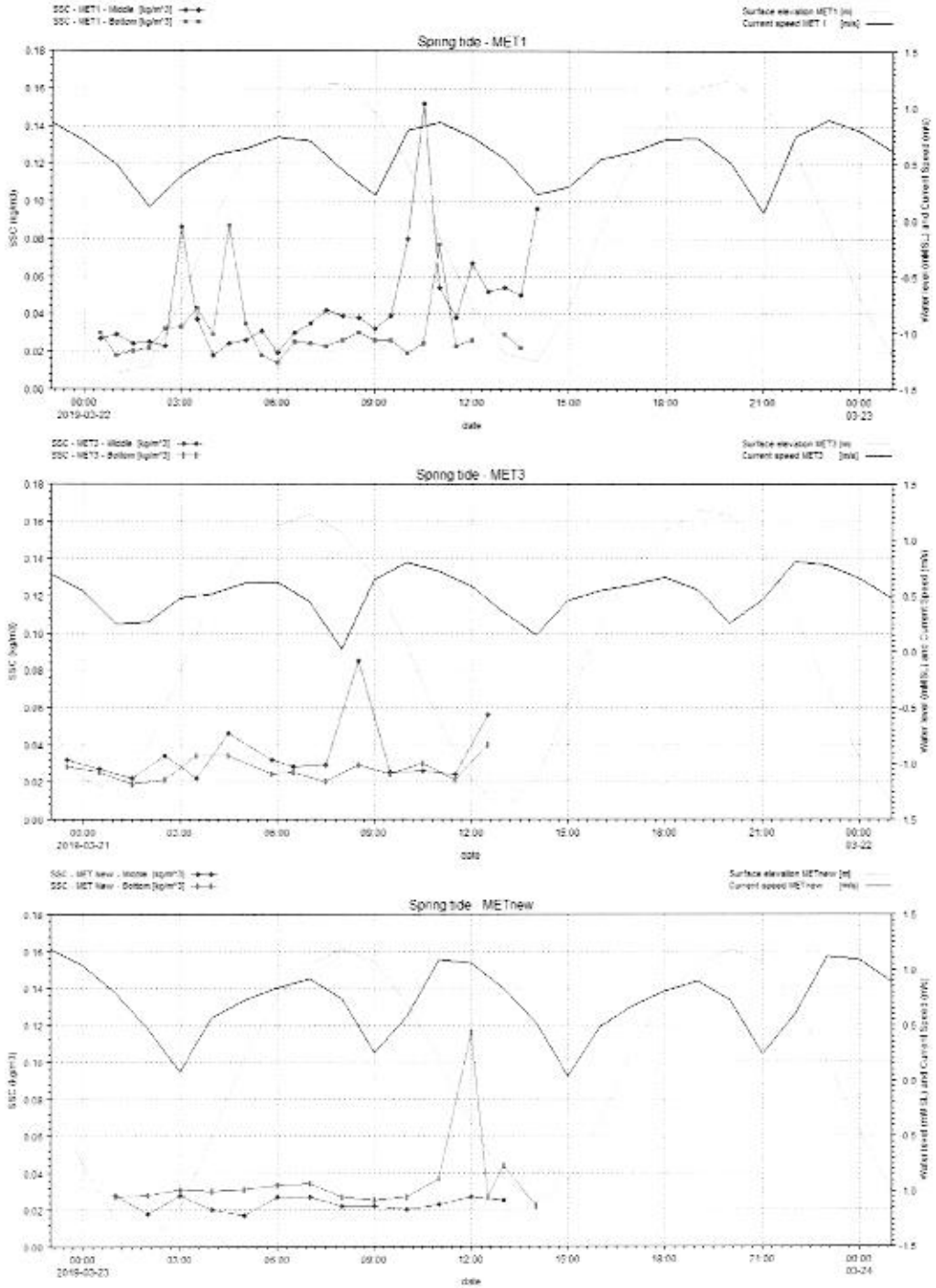

Source: Mott MacDonald, 2019. Contains TCI data, 2019.

3.3.1.2 Turbidity measurements – Aqualogger

To measure turbidity, a measurement device, Aqualogger, was deployed at MET1 station from the 15th of March 2019 until 1st of April 2019 to obtain time-series SSC data for single location as part of the TCI survey campaign. The turbidity measurements were used to derive SSC after the instrument calibration. For additional information regarding the calibration and the derivation of the SSC, please refer to TCI (2019) report.

The measured SSC time-series provided by TCI (2019) are shown in Figure 38. Longer SSC time-series are not available at this time. Figure 39 compares the Aqualogger data with the SSC values derived from the Niskin Bottle samples. Please note that the Aqualogger data was digitized from the TCI report, as the raw data was not provided.

Figure 38: Aqualogger results of SSC (mg/l) – Please note that the time axis is in local time (GMT+ 5 hours)

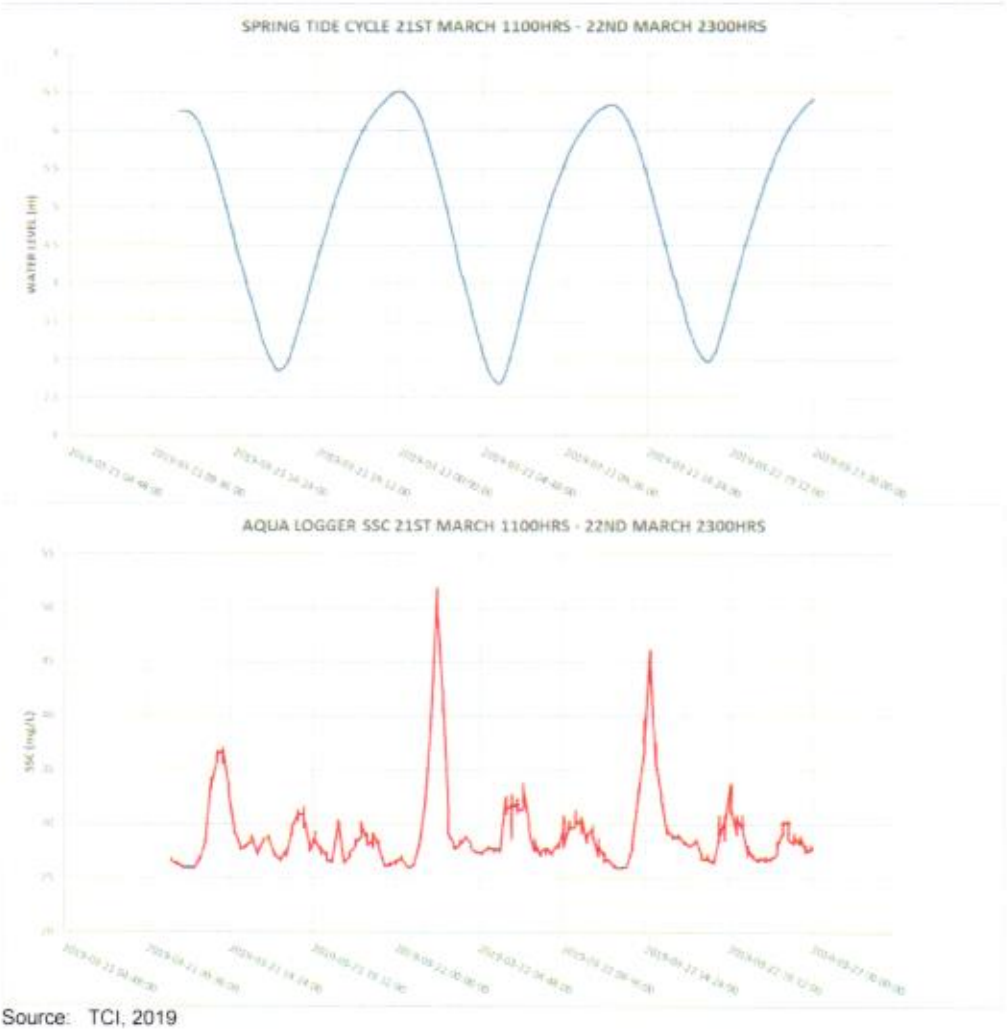

Source: TCI, 2019

Figure 39: Niskin bottle SSC (black lines) compared to Aqualogger SSC (red line) for the same location and time. Please note that the model SSC is expressed in kg/m^3 instead of mg/l – 0.1kg/m^3 is equal to 100mg/l.

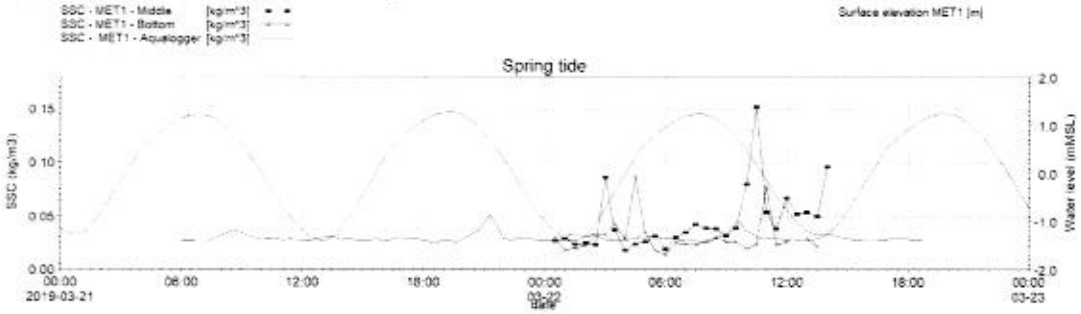

Source: Mott MacDonald, 2019. Contains TCI data, 2019.

From Figure 39, it can be noted that there are discrepancies between the two datasets. The SSC obtained using the Aqualogger are considerably smaller than the data recorded using the Niskin bottles. While both datasets indicate peak concentration during the ebb tide, Niskin bottle data are three to five time higher than the Aqualogger data. While the reasons for this disparity cannot be determined, it is understood that TCI used water samples to calibrate the Aqualogger data and thus much better agreement between the two data sets would be anticipated.

Being unable to reconcile the differences between SSC values from the Aqualogger instrument and the Niskin bottles a decision was made to calibrated the MT model using the SSC values from the Niskin bottles. This decision was based on the observation that: (a) the higher SSC values from the Niskin bottle sample analyses represents a more conservative approach; and (b) the analysis used to obtain SSC values from the water samples is simple and usually reliable unlike the Aqualogger data which can be compromised by materials in the water column other than cohesive sediments (e.g. algae) and requires a calibration procedure to derive SSC values.

3.4 Mud Transport model inputs and parameter setting

In the MT model the erosion, transport and accretion of sediments is governed by the hydrodynamic conditions derived from the HD model. The bottom sediments are described using three vertical layers with each layer having a defined thickness, a bulk density value and threshold erosion/accretion properties and rates. The bed layers are organised so that the "weakest" layer (typically fluid mud or newly deposited sediment) is defined as the uppermost layer. Layers beneath this have increasing bulk density and shear strength to reflect the natural consolidation and compaction of cohesive sediments. The properties of these layers are defined further in Section 3.4.2. If mobilised the sediment is transported by the currents predicted by the hydrodynamic module.

Two diagrams showing how the mud transport model parameters are defined and the main processes are shown in Figure 40.

Figure 40: Mud transport model parameters and processes

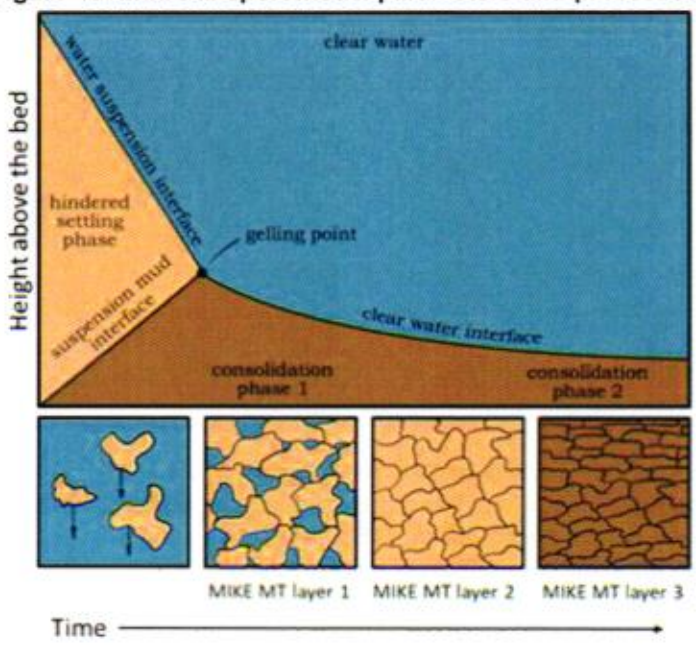

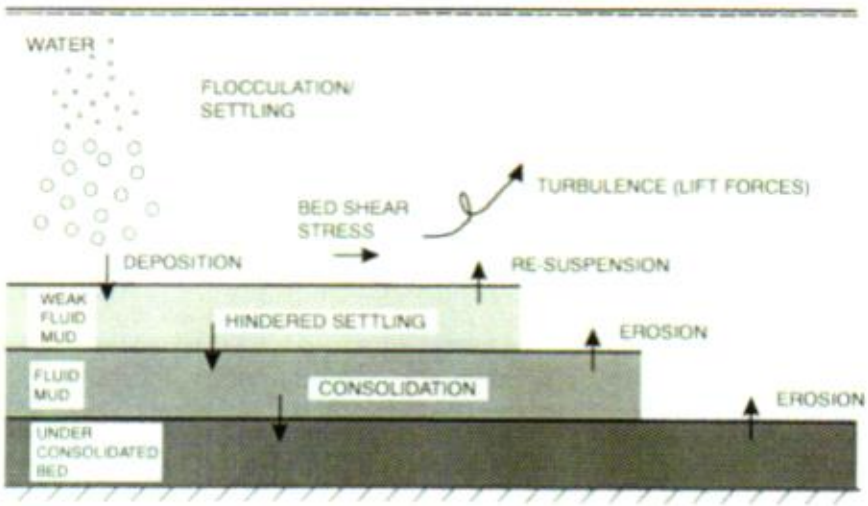

Source: Mike by DHI, 2017

3.4.1 Hydrodynamic and suspended sediment parameters

Critical bed shear stress values are defined in the MT model to describe when the suspended sediment will start to erode or accrete. Following MT model guidelines, the critical shear stress for deposition was defined as being constant throughout the model and set to 0.1 N/m^2. This is a calibration factor, which is at the upper end of the appropriate range, but one that would be more

conservative for estimating deposition. In reality, the threshold bed shear stress for erosion and accretion may be different (*cf.* Whitehouse *et al.*, 2000).

In the MT module, the model uses a constant settling velocity when suspended sediment concentrations are below 0.01kg/m^3. Above this concentration, the model calculates a settling velocity value that depends upon the suspended sediment concentration in the water column, accounting for the flocculation of the suspended sediment particles when the ambient conditions are suitable, and for hindered settling when particle concentrations are sufficiently high.

3.4.2 Bed parameters

As there is insufficient information available to define the variability in either bed or suspended sediment properties across the model domain, for simplicity the erosion and deposition characteristics of the sediments in the MT model are defined as being spatially invariant. Thus, the properties of each of the three sediment layers across the MT model domain are defined as being constant in composition.

Appropriate values for the erosion coefficient, critical bed shear stress and dry bulk density of each layer were estimated using recommended empirical equations in Whitehouse *et al.* (2000) and the information available from the boreholes. A transition coefficient (representing consolidation) can be used in the MT module to determine a rate at which the properties of the sediment from upper layers are transformed to that of the sediment in lower layers. This coefficient was set to a value of 10^{-7} kg/m^2/s for the transition between layer 1 and layer 2, and a value of 10^{-7} kg/m^2/s for the transition between layer 2 and layer 3. These values are founded on experience and broadly in agreement with DHI recommendations, where transition values between 10^{-8} Kg/m^2/s and 10^{-6} Kg/m^2/s are indicated (DHI, 2006). It is noted that in the MT model, the consolidation of bed sediments is generally only relevant over times-scales of several weeks or more. Therefore, over the period of the present simulations, changes in bed consolidation were expected to be negligible and thus will have little impact on the model calibration and results.

As limited information was available to define the density of the sediment around the Project site, the borehole information (Section 3.2.4) was used in combination with the recommended values in the literature. It is important to note that the boreholes do not provide information for the superficial recently deposited sediments, but instead represent the nature of the slightly deeper consolidated material.

To account for different sediment consolidation in the MT model, the density of the three layers were variable with a value of: (a) 100 kg/m^3 defined the uppermost soft unconsolidated layer; (b) 400 kg/m^3 for the middle layer; corresponding to medium consolidated bed (1 month to 1 year consolidation); and (c) 1000 kg/m^3 for the deepest, most consolidated third layer (Table 10). The density of the third layer is of the same order of magnitude as reported in the borehole information.

Table 10: MT model parameter settings

Layers	Layer Thickness (m)	Erosion Coefficient x 10^{-4}	Critical Sheer Stress	Dry Density
		(kg/m^2/s)	(N/m^2)	(kg/m^3)
1	0.01	0.2	0.4	100
2	0.20	1	2	400
3	10.00	1	3	1000

Source: Whitehouse et al., 2000; Mott MacDonald, 2015

After the initial MT model run, the thickness of the sediment layers was adjusted using a data post-processing routine so that sediments were not present at locations where the peak bed shear

stress exceeded the critical stress for erosion of a given sediment layer. It is considered that this approach approximates to what would naturally happen if a uniform sediment bed was exposed to the variable bed shear stress distribution in the estuary. This is used as a starting bed layer map for a "cold start" simulation. The initial conditions for subsequent simulations, were then taken from the end of the "cold start" simulation.

3.4.3 Boundary conditions

It has been assumed that the sediment available in the estuary is re-worked sediment from the estuary itself. Owing to extensive water extraction for irrigation and dams at many locations along the river course, the delta area around the project site now receives very little sediment from fluvial sources, and therefore, no fluvial input has been considered in the model. There is no information regarding the offshore suspended concentrations to define the model offshore boundary. It has been assumed that these concentrations are very small, of the order of 15mg/l for a non-monsoon period.

3.5 Calibration – Spring tide results

Calibration involves varying model parameters, boundary conditions, bathymetry, bed and suspended properties such as erosion and deposition thresholds, densities, etc., to reproduce real world data as accurately as possible within the model requirements and limitations. Model calibration was undertaken using the Niskin bottle results, as described in Section 3.3.1.

The final model calibration is shown in Figure 41 for the 3 sampling locations during the Spring tide period. Please note that sensitivity tests were undertaken in order to determine the final calibration parameters. These sensitivity tests are described in Section 3.7. In general, predicted SSC values have the same patterns over the tidal cycle. Peaks in concentrations are observed during the ebb tide, especially at MET1 and MET3. Background concentrations are lower, between 20 to 40mg/l, as per the measured data. There is a slight delay in the modelled peaks of SSC. Hhowever, the peak magnitudes are of the right order. This is clearly observed in MET1 and MET3 results.

It is noted that the model results for METnew do not reproduce the short peak of SSC observed in the measured data (which is only present in one observation). The model produces a later and longer peak in SSC during the late ebb and early flood in the tide. While being slightly out of phase, the concentrations simulated by the model are of the right order of magnitude, both for the peaks and the background concentrations.

The phase difference between the observed and modelled SSC peak values can be attributed to a range of possible factors, for example: (a) passing vessels or other local bed disturbances that artificially elevated SSC values at the time of the water sampling; (b) advection of higher concentration of suspended sediment at the time of sampling (e.g. fast flowing water runoff from an adjacent creek); and bed disturbance and local resuspension caused by the sampling process itself.

Figure 41: Comparison between measured (black line) and modelled (red line) suspended sediment concentration during Spring tide conditions at the sampling locations. Please note that the model SSC is expressed in kg/m^3 instead of mg/l – 0.1kg/m^3 is equal to 100mg/l.

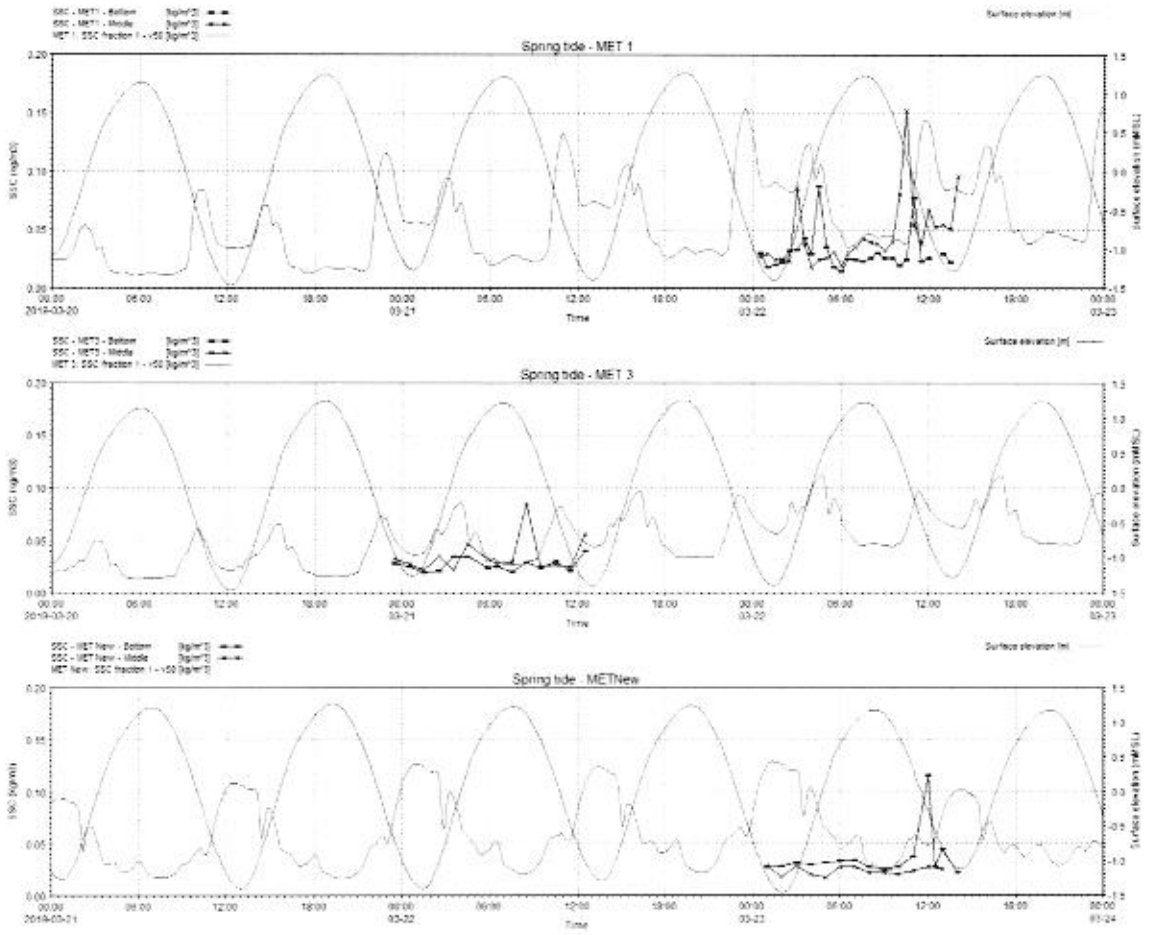

Source: Mott MacDonald, 2019. Contains TCI data, 2019

It is important to note that the main aim of the MT model is to determine the spatial and temporal behaviour of cohesive sediments at the project site and to understand the potential deposition expected so that potential dredging requirements can be estimated. While the short peaks in SSC are important it is equally important that the model is able to simulate the observed background SSC values accurately as these determine the rate and amount of accretion at the project site. In this regard the MT model calibration has achieved good agreement between observed and predicted SSC behaviour.

3.6 Validation – Neap tide results

Validation is the process of comparing the model against a different set of data (or tidal range) using the model parameters/setup derived during the calibration to prove that the model is robust enough to be applied to different periods of time or input conditions. Validation was also undertaken using the SSC data from the Niskin bottle measurements reported in Section 3.3.1.

The final model validation is shown in Figure 42 for the 3 sampling locations during the Neap tide period. The figure shows that due to the lower current speeds, there are no SSC peaks during the ebb flows. The figure also shows that the background concentrations are generally lower with a value around 20mg/l. The simulated model results show similar concentrations to those measured on site, although the model results under predict the SSC slightly. In general, however, concentrations are very small with the model predicting 10mg/l, while the measured data is around the 20mg/l over these neap tides.

The slightly lower concentrations predicted by the model during the validation stage may be related to the deposition threshold value being a little too high, This reduces the amount of sediment in suspension. Since no information regarding deposition rates is available at this stage, the potentially larger deposition is considered to be conservative in this case, since the model aim is to determine the potential for accretion of the dredging channels. Deposition from such low concentrations is also considered to be small.

Figure 42: Comparison between measured (black line) and modelled (red line) suspended sediment concentration during Neap tide conditions at the sampling locations. Please note that the model SSC is expressed in kg/m^3 instead of mg/l – 0.1kg/m^3 is equal to 100mg/l.

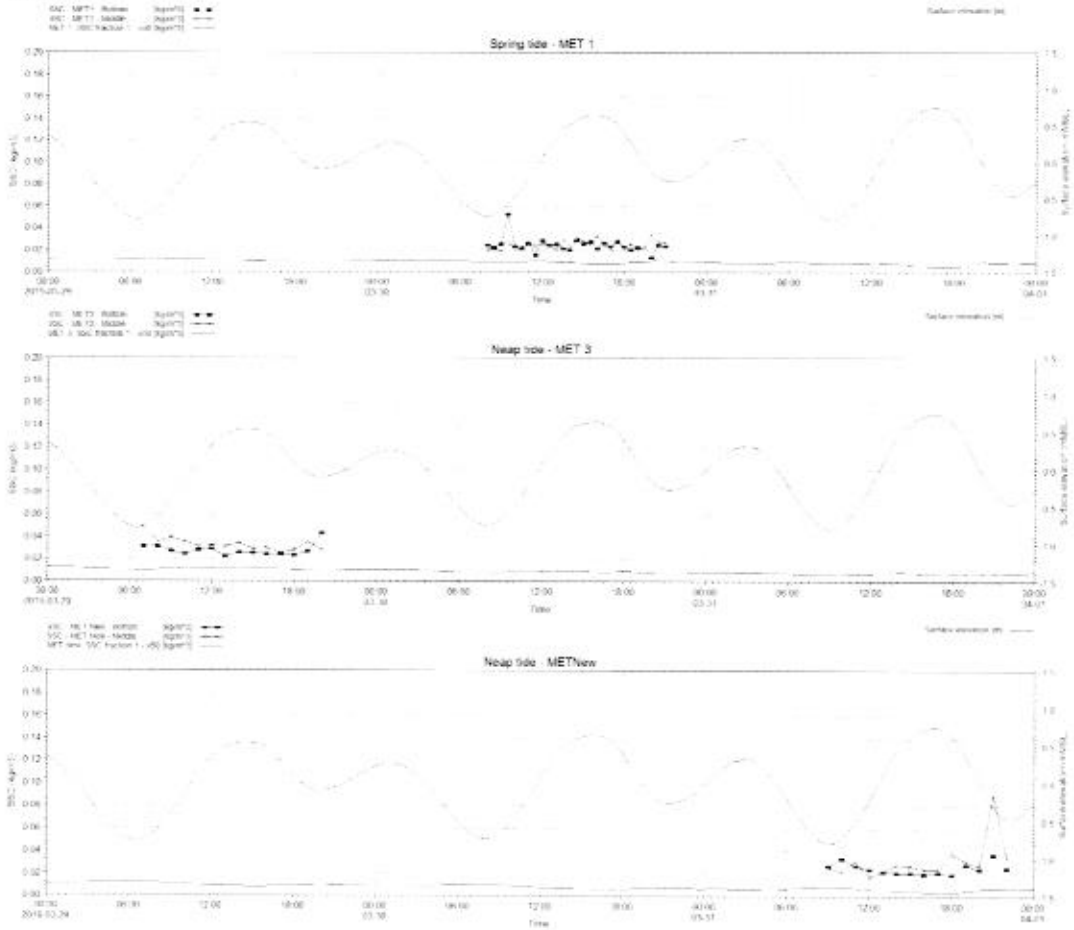

Source: Mott MacDonald, 2019. Contains TCI data, 2019

3.7 MT model sensitivity tests

Model sensitivity tests seek to establish and to quantify how the MT model output values are affected by changes to the model input values. Although constrained by data availability, sensitivity tests have been undertaken to assess model responses to uncertainties in:

- Sediment settling velocity; and
- Monsoon season.

3.7.1 Settling velocity

The settling velocity is dependent on the size of the particles in the water column. If the concentration of suspended sediment is high enough, other factors act such as salinity and/or temperature changes can affect the physical and dynamical properties of the suspended sediment (e.g. flocculation). When this happens collisions between particles/flocs will increase and floc size will increase further leading to higher settling velocities.

In the MT module, the settling velocity is constant when suspended sediment concentration values are less than 0.01kg/m^3. Above this concentration value, the MT model defines the settling velocity by accounting for the SSC value and the shear stress in the water column, so that flocculation of the particles is included. In the sensitivity test, the settling velocity coefficient in the model was varied to determine its effect on SSC values. Figure 43 shows the concentration profile when flocculation is included in the model and it highlights the settling velocity coefficient used in the sensitivity test.

Figure 43: Applied concentration profile when flocculation is selected in the MT module.

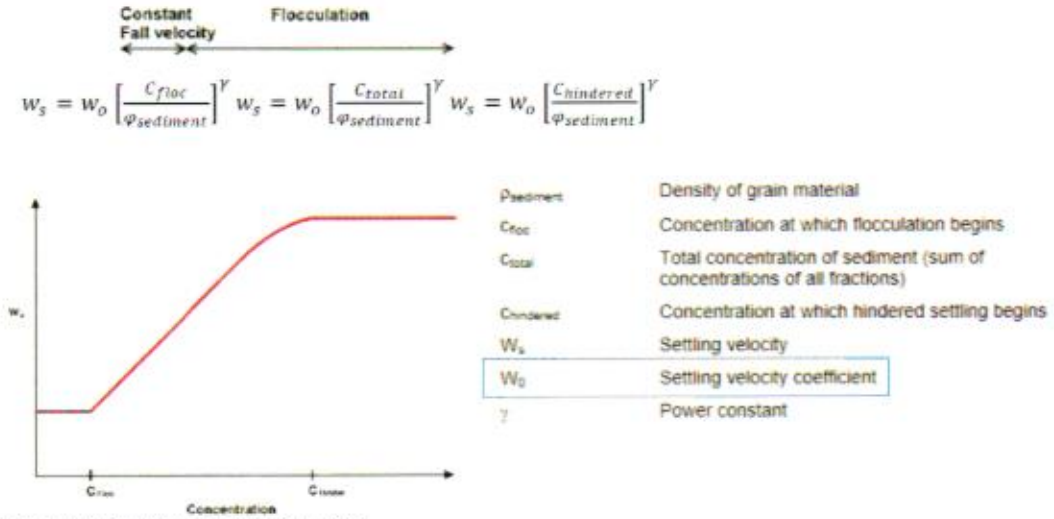

Source: Modified from Mike by DHI, 2017

As expected, and as shown in Figure 44, increasing the settling velocity coefficient in the model by 45% from 7.5 to 12, the predicted SSC decreased. The figure indicates that slightly lower concentrations of sediments are predicted at MET1 sampling location, with differences between the 5 to 10mg/l.

Thus, while settling velocity has been demonstrated to control to some extent SSC values, the effect is significantly smaller than the variation in observed concentrations. Therefore, for the

range of settling velocity values tested, it was judged to have relatively little effect on the overall sedimentation regime. Please note that Figure 44 shows sensitivity test results and not the final calibration run.

Figure 44: Modelled suspended sediment concentration during Spring tide conditions MET1 sampling location. The predicted SSC values using an increased settling velocity are shown by the green line. Please note that the model SSC is expressed in kg/m3 instead of mg/l – 0.1kg/m3 is equal to 100mg/l.

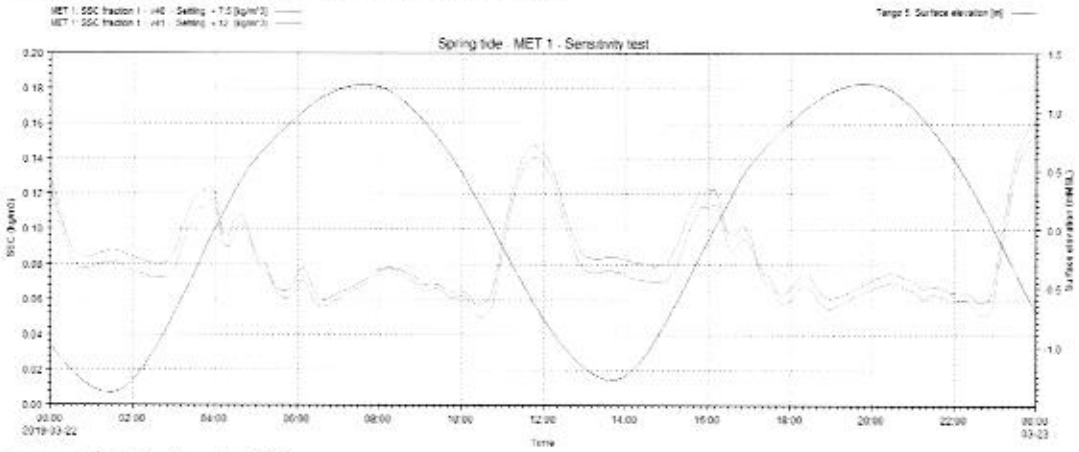

Source: Mott MacDonald, 2019

Since no information regarding settling velocity was available, it was decided to set the settling velocity coefficient to 7.5 to ensure that, especially during neap tide, not all the suspended sediment was settling, and therefore maintaining the measured background concentration measured by TCI during the neap tide period.

3.7.2 Monsoon season

During the monsoon season, May/June to August/September, it is expected that the SSC in the estuary is considerably higher than that measured during the survey. This increase in the available material is expected due to higher offshore concentrations entering the estuary, attributable to the larger wave action and (potentially) the input from the river sources. According to EMC (2014), during the flood season (June to September) in the Indus River (located south of the site), the suspended load rises to about 400 mg/l in Khobar Creek. This suspended load appears to be similar to what has been observed closer to the project site during monsoon season.

Based on available information and a conservative approach we have assumed a high offshore SSC value of 400 mg/l for the monsoon runs over a Spring-Neap cycle. These larger SSC values represent suspended sediment arising from all identified sources. To best represent the bottom stirring caused by wave action and the associated reduction in deposition offshore in the monsoon simulations no sediment deposition was allowed in the offshore areas.

The effect of the monsoon season on the SSCs at the MET1 during the spring tide and the neap tide is shown in Figure 45. This figure shows that the background suspended sediment concentrations at the site are increased four-fold up to more than 200mg/l indicating that there is a significant amount of suspended material entering the estuary. An assessment of the monsoon season effects on SSC values and associated deposition in the estuary is considered further in Section 3.8.3.

Figure 45: Modelled suspended sediment concentration during Spring tide (a) and Neap tide (b) conditions MET1 sampling location. The predicted SSC values using increased offshore concentrations are shown by the green line. Please note that the model SSC is expressed in kg/m³ instead of mg/l – 0.1kg/m³ is equal to 100mg/l.

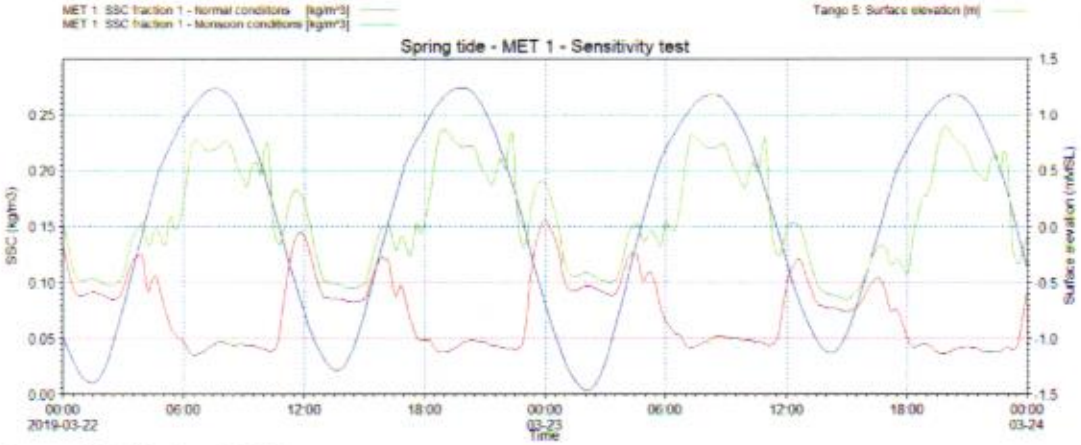

Source: Mott MacDonald, 2019

3.8 MT model results

3.8.1 Baseline model

The highest observed SSCs within the study area tend to occur during the ebb tide on Spring tides. SSCs in the vicinity of the project site and at the site (MET1) are, for the most part, between 20mg/l and 40mg/l with short-term peaks up to 150 mg/l (Figure 41). During neap tides, the background concentrations are smaller, being under 40mg/l (Figure 42).

The model shows that in general, SSCs in the study area are low and therefore, the existing deposition is limited by the amount of material in suspension.

The model results indicate that the accretion around the study area, for the baseline conditions, is limited, of the order of millimetres per year. The estimated model accretion is highly dependent on the density of the bed material, and it has been calculated using a dry density of 400 Kg/m^3 (layer 2 density, corresponding to a bulk density of 1270 kg/m^3) and 1000 Kg/m^3 (layer 3 density, corresponding to a bulk density of 1640 kg/m^3). These represent partial and fully consolidated sediment.

The simulated annual accretion rates are shown in Figure 46 for the two sediment densities. The accretion rates have been calculated using the Spring-Neap cycle deposition results and extrapolated to one year.

The total material deposited and eroded over the 15-day simulation, in g/m^2, has been multiplied up to 1-year period and transformed into a bed thickness change using the material dry density. Due to the uncertainties related to the bed properties alluded to above, the results are always presented using the second- and third-layer density values,. Please note that these accretion rates do not include any seasonal effects and are explored further when the proposed layout is analysed in Section 3.8.2.

Figure 46: Net annual deposition rate – Baseline conditions. a) Deposition calculated using a dry density of 400 kg/m³ (bulk density 1270 kg/m³). b) Deposition calculated using a dry density of 1000 kg/m³ (bulk density 1640 kg/m³).

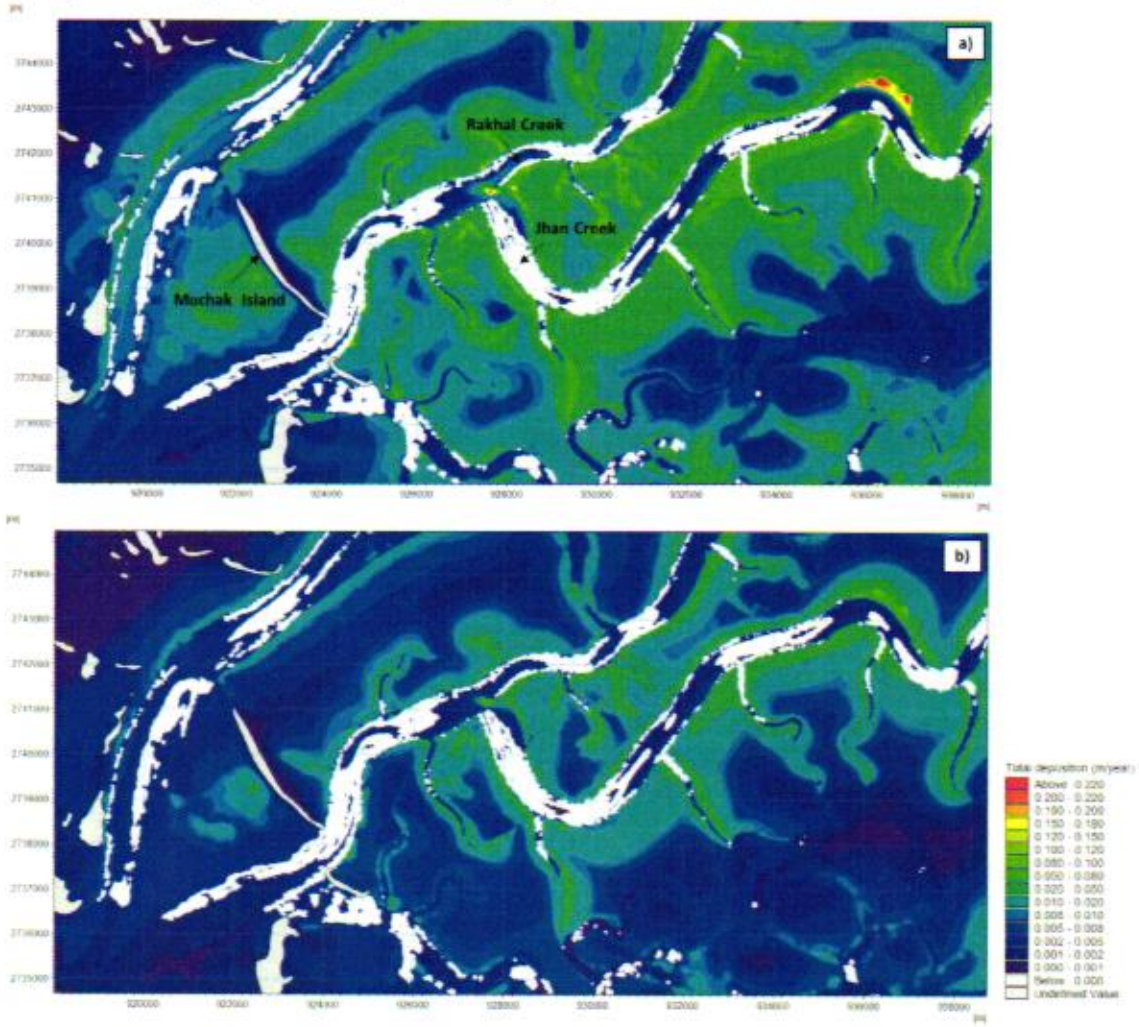

Source: Mott MacDonald, 2019

As expected, the model shows that accretion is mainly confined to the mangrove/intertidal areas. Accretion is also observed in the intertidal area in front of Muchak Island. Here the model indicates that accretion is limited to millimetres per year with higher accretion rates up to 0.2m where Rakhal Creek and Jhan Creek meet just north of the site.

3.8.2 Proposed layout

The model was run with the proposed dredging areas for the approach channel and turning circle included, as described in Section 2.4. Figure 47 shows simulated SSC for the baseline (red line) and the proposed layout (green line) at the three sampling locations. The figure shows that the dredging of the approach channel, turning circle and berths has results in almost no change to SSC values in the vicinity of the site.

Figure 47: Changes between the simulated baseline SSC (red line) and proposed SCC (green line) for the three-sampling location during Spring tide. Please note that the model SSC is expressed in kg/m^3 instead of mg/l – 0.1kg/m^3 is equal to 100mg/l.

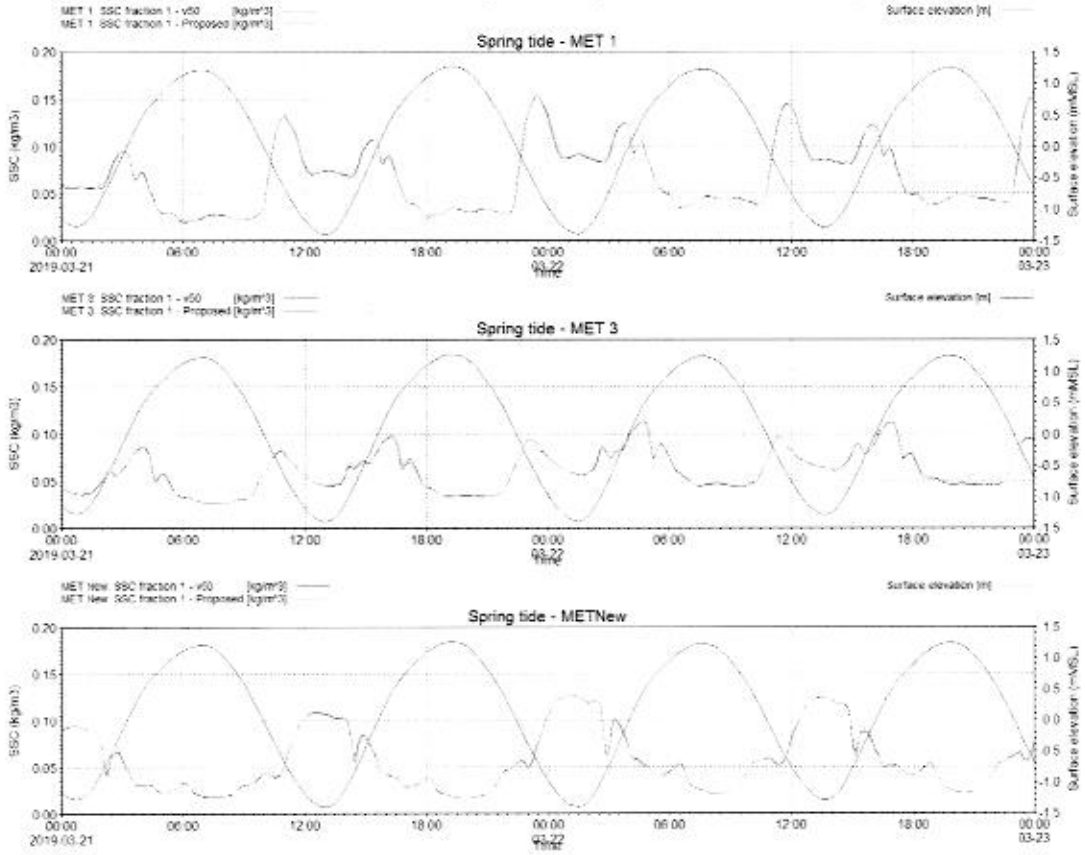

Source: Mott MacDonald, 2019

It is considered that the minor changes in SSC values are related to the small local changes in current speeds attributable to the new bathymetry. These small changes in currents speeds are described in the hydrodynamic model report (Mott MacDonald, 2018) and in Figure 48 below which shows some limited areas where the current speeds were increased, both during ebb and flood conditions, potentially causing some very small changes to local SSC values.

Figure 48: Spatial difference in current speed (baseline vs post dredge scenario) during typical spring tide show the difference between flood and ebb

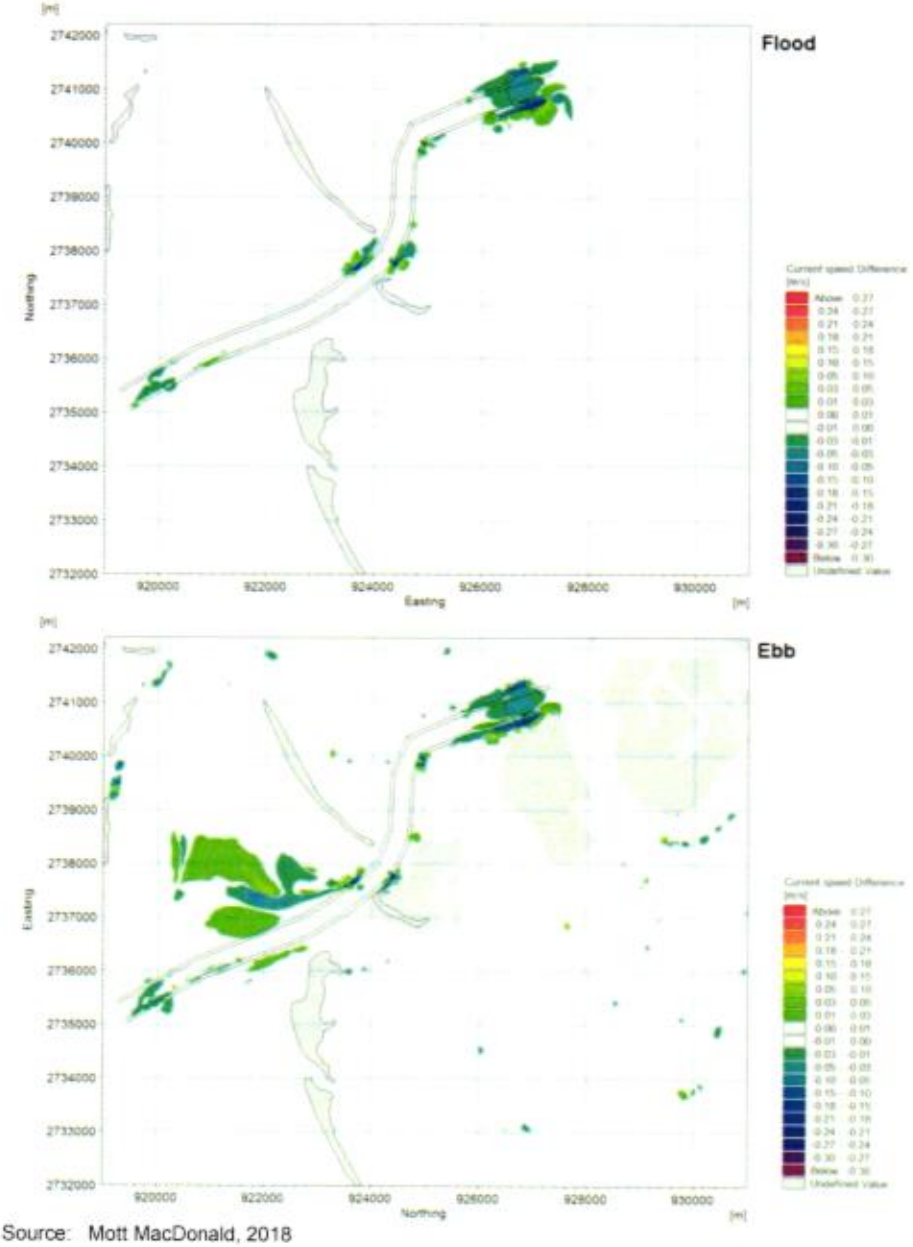

Source: Mott MacDonald, 2018

Figure 49 shows the changes in the maximum suspended sediment concentration between the proposed layout and the baseline conditions during the Spring-Neap simulation. As indicated by the time-series from the sample locations (Figure 47), the maximum SSC values show small localised increases up 10mg/l around the project site, probably due to the small variation in the local currents. Please note that the isolated spots in Figure 47 are attributed to the model elements wetting and drying at different times in the model, and they do not represent a real increase/decrease in the SSC.

Figure 49: Changes in maximum suspended sediment concentration between the proposed layout and the baseline over a Spring-Neap cycle.

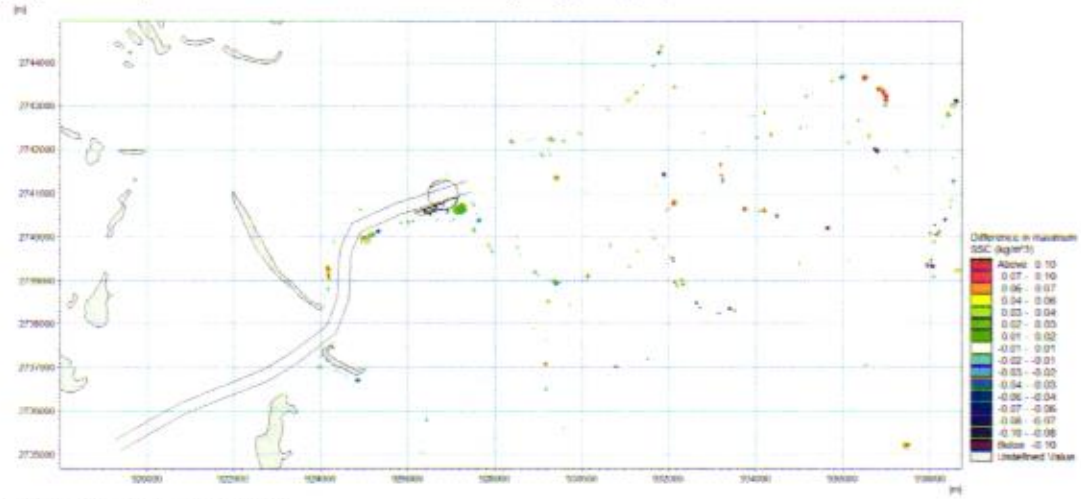

Source: Mott MacDonald, 2019

The predicted net annual accretion expected at the site, including the proposed dredging scheme, is shown in Figure 50 together with the baseline net annual deposition rate. This accretion has been calculated using a dry density of 400kg/m^3 for one year. Figure 51 shows the same comparison, however using a dry density of 1000kg/m^3, therefore the magnitudes are smaller due to the more dense and consolidated material. Similar to the baseline case (Figure 46), the model results show net accretion in the mangrove areas and the intertidal, especially in front of Muchak Island and north of the site, were the two creeks meet. The model results also indicate that there is some accretion expected at the proposed berth locations and turning circle (Figure 50b and Figure 51b). This accretion varies between 0.1m/year and 0.2m/year depending of the density of the sediment use in the calculation.

Figure 50c and Figure 51c show the differences in deposition between the baseline and the proposed layout results. Both figures indicate that the changes in the deposition patterns are mainly limited to the berths/turning circle south edge, where deposition is increased by the proposed layout up to 0.2m per year.

The deposition changes described above are mainly related to the changes in the hydrodynamic conditions attributable to dredging at the site. Figure 48 shows that currents tend to decrease slightly in the berth pocket, due to the deepening of the bathymetry, and therefore the cause of the higher deposition observed in the sediment model results. However, the accretion rates predicted for cohesive sediments are small, and it is considered that they do not represent a problem to the required minimal depths for the approach channel and tuning circle. Please note that the deposition described in this section does not include any seasonal effect. This is explored further in Section 3.8.3.

Figure 50: Net annual deposition rate (m/year) – Baseline (a), proposed layout (b) and differences in accretion (proposed minus baseline) (c). This deposition has been calculated using a dry density of 400kg/m³ (bulk density 1270 kg/m³)

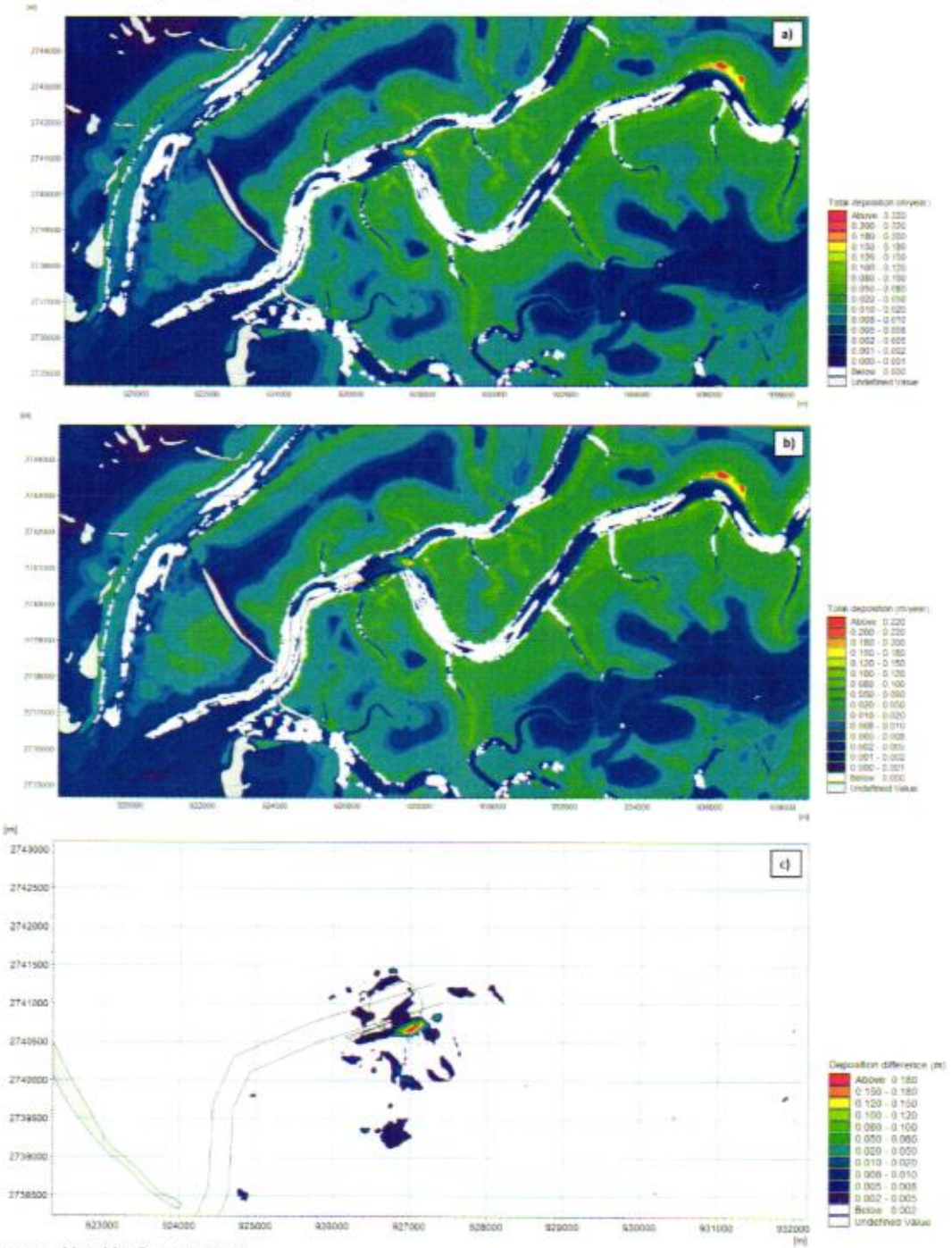

Source: Mott MacDonald, 2019

Figure 51: Net annual deposition rate (m/year) – Baseline (a), proposed layout (b) and differences of accretion (proposed minus baseline) (c). This deposition has been calculated using a dry density of 1000kg/m³ (bulk density 1640 kg/m³)

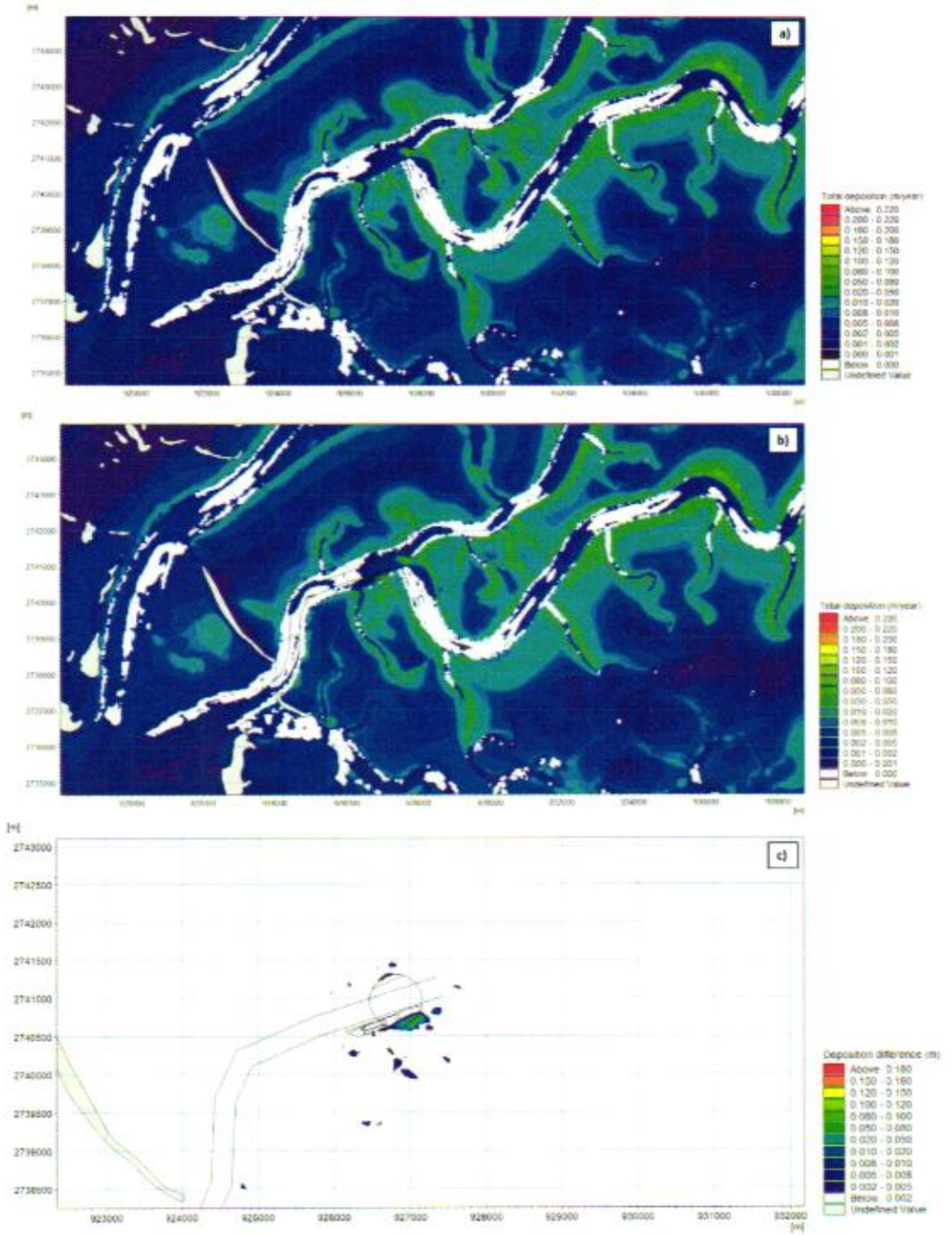

Source: Mott MacDonald, 2019

3.8.3 Monsoon season assessment

Increased offshore concentrations have a significant effect on the SSC values in the estuary and the study site related to wave action and the stirring of the offshore mud banks during the monsoon, and/or to material from the southern Indus River. The changes in SSC values at the sampling locations, for a spring tide during the monsoon simulation is shown in Figure 52. This assumes SSC comprise cohesive sediments with a concentration of 400mg/l offshore. Compared to the normal conditions, the background SSC values are increased by a factor of 4 at the three sampling locations, indicating the material entering the estuary from offshore changes considerably the suspended concentration patterns at the site (MET1) and the nearby locations (MET3 and METnew).

Figure 52: Modelled suspended sediment concentration during Spring tide conditions at the sampling locations for the proposed layout, normal conditions (red line) and the proposed layout, monsoon conditions (green line). Please note that the model SSC is expressed in kg/m^3 instead of mg/l – 0.1kg/m^3 is equal to 100mg/l.

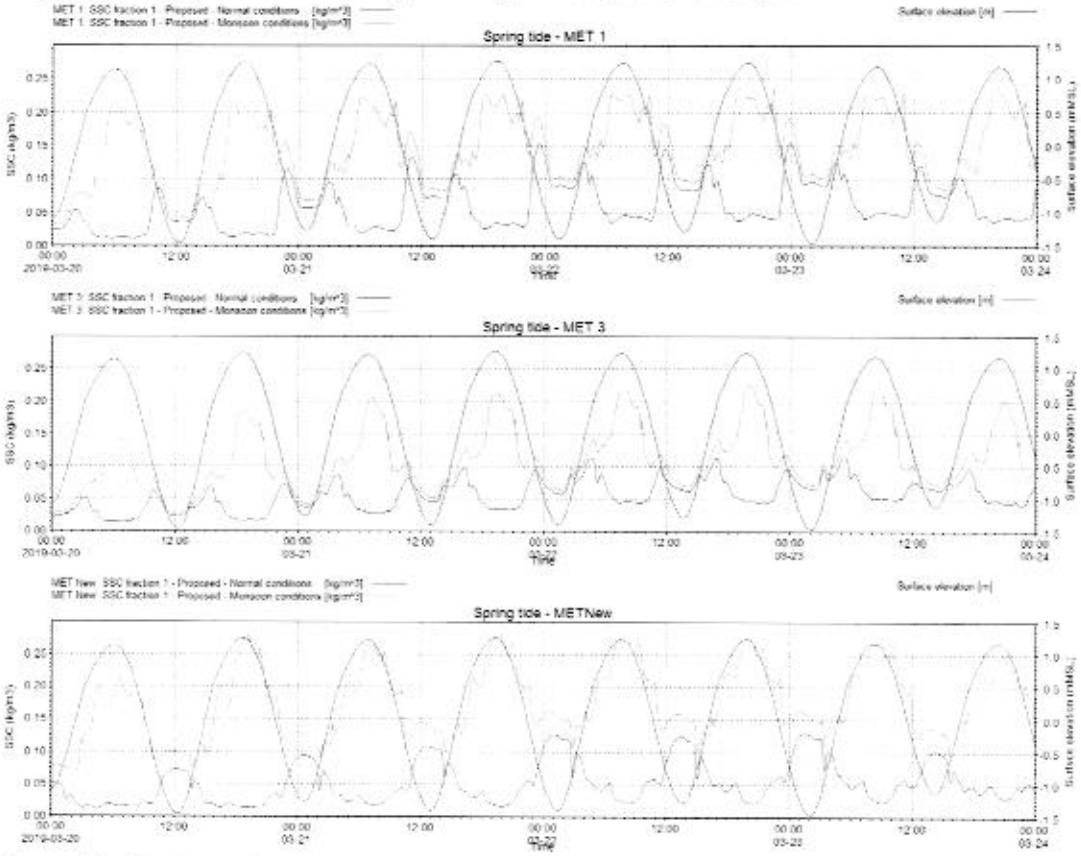

Source: Mott MacDonald, 2019

Figure 53 compares the maximum suspended sediments simulated in the estuary during: (a) normal conditions, and (b) during the assumed monsoon conditions. The figure shows that there is a considerable increase in the SSC values for the whole estuary due to the higher offshore concentrations. Of interest for the present study, concentrations at the project site during the monsoon season increase by around 50% from 150mg/l to 230mg/l.

Figure 53: Maximum SSC around the study site for the proposed layout during normal conditions (a) and monsoon conditions (b). Please note that the model SSC is expressed in kg/m³ instead of mg/l – 0.1kg/m³ is equal to 100mg/l.

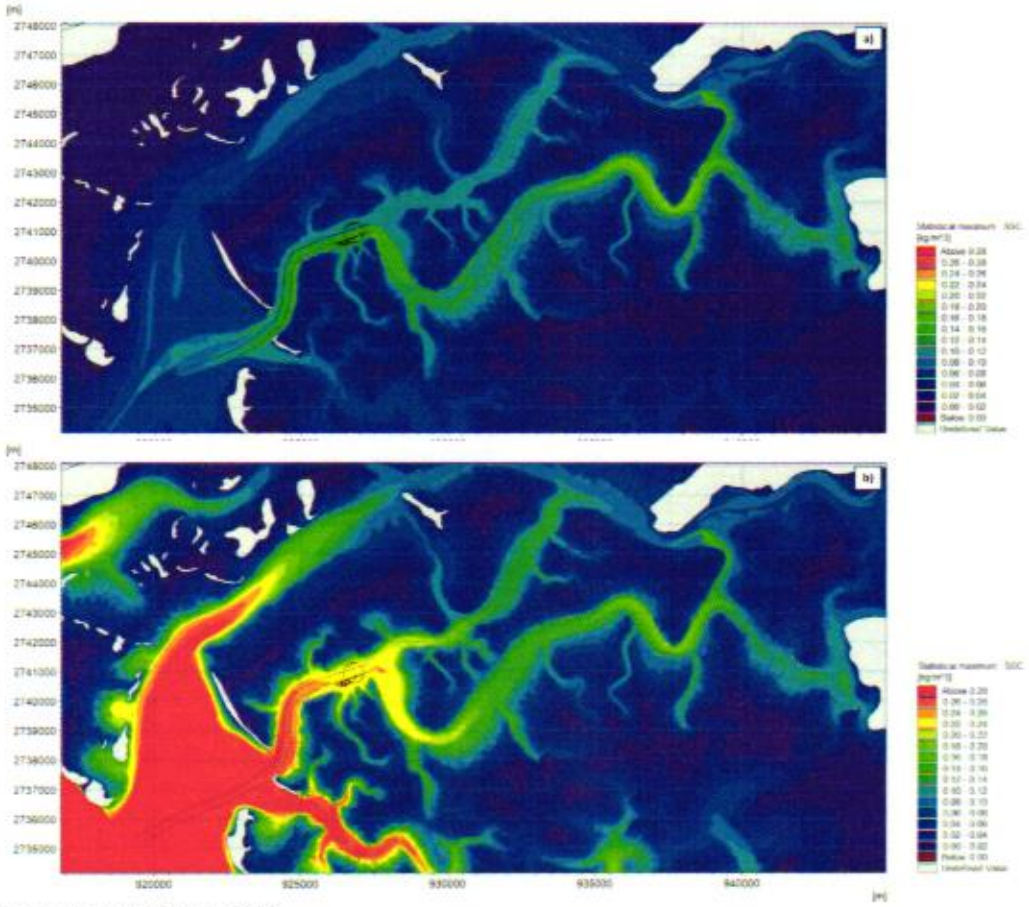

Source: Mott MacDonald, 2019

It is considered that the higher suspended sediment concentrations entering the estuary would have an effect on the deposition rates expected at the Project site and in the dredged channels. In order to including the monsoon in estimates of the annual deposition rates, it has been assumed that the monsoon lasts for 4 months (June to September) and that the rest of the year has 'normal' conditions. This is a conservative approach, since in reality the monsoon conditions would vary during the 4 months, with periods with less suspended sediments available due to a smaller wave climate or river inputs.

The estimated annual deposition rates are shown in Figure 54 (dry density of 400kg/m^3) and Figure 55 (dry density of 1000kg/m^3), together with the normal conditions results, in order to allow comparison and appreciate the effect of the 4 months monsoon conditions on the results.

The results show that the annual deposition rates are increased during the monsoon resulting in deposition rates up to 0.5m/year for some areas on the edge of the turning circle and berth pockets (assuming a dry bulk density of 400kg/m^3). There is also some evidence of an increase in the expected deposition in the approach channel, up to 0.3m/year, when the lower sediment density is used. This is attributed to the proximity to the higher than normal offshore suspended sediment concentrations.

Figure 54: Net annual deposition rate (m/year) – (a) Proposed layout with 12 months of normal conditions, (b) proposed layout including 4 months of monsoon conditions and 8 months of normal conditions, and (c) zoom into turning circle for the results including 4 months of monsoon and 8 months of normal conditions. This deposition has been calculated using a dry density of 400kg/m³ (bulk density 1270 kg/m³). Please note that the figures do not have the same colour legend as the previous deposition figures.

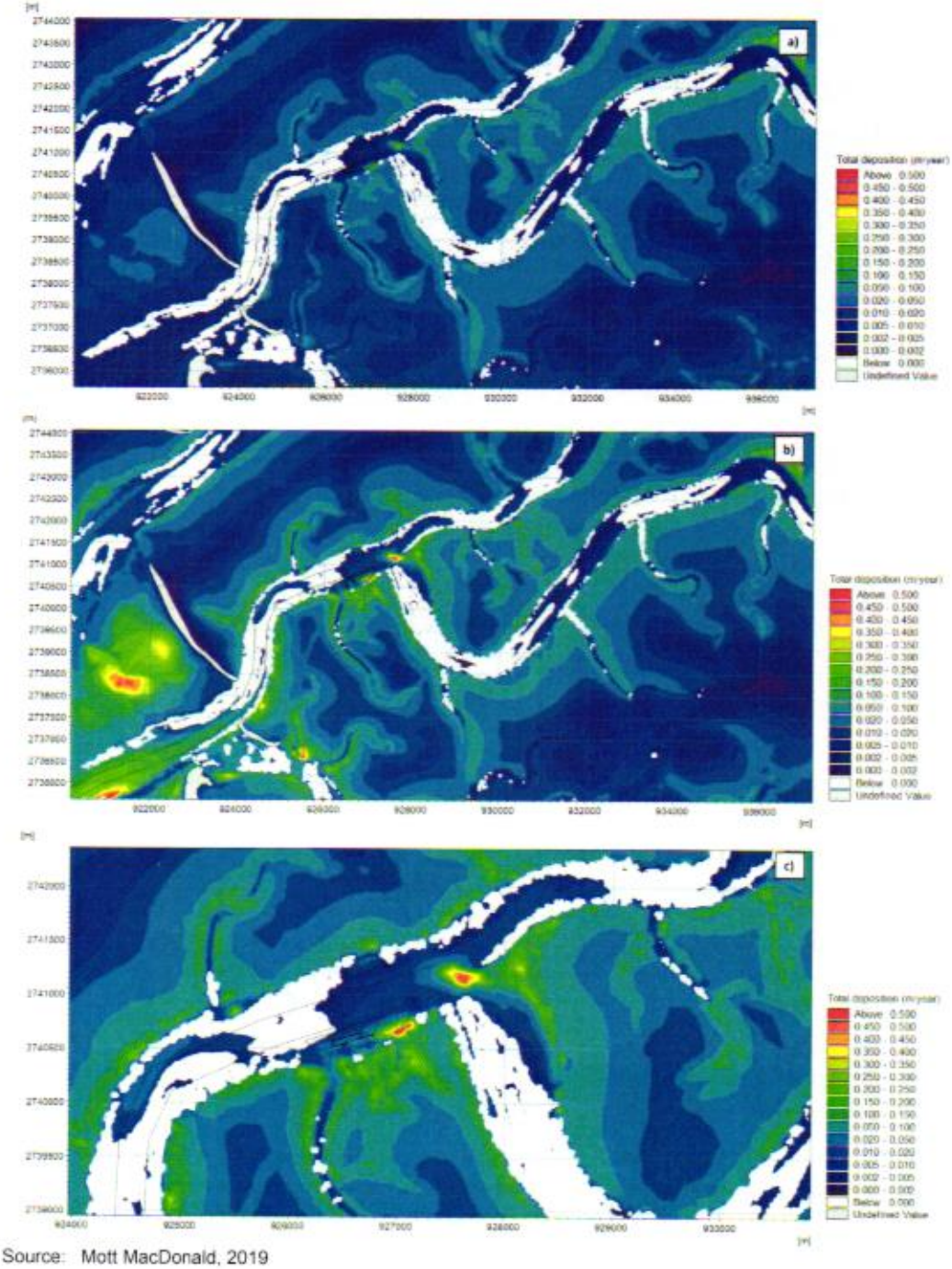

Source: Mott MacDonald, 2019

Figure 55: Net annual deposition rate (m/year) – (a) Proposed layout with 12 months of normal conditions, (b) proposed layout including 4 months of monsoon conditions and 8 months of normal conditions, and (c) zoom into turning circle for the results including 4 months of monsoon and 8 months of normal conditions. This deposition has been calculated using a dry density of 1000kg/m^3 (bulk density 1640 kg/m^3). Please note that the figures do not have the same colour legend than the previous deposition figures.

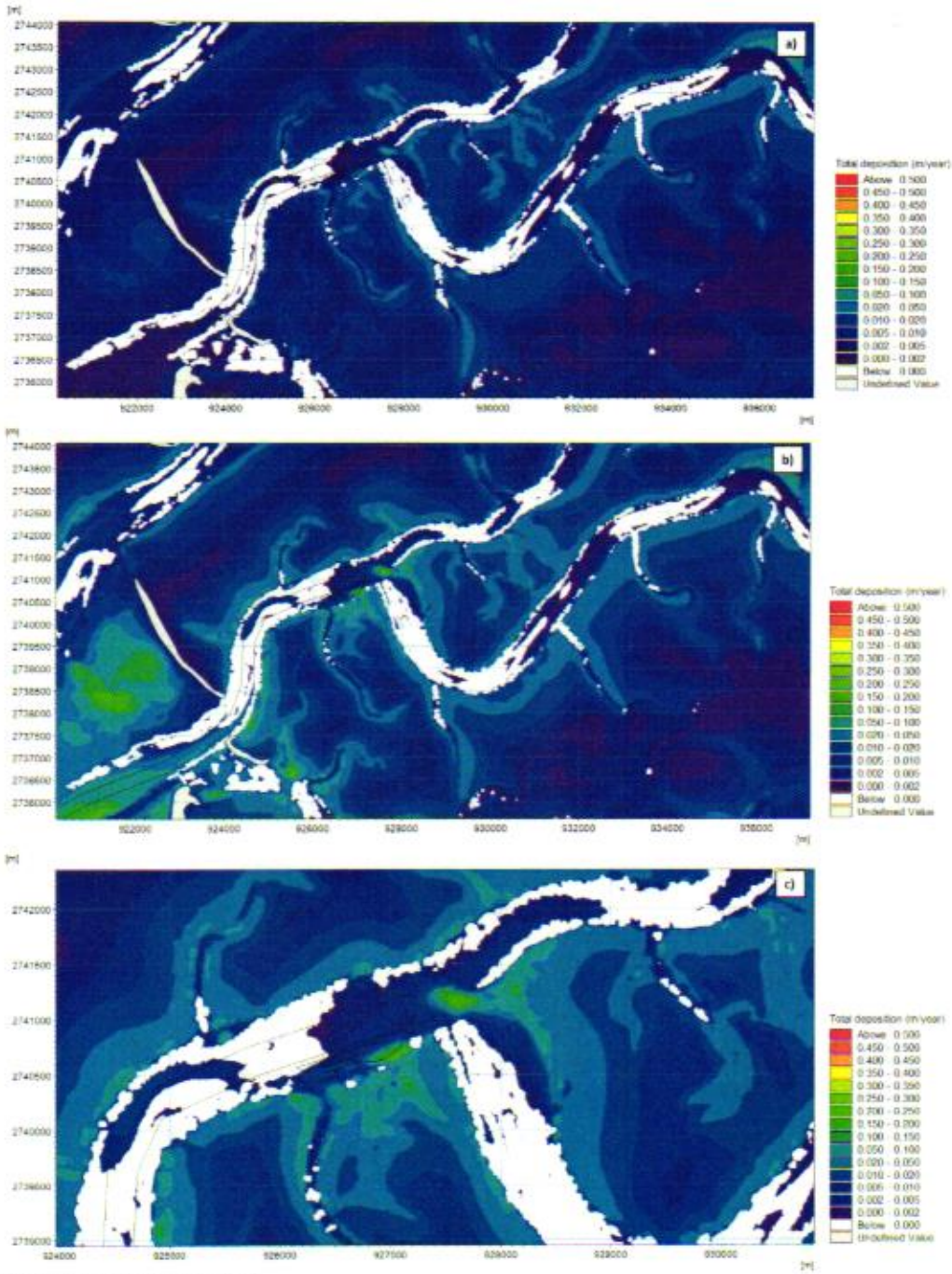

Source: Mott MacDonald, 2019

3.9 Summary and Conclusions

A MIKE21 FM MT mud transport model for the Pakistan FRSU – FEED, was setup to determine the cohesive sediment transport regime in the study area. The model was also used to understand accretion rates in the nearshore and approach channels, turning circle and berth facilities.

Limited information was available to calibrate the mud transport model. An extensive literature review was undertaken to gain a general understanding of the available suspended sediment concentrations in the estuary and their variability over the year. From this review, it was concluded that in general, the suspended sediment concentration in the estuary is small and in the range of 25 to 180mg/l, with the larger values expected during the monsoon season (June to September). According to the literature, the sediment available in the estuary is mainly reworked material, since there is a very limited input from the rivers.

Survey data used to calibrate the model from TCI in March 2019 showed background SSC values between 20mg/l and 40mg/l, with peak concentrations during the ebb tide of up to 150mg/l. The calibrated model demonstrated good skill in simulating the temporal spring tide concentration characteristics and reproduced the magnitude of the observed peaks in SSC values during the ebb tide. However, during neap tides, the model tended to slightly underestimate the suspended sediment load by approximately 10mg/l. However, since the suspended sediment concentrations are low, this underestimation is considered not to affect the model results greatly, especially when the monsoon seasonal effects are factored in.

A summary of model results showing cohesive sediment deposition rates at three locations is shown in Table 11 and Table 12 for different assume dry bulk density values and for 12 months of Spring-Neap cycles and for 4 months of monsoon conditions and 8 months of Spring-Neap cycles.

Table 11: Summary of estimated deposition rates calculated using a dry density of 400kg/m^3 (bulk density 1270 kg/m^3).

Area	Deposition during normal conditions 12 months of Spring-Neap cycles	Deposition during monsoon conditions 4 months of monsoon conditions + 8 months of Spring-Neap cycles
Approach channel	0.003 - 0.006 m/year	0.07 - 0.3 m/year
Turning circle	0.004 – 0.2 m/year	0.01 – 0.45 m/year
Berth	0.006 - 0.02 m/year	0.01 – 0.05 m/year

Source: Mott MacDonald, 2019

Table 12: Summary of estimated deposition rates calculated using a dry density of 1000kg/m^3 (bulk density 1640 kg/m^3).

Area	Deposition during normal conditions 12 months of Spring-Neap cycles	Deposition during monsoon conditions 4 months of monsoon conditions + 8 months of Spring-Neap cycles
Approach channel	0.001 - 0.002 m/year	0.03 – 0.1 m/year
Turning circle	0.001 – 0.08 m/year	0.003 – 0.2 m/year
Berth	0.002 - 0.008 m/year	0.006 – 0.05 m/year

Source: Mott MacDonald, 2019

When interpreting the model results it is important to understand the model limitations. The model was calibrated with the existing available information collected outside the monsoon season in March 2019. To better understand the influence and implications of the monsoon season, it is highly recommended to collect data during this period of the year to check that the values assumed in this modelling study are appropriate.

Despite the limited model calibration data and the assumptions made in this study to accommodate this, it is considered that the model results are broadly conservative and reflect the expected cohesive sediment behaviour and associated accretion around the Project site and more widely in the approach channel. Nevertheless, the mud transport result presented in his study must only be used as a guide to likely sedimentation rates and if used to assess dredging requirements must also include some element of uncertainty to mitigate risks.

4 Conclusions and Recommendations

JGC corporation (JGC) is undertaking Basic Design services for the marine facilities associated with FEED Design services in Chann Waddo Creek, near Port Qasim, Karachi, Pakistan.

The primary aim of FEED was to quantify sedimentation in the approach and nearshore channels, berth and turning basin areas (Figure 56). The offshore region and islands around the nearshore channel are understood to be characterised by fine sand. In contrast, sediments in the approach channel comprise silt and clay. These different sediment types are thought to merge gradually in the area adjacent to Muchak Island. To correctly represent the different dynamical properties of these sediment types, two modelling approaches have been undertaken in this second phase of the works:

- Sand transport model (ST) – for the non-cohesive sandy sediment in the nearshore and approach channel; and
- Mud transport model (MT) – for the muddy cohesive sediments in the approach channel, berthing and turning basin.

Figure 56: Study area – channels definition and project site

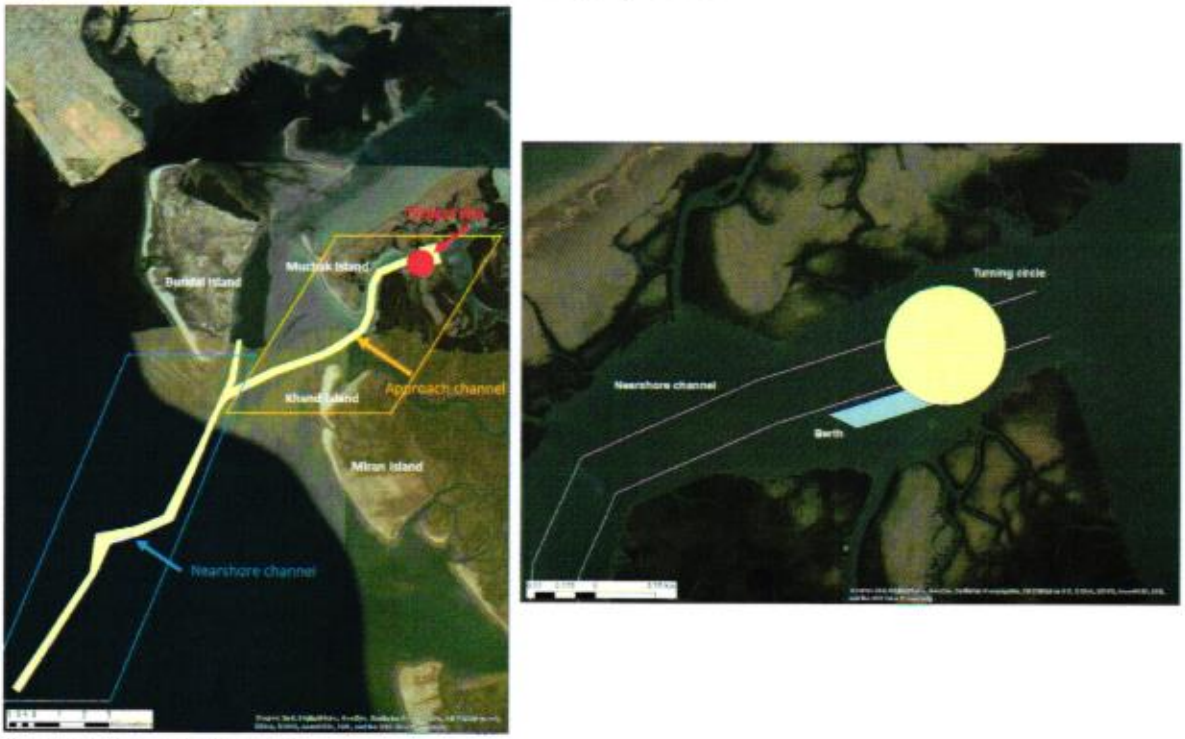

Source: Mott MacDonald, 2019

1843

According to the sand transport results:

- There are important potential net sand transport pathways, both in the nearshore and in the approach channels which can lead to significant deposition. The nearshore sediment is generally driven towards the channels and then offshore creating deposition in the channel and an intertidal sandbank growing in an offshore direction, as the tidal flow is ebb-dominant;
- The predicted sand accretion location in the nearshore channel agrees broadly with the existing anecdotal dredging records;
- The results indicate accretion of up to 2m in the entrance to the approach channel, mainly in the areas close to the islands;
- In the area of the turning circle and the berth, no significant sand accretion is observed, and there is evidence of localised erosion in these areas; and
- Annual sand accretion of the order of 1.2 million m^3 is predicted in the approach channel, as defined in Figure 27 between boxes 1 to 12.
- In the nearshore channel the annual accretion is estimated of the order of 1.8 million m^3 over the simulated year. It is understood from anecdotal evidence that around 3 million m^3 has been dredged per annum previously. From this evidence, the nature of the material dredged is unclear. It is possible therefore that the accretion predicted in this report underestimates the actual accretion at the site. This may be due to model limitation and the selected approach. Note however that in absence of a detailed sediment type/particle size distribution map there will always be some level of uncertainty attached to these results.

According to the mud transport results:

- Limited mud accretion is observed during normal conditions (spring-neap cycle) in all the study area, including the approach channel, turning circle and berthing basin. However, as would be expected, there is a supply of sediment onto the intertidal areas where the mangroves grow. The maximum accretion is observed towards the southern edge of the turning circle reaching a maximum estimate of 0.2m/year.
- When the monsoon season is considered, for a period of 4 months, the deposition of the mud in the study area is increased considerably. The approach channel accretes up to 0.3m/year, while the south edge of the turning channel reaches 0.45m/year. Note however, that the deposition is considered conservative, assuming a constant high concentration (400mg/l) of offshore supply of material during four consecutive months. In reality, monsoon conditions will vary over the June to September period.
- The deposition calculated during the mud transport simulations are based on a large amount of assumption, but with expert judgement. Without additional data, there will be some uncertainty.
- To reduce uncertainty, it would be advised to obtain more information regarding the suspended sediment concentration in the estuary during monsoon conditions, as well as additional information on sediment properties.

The results obtained from both models show that, in general, the approach channel is mainly dominated by sand processes, with some additional mud deposition during the monsoon season. Whereas, the area of the turning circle and the berths is dominated by deposition of cohesive sediments.

The volume of sand and mud deposited in the approach channel and project site have been added together. A table with the estimated deposition over the years is included in Appendix A. Please note that the results showed in the table assumed:

- The average bed level for each box has been assumed.

- The average annual deposition for the sand and the mud results per box has been used.
- Although the average condition bed level has been used, there may be some localised areas of higher deposition and therefore, regular bathymetry survey should be undertaken.
- Erosion rates (negative rates) would not occur indefinitely and therefore they have been removed from the analysis.
- Assessment of the risk allowance to be made by JGC.
- The results presented in the table should be treated as indicating the expected sediment accretion rates and locations rather than absolute figures. It is noted also that sediment transport formulae and models have a significant empirical foundation and often relate best to the data set upon which they were derived.
- At best sediment transport can only be predicted to within a factor of two or three, as per literature review three (e.g. Schoonees & Theron, 1995; Camenen & Larroudé, 2003; Winter, 2007; Papanicolaou *et al.*, 2008; Amoudry & Souza, 2011) and thus model precision must always be treated with caution and allowances made for inaccuracies.

Finally, to reduce some of the uncertainty in the model results (due to limited data), it would be advisable to collect more sediment data. This would be aimed at improving knowledge of the sediment type distribution across the delta, obtaining longer term SSC measurements (to encompass monsoon seasons) and also sediment properties such as erosional threshold, surface bed densities and settling velocities. The data could help to refine and verify the models further.

It would also be advisable to undertake bathymetry surveys both before and after the monsoon season, to gain an improved understanding of the seasonal effect upon the depositional regime of the area. This would help in validating the deposition within the model to improve predictions of accretion rates with the proposed scheme.

This report is based on best presently available data and predictions. Climate change within the design life of the project is always to be expected; the consequences of which are unknown. It can, however, be expected that such consequences would have an impact on the conclusions reached herein.

5 References

Amoudry, L. O. & Souza, A. J. 2011. Deterministic coastal morphological and sediment transport modelling: a review and discussion. Reviews in Geophysics, https:// doi.org/ 10.1029/2010RG000341.

Camenen, B. & Larroudé, P., 2003. Comparison of sediment transport formulae for the coastal environment. Coastal Engineering. Volume 48(2), 111-132

Danish Hydraulic Institute (DHI), 2006. *MIKE 21 Flow Model, Mud transport Module (MT)*, User's Manual, 80pp.

Dean, R.G., 1991. *Equilibrium Beach Profiles: Characteristics and Applications*. Journal of Coastal Research, 7:1, 53-84

EMC, 2014. Draft Environmental Impact Assessment Volume 1. PAK: Engro Fast Track LNG Regasification Project. Project Number: 48307-001

Evans, G. P., 1993. *A framework for marine and estuary model specification in the UK*. Report No. FR0374, Foundation for Water Research, 58pp.

Global Environmental Management Services (GEMS), 2017. ESIA of Pakistan Gasport Ltd. LNG Import Terminal 2, Port Qasim, Pakistan, 256pp.

Harrison, P.J., Khan, N., Yin, K., Saleem, M., Bano, N., Nisa, B., Ahmed, S. I., Rizvi, n. and Azan, F., 1997. Nutrient and phytoplankton dynamics in two mangrove tidal creeks of the Indus River delta, Pakistan. Marine Ecology Progress Series, 157: 13-19.

Kirby, R., 2002. *Chapter 4: Distinguishing accretion from erosion-dominated muddy coast*. From Muddy coast of the word: Process, deposition and function. Elsevier Science

Lumborg, U. & Windelin A., 2003. Hydrography and cohesive sediment modelling: application to the Rømø Dyb tidal area. *Journal of Marine Systems*, 38,287-303.

Mehta, A., Hayter, J. E., Parker, R. W., Krone, R., Teeter, A. M.,1989. Cohesive Sediment Transport. I: Process Description. Journal of Hydraulic Engineering, DOI: 10.1061/(ASCE)0733-9429(1989)115:8(1076)

Mott MacDonald, 2018. Pakistan FSRU - Hydrodynamic Modelling Study. 396490-002-A

Mott MacDonald, 2018. Pakistan FSRU Project Pre-FEED - Wave Modelling Study. 39639-003-A

Naz, F., Qureshi, N. A. & Saher, N. U., 2014. Temporal variations of mesozooplankton abundance and biomass in the mangrove creek area along the Karachi coast, Pakistan. *Acta Oceanol. Sin.*, 33(12), 222–230, DOI: 10.1007/s13131-014-0548-9.

Papanicolaou, A. N., Elhakeem, M., Krallis, G., Prakash, S. & Edinger, G., 2008. Sediment Transport Modelling Review—Current and Future Developments. Journal of Hydraulic Engineering, https://doi.org/10.1061/(ASCE)0733-9429(2008)134:1(1)

STS, 2018. Factual Geotechnical Investigation Report for Geotechnical Investigation for Pakistan FSRU Project, Report Ref. K18-1143-101, 523pp.

TCI, 2019. Field Data Collection for Sedimentations Studies for Tabeer Energy FSRU Terminal Port Qasim. May 2019.

Schoonees, J. S. & Theron, A. K., 1995. Evaluation of 10 cross-shore sediment transport/ morphological models. Coastal Engineering, Vol: 25(1), 1-41

Whitehouse, R. J., Soulsby, R. L., Roberts, W. & Mitchener, H. J., 2000. *Dynamics of estuarine muds*. Thomas Telford.

Williams, J. J. & Esteves, L. S., 2018. Guidance on setup, calibration, and validation of hydrodynamic, wave and sediment models for shelf seas and estuaries, *Advances in Civil Engineering*, Article ID 5251902, 25 pages. https://doi.org/10.1155/2017/5251902.

Winter, C., 2007. On the evaluation of sediment transport models in tidal environments. Sedimentary Geology, Vol. 202(3), 562-571.

1847

Appendices

A. Deposition rates table

Table 13: Accumulated depth level change (m) resulting from the deposition of sand and mud material, per box. The highlighted (orange) results are showing that the deposition rate has reached the minimal depth of -14mCD. Please note that the values of the table do not include any factor to allow for model inaccuracies. Please refer to the calculation assumptions below for further information.

			Accumulative depth level change (m) without dredging															
Box	Location	Area (m2)	Present day - 2019 Assumed Avg. Bed Level (mCD)	ST Average Total Net Deposition (m/year)	MT Average Total Net Deposition (m/year)	Total deposition (m/year)	2020	2021	2022	2023	2024	2025	2026	2027	2028	2029	2030
1-1	Approach	258,882	-15.77	0.41	0.104	0.517	-15.26	-14.74	-14.22	-13.71	-13.19	-12.67	-12.15	-11.64	-11.12	-10.60	-10.09
1-2	Approach	253,107	-16.51	0.27	0.098	0.369	-16.14	-15.77	-15.40	-15.03	-14.66	-14.29	-13.92	-13.55	-13.18	-12.81	-12.45
10-1	Berths	32,760	-15.50	0.00	0.000	0.000	-15.50	-15.50	-15.50	-15.50	-15.50	-15.50	-15.50	-15.50	-15.50	-15.50	-15.50
10-2	Berths	58,853	-14.00	0.08	0.035	0.115	-13.88	-13.77	-13.65	-13.54	-13.42	-13.31	-13.19	-13.08	-12.96	-12.85	-12.73
11-1	Turning	270,585	-21.01	0.00	0.010	0.010	-21.00	-20.99	-20.98	-20.97	-20.96	-20.95	-20.94	-20.93	-20.92	-20.91	-20.90
11-2	Turning	278,013	-19.19	0.00	0.047	0.047	-19.14	-19.09	-19.05	-19.00	-18.95	-18.90	-18.86	-18.81	-18.76	-18.71	-18.67
12-1	Approach	81,432	-17.00	0.00	0.002	0.002	-17.00	-17.00	-16.99	-16.99	-16.99	-16.99	-16.98	-16.98	-16.98	-16.98	-16.98
12-2	Approach	82,462	-18.69	0.73	0.002	0.735	-17.95	-17.22	-16.48	-15.74	-15.01	-14.27	-13.54	-12.80	-12.07	-11.33	-10.60
2-1	Approach	313,585	-17.87	0.25	0.185	0.434	-17.43	-17.00	-16.56	-16.13	-15.69	-15.26	-14.83	-14.39	-13.96	-13.52	-13.09
2-2	Approach	298,192	-17.43	0.00	0.172	0.172	-17.26	-17.08	-16.91	-16.74	-16.57	-16.39	-16.22	-16.05	-15.88	-15.70	-15.53
3-1	Approach	121,473	-23.62	0.00	0.123	0.123	-23.50	-23.38	-23.25	-23.13	-23.01	-22.88	-22.76	-22.64	-22.52	-22.39	-22.27
3-2	Approach	113,866	-23.36	0.00	0.081	0.081	-23.27	-23.19	-23.11	-23.03	-22.95	-22.87	-22.79	-22.71	-22.63	-22.55	-22.47
4-1	Approach	171,875	-32.03	0.77	0.065	0.835	-31.19	-30.36	-29.52	-28.69	-27.85	-27.02	-26.19	-25.35	-24.52	-23.68	-22.85
4-2	Approach	151,214	-30.00	0.97	0.000	0.970	-29.03	-28.06	-27.09	-26.12	-25.15	-24.18	-23.21	-22.24	-21.27	-20.30	-19.33
5-1	Approach	122,000	-21.66	1.29	0.000	1.290	-20.36	-19.07	-17.78	-16.49	-15.19	-13.90	-12.61	-11.32	-10.03	-8.74	-7.45
5-2	Approach	104,427	-23.43	0.41	0.000	0.410	-23.03	-22.62	-22.21	-21.80	-21.39	-20.98	-20.57	-20.16	-19.75	-19.34	-18.93
6-1	Approach	163,937	-19.75	0.00	0.000	0.000	-19.75	-19.75	-19.75	-19.75	-19.75	-19.75	-19.75	-19.75	-19.75	-19.75	-19.75
6-2	Approach	162,182	-23.82	0.00	0.000	0.000	-23.82	-23.82	-23.82	-23.82	-23.82	-23.82	-23.82	-23.82	-23.82	-23.82	-23.82
7-1	Approach	96,043	-32.91	0.57	0.012	0.585	-32.32	-31.74	-31.15	-30.57	-29.98	-29.40	-28.81	-28.23	-27.64	-27.06	-26.47
7-2	Approach	82,382	-23.34	1.40	0.000	1.397	-21.94	-20.55	-19.15	-17.75	-16.35	-14.96	-13.56	-12.16	-10.76	-9.37	-7.97
8-1	Approach	163,324	-24.52	1.30	0.000	1.304	-23.22	-21.92	-20.61	-19.31	-18.00	-16.70	-15.39	-14.09	-12.78	-11.48	-10.18
8-2	Approach	152,737	-23.37	0.00	0.000	0.000	-23.37	-23.37	-23.37	-23.37	-23.37	-23.37	-23.37	-23.37	-23.37	-23.37	-23.37
9-1	Approach	111,319	-20.16	0.00	0.000	0.000	-20.16	-20.16	-20.16	-20.16	-20.16	-20.16	-20.16	-20.16	-20.16	-20.16	-20.16
9-2	Approach	111,155	-19.88	0.00	0.00	0.004	-19.87	-19.87	-19.86	-19.86	-19.86	-19.85	-19.85	-19.84	-19.84	-19.83	-19.83

Source: Mott Macdonald, 2019

Notes: In order to derive the deposition rates of Table 13. It has been assumed that:

- The average bed level for each box has been assumed.
- The average annual deposition for the sand and the mud results per box has been used.
- Although the average condition bed level has been used, there may be some localised areas of higher deposition and therefore, regular bathymetry survey should be undertaken.
- Erosion rates (negative rates) would not occur indefinitely and therefore they have been removed from the analysis.
- Assessment of the risk allowance to be made by JGC.
- The results presented in the table should be treated as indicating the expected sediment accretion rates and locations rather than absolute figures. It is noted also that sediment transport formulae and models have a significant empirical foundation and often relate best to the data set upon which they were derived.
- At best sediment transport can only be predicted to within a factor of two or three, as per literature review three (e.g. Schoonees & Theron, 1995; Camenen & Larroudé, 2003; Winter, 2007; Papanicolaou et al., 2008; Amoudry & Souza, 2011) and thus model precision must always be treated with caution and allowances made for inaccuracies.